Electromagnetic Properties of 2-dimensional $d_{x^2-y^2}$ Symmetry Superconductors

By

Peter N. Arberg, B.Sc., M.Sc.

A Thesis

Submitted to the Faculty of Graduate Studies

in Partial Fulfillment of the requirements

for the Degree

Doctor of Philosophy

McMaster University

June 1995

DOCTOR OF PHILOSOPHY (1995)
(PHYSICS)

McMASTER UNIVERSITY
Hamilton, Ontario

TITLE: Electromagnetic Properties of
2-dimensional $d_{x^2-y^2}$ Symmetry
Superconductors

AUTHOR: Peter N. Arberg,
B.Sc. (Brock University),
M.Sc. (Brock University)

SUPERVISOR: DR. J.P. CARBOTTE

NUMBER OF PAGES: vii, 125

Electromagnetic Properties of 2-dimensional $d_{x^2-y^2}$ Symmetry Superconductors

Oh, pilot of the storm who leaves no trace
Like sorts inside a dream
Leave the path that led me to that place
Yellow desert stream

J. Bonham, J. Page, R. Plant.

ABSTRACT

A 2-dimensional $d_{x^2-y^2}$ symmetry superconductor is studied. The model used is a two dimensional Hubbard model with tight binding electrons in the plane with both nearest neighbor and next nearest neighbor hopping. The superconductivity is stabilized by anti-ferromagnetic spin fluctuations and is described by the Eliashberg theory.

With this model a general set of Eliashberg equations are derived which are valid for any electronic band structure and also the details of the electron-boson interaction can be included, and impurity scattering of arbitrary strength. This is possible because no model for the electronic density of states has been taken and thus all of the details of the density of states including the van Hove singularity can be accounted for fully. This leads to a non-trivial difference not previously seen between impurity scattering in the Born limit and that of impurity scattering in the unitary limit. The Eliashberg equations are solved numerically, and the effect of band structure and impurity scattering on the critical temperature is examined.

General expressions for the London penetration depth and the optical conductivity are derived. These are calculated for different impurity concentrations and scattering strengths, and band structures. It is found that the inverse square of the low temperature penetration depth is linear in temperature. This behavior can be changed to quadratic by adding small concentrations of impurity scattering in the unitary limit or by large concentrations of scattering in the Born limit. The conductivity of the normal state as well as that in the superconducting state also have a large dependence on the type of scattering included. The optical conductivity in the superconducting state shows no evidence of a gap in the spectrum in contrast to conventional superconductors. These results are compared with experimental observations on impurity doped high-T_c superconductors where similar behavior is observed.

ACKNOWLEDGMENTS

I would like to thank my supervisor Dr. Jules Carbotte for his insight and guidance throughout my work here at McMaster. I could not have asked for a better supervisor.

I would also like to thank Dr. Bozidar Mitrovic for always encouraging my studies throughout my university years from the undergraduate to graduate level. He is another outstanding supervisor.

There are present and past students and post-doctoral fellows and others I would like to thank. These include (in no particular order): Mohammed Mansor (now a Dr.), Ron Rogge (also now a Dr.), Dwayne Branch, Jennifer Rendall, Bill Atkinson, Bill Minor, Chris O'Donovan, Charles Curry, Armando Gama, Rachid Ouyed, Dr. Frank Marsiglio, Dr. Elisabeth Nicol, Dr. Ciao Jiang, Dr. Stefan Lenck, Dr. Gregg Cripps.

Also to be thanked is the office staff including Jackie, Wendy, Cheryl and Rosemary for always being helpful and cheery despite sometimes trying circumstances.

Most of all I would like to thank my parents and Kanan (also now a Dr.) for extraordinary support and wonderful friendship.

Table of Contents

1. Introduction

1.1. Superconductivity

The discovery of ceramic superconductors in 1986 (Bednorz and Müller, 1986) has sparked great interest in the field of high temperature superconductivity where high temperature in this context refers to superconductors with critical temperatures in excess of *30 K*. Although this discovery of superconductivity in the ceramic material Ba-La-Cu-O has a rather modest (by present standards) critical temperature (T_c=*30 K*), it is a large enhancement over the previous known superconductors. These are for example, mercury (Hg; the first known superconductor discovered in 1911) with T_c =*4.2 K*, lead (Pb) with T_c =*7.2 K* among others and the so called A-15 compounds. The A-15 compounds (V_3Si,

V_3Ga , Nb_3Al , Nb_3Ge , and others) had the highest critical temperature until the 1986 discovery and were known superconductors in the 1970's (Shen, 1972). These compounds typically have critical temperatures of the order of *20 K* with Nb_3Ge having the highest, T_c=*23 K* (Kihlstrom *et al.*, 1981; Golovashkin *et al.*, 1981). All of the pre-1986 superconductors have the common features of a metallic normal state including the organic superconductors first discovered in 1979 with $(TMTSF)_2PF_6$[1] with T_c=*1.2 K* under a pressure of *6.5 kbar* (Jerome *et al.*, 1980; see Ishiguro and Yamaji, 1990 for a complete list of the organic superconductors and their properties), and their superconducting state is well described by electron-phonon mediated superconductivity (with the exception of the organic superconductors and the heavy fermion superconductors (Stewart, 1984) where it is still unclear as to the underlying interaction which is responsible). These electron-phonon coupled superconductors are also known as conventional superconductors. The discovery of superconductivity in Ba-La-Cu-O quickly lead to the discovery of superconductivity in other copper-oxides, for example Y-Ba-Cu-O (Chu *et al.*, 1987) with T_c=*93 K*; Tl-Ba-Ca-Cu-O (Sheng and Herman, 1988a, 1988b; Hazen *et al.* 1988) with T_c=*125 K*.

[1] bistetra-methyl-tetraselenafulvalene-hexaflourophosphate

1.2. BCS Theory - Overview

Although the phenomenon of superconductivity was discovered in 1911, a microscopic theory of superconductivity was not forth-coming until 1957. The theory was proposed by Bardeen, Cooper and Schrieffer (1957) and is now known as the BCS theory of superconductivity. A very detailed and lucid description of BCS theory can be found in de Gennes (1966). The key element in the theory is that a system containing an inert Fermi sea plus two electrons at the Fermi surface in opposite momentum and spin states ($|\mathbf{k}\uparrow\rangle$ and $|-\mathbf{k}\downarrow\rangle$) with an overall attractive interaction (no matter how small) has a lower energy than the same system with the two electrons being in any other momentum - spin state. This pair of electrons is known as a Cooper pair and is the starting point for the BCS theory of superconductivity. The superconducting state arises when one constructs a system of Cooper pairs such as

$$|\Phi\rangle_{BCS} = \prod_{\mathbf{k}} (u_{\mathbf{k}} + v_{\mathbf{k}} c^{+}_{\mathbf{k}\uparrow} c^{+}_{-\mathbf{k}\downarrow})|0\rangle \qquad : 1\text{-}1$$

where $|\Phi\rangle_{BCS}$ is the BCS wave function, $|0\rangle$ is the vacuum, the product is over all electronic plane wave states, $c^{+}_{\mathbf{q}\sigma}$ creates an electron in plane wave state with momentum $\mathbf{q}$ and spin σ, $v_{\mathbf{k}}(u_{\mathbf{k}})$ are variational parameters which turn out to be the probability amplitude for finding an electron(hole) with momentum $\mathbf{k}$. The theory leads to a critical temperature

$$T_c = 1.13\omega_c e^{-\frac{1}{N(0)V}} \qquad : 1\text{-}2$$

where $N(0)$ is the electronic density of states at the Fermi surface, V is the pairing potential between two electrons (and is positive) and ω_c is a cut-off energy for the interaction[2]. Although T_c cannot be predicted by microscopic means only, the theory has been a great success and it does give several universal numbers such as

$$\frac{2\Delta(0)}{T_c} = 3.54 \qquad : 1\text{-}3$$

$$\frac{\gamma T_c^2}{H_c^2} = 0.17 \qquad : 1\text{-}4$$

where $\Delta(0)$ is the zero temperature limit of the superconducting gap, T_c is the critical temperature, H_c is the thermodynamic critical field and $\gamma = \frac{2}{3}\pi^2 N(0)$. While the BCS theory does not give quantitative agreement with experiment it does however give excellent qualitative agreement in a wide range of materials.

1.3. *Eliashberg Theory - Overview*

While the BCS theory gives qualitative behavior for so called weak coupling superconductors (i.e. Al, Sn) it fails for so called strong coupling

---

[2]Throughout this work the units are chosen such that $\hbar=k_B=c=1$.

superconductors (i.e. Pb, Hg). A general theory was developed by Eliashberg (1960a, 1960b). This theory takes into account the repulsive Coulomb interaction between electrons and the attractive interaction between the electrons induced by the electron-phonon interaction. The basis for the Eliashberg theory (or strong coupling) theory is a system of Cooper pairs as in BCS (weak coupling) theory. The two theories depart in the treatment of the interactions between the electrons. BCS theory assumes there is a net attraction between electrons near the Fermi surface and treats this interaction as a constant. Strong coupling theory includes the interactions from a microscopic level and then the superconducting state arises from the electron-phonon interaction. However the price one pays is that the Eliashberg equations must be solved by numerical means. Despite this difficulty, the solutions obtained and the physical properties, both thermodynamic and transport are in excellent quantitative agreement with experimental results (see Carbotte, 1990).

The Eliashberg theory has been a tremendous success in condensed matter theory. Included in the success is the incorporation into the theory of electron scattering from magnetic impurities in the weak limit, Born approximation (Abrikosov and Gor'kov, 1960, 1961; Ambegaokar and Griffin, 1965; Skalski *et al.*, 1964, Maki, 1969; Schachinger *et al.*, 1980) and in the strong limit, T-matrix approach (Rusinov, 1969a, 1969b; Shiba, 1968). Also studied has been anisotropic effects of the Fermi surface (Allen, 1980; Daams and Carbotte, 1980a,

1980b, 1981; Allen and Mitrovic, 1982; Zarate and Carbotte, 1983a, 1983b; Whitmore, 1984). Energy dependent electronic density of states has also been examined (Pickett, 1980, 1982; Mitrovic and Carbotte, 1981, 1983a, 1983b; Carbotte, 1982; Kieselmann and Rietchel, 1982). This theory with all of these additional features has been able to successfully account for the properties of many superconducting systems.

1.4. *High T_c Superconductivity*

The Eliashberg theory fails to properly describe the heavy fermion superconductors and the high T_c ceramic superconductors. It is believed that the heavy fermion superconductors can be described by an Eliashberg type theory where the superconducting order parameter is anisotropic in k-space and with the superconductivity stabilized by anti-ferromagnetic spin fluctuations (Fulde *et al.*, 1988). The case of the high T_c superconductors is less clear. There are many different theories (Varma, 1988; Kresin *et al.*, 1993) for explaining the properties of the oxide superconductors but as of yet there is no definitive theory. A common point among these superconductors is that they are metallic in the a-b plane due to the presence of Cu-O planes and closer to insulating in the c direction (Batlogg *et al.*, 1993). This makes these materials highly anisotropic and any theoretical model must incorporate this aspect. Another aspect that must be

incorporated is that the superconducting gap exhibits $d_{x^2-y^2}$ symmetry in the a-b plane (Annett and Goldenfeld, 1992). Many experiments indicate that this could be the case, for example, the temperature dependent penetration depth (Hardy *et al.*, 1993), the superconducting quasi-particle density of states from tunneling experiments (Jiang *et al.*, 1993; Liu *et al.*, 1993), angle resolved photoemission (Wells *et al.*, 1992; Shen *et al.*, 1993). Another common feature is that the undoped materials (i.e., $La_{2-x}Sr_xCuO_4$ with $x=0$) are insulators with an anti-ferromagnetic ground state (Kitazwa. 1990). The superconducting state is believed to be stabilized by anti-ferromagnetic spin fluctuations (Millis *et al.*, 1988, 1990, Bulut and Scalapino 1992; Miyake *et al.*, 1986) which gives a repulsive interaction between the electrons in the s-wave channel and an attractive in the d-wave channel. A possible model which incorporates these ideas is a 2-dimensional Hubbard model describing electrons hopping between lattice sites and an electron-boson (anti-ferromagnetic spin fluctuation) interaction which is attractive in the d-wave channel and having $d_{x^2-y^2}$ symmetry (Millis *et al.*, 1990, Monthoux *et al.*, 1991, 1992).

1.5. Thesis Layout

This 2-dimensional $d_{x^2-y^2}$ symmetry model is described in chapter 2 along with the strong coupling theory of superconductivity. The Eliashberg equations

within this model are solved numerically for the critical temperature and some results for T_c as function of chemical potential and impurity scattering strength, both in the weak and strong limits are given. Chapter 3 describes the London penetration depth and presents results of the calculation and their relationship to the experimental results. Chapter 4 is concerned with the optical conductivity within this model. The theory of optical conductivity is described and results are shown and compared with the results found via experiment. The final chapter discusses results and gives conclusions concerning what can and what cannot be described with this model as it pertains to the high T_c superconductors.

2. Theory

2.1. The Hubbard Hamiltonian

Since the superconductivity in the high T_c superconductors is believed to occur mainly in the Cu-O planes and conduction occurs via electron hopping between lattice sites, an appropriate model is the 2-dimensional Hubbard model on a square lattice. The Hamiltonian for the model is (Hubbard, 1963)

$$H = \sum_{i\delta\sigma} W_\delta c^+_{i\sigma} c_{i+\delta\sigma} \qquad : 2.1$$

where

$$W_\delta = \int d\vec{r}\, \psi_i(\vec{r}) \psi_{i+\delta}(\vec{r}) \qquad : 2.2$$

is the overlap integral in the tight-binding approximation between an electron on site i and one on site $i+\delta$; $c^{*}_{i\sigma}$ ($c_{i\sigma}$) creates (destroys) an electron on site i with spin σ. For a square lattice with nearest neighbor and next nearest neighbor interactions between electrons, i.e.,

$$W_{\delta} = -t\begin{cases} 1 & \text{nearest neighbour,} \\ -B & \text{next nearest neighbour,} \\ 0 & \text{otherwise} \end{cases} \qquad : 2.3$$

where t is the hopping amplitude for nearest neighbor hopping and B is the strength of next nearest neighbor hopping. Then by transforming to k-space.

$$\begin{aligned} c_{i\sigma} &= \sum_{\mathbf{k}} e^{i\mathbf{k}\cdot\mathbf{r}_i} c_{\mathbf{k}\sigma} \\ c^{+}_{i\sigma} &= \sum_{\mathbf{k}} e^{-i\mathbf{k}\cdot\mathbf{r}_i} c^{+}_{\mathbf{k}\sigma} \end{aligned} \qquad : 2.4$$

then the Hamiltonian becomes

$$H = \sum_{\mathbf{k}\sigma} E_{\mathbf{k}} c^{+}_{\mathbf{k}\sigma} c_{\mathbf{k}\sigma} \qquad : 2.5$$

where $c^{*}_{k\sigma}$ ($c_{k\sigma}$) creates (destroys) an electron in state k with spin σ and

$$E_{\mathbf{k}} = -2t(\cos k_x a + \cos k_y a - 2B\cos k_x a \cos k_y a) \qquad : 2.6$$

and a is the lattice parameter (where from this point on $a=1$), and the summation is over the 2-dimensional square Brillouin zone, $\mathbf{k}\in[-\pi,-\pi]\times[\pi,\pi]$. Define

$$\begin{aligned} \varepsilon_{\mathbf{k}} &= E_{\mathbf{k}} - \mu \\ &= -2t(\cos k_x + \cos k_y - 2B\cos k_x \cos k_y) - \mu \end{aligned} \qquad : 2.7$$

where μ is the chemical potential.

The Fermi surfaces for various chemical potentials and next nearest neighbor hopping strengths (B=0, B=0.16 suitable for La-Sr-Cu-O, and B=0.45 suitable for Y-Ba-Cu-O) are shown in Figure 2.1. The electronic density of states

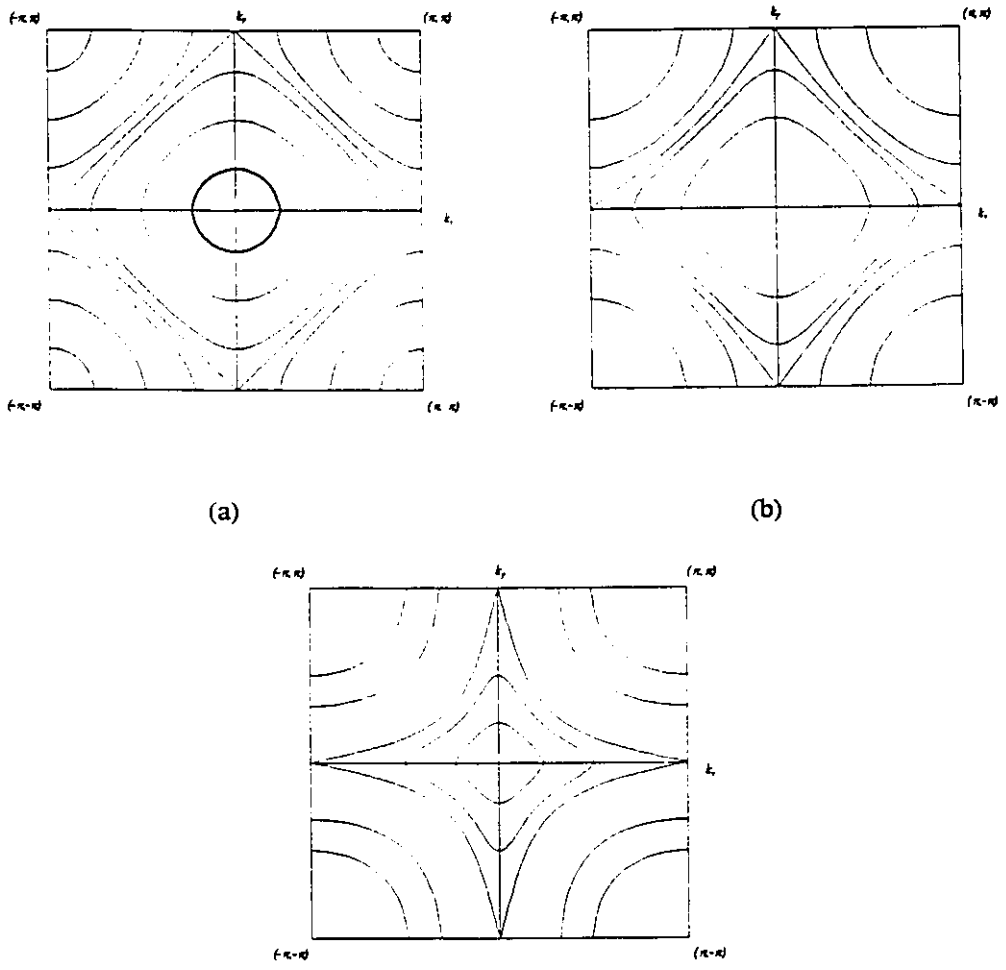

Figure 2.1 **Fermi surfaces for tight-binding Hubbard model dispersion in the first Brillouin zone. (a) For *B=0*, and *μ/2t=3.5, 2.0, 0.5, 0.0, -2.0, -0.5, -3.5* from the outside curves and inwards; (b) For *B=0.16* and *μ/2t=2.0, 0.0, -0.64, -1.0, -2.0*; (c) For *B=0.45* and *μ/2t=2.0, 0.0, -1.8, -2.0, -2.15*.**

for this tight-binding electron dispersion is shown in Figure 2.2. The feature to be pointed out is the van Hove singularity at $\mu=0$ for the case with no next nearest neighbor hopping and the additional van Hove singularity for the finite B cases (most clearly evident for $B=0.45$). The original theories of superconductivity (both BCS and Eliashberg theories) assumed that the density of states is constant near the Fermi energy. This is a very good assumption for 3-dimensional superconductors and energies within the Debye frequency of the Fermi energy. As can be seen here, this is not a reasonable assumption for this tight-binding dispersion. Later work on conventional superconductivity has incorporated a van Hove singularity in the electronic density of states (Dzyaloshinskii, 1987; Xing *et al.* 1991; Newns *et al.*, 1992; Pattnaik *et al.*, 1992; Mansor, 1994) and explicitly substituting this model for the density of states. This work does not use any explicit form for the density of states, hence all of the features of the density of states are included implicitly.

In past work the summations over k are replaced by density of states integrals and the density of states is assumed to be constant and hence can be pulled out of the integrand. The prescription then is

$$\sum_{\mathbf{k}} F(\varepsilon_{\mathbf{k}}) \rightarrow N(0)\int d\varepsilon F(\varepsilon) \qquad : 2.8$$

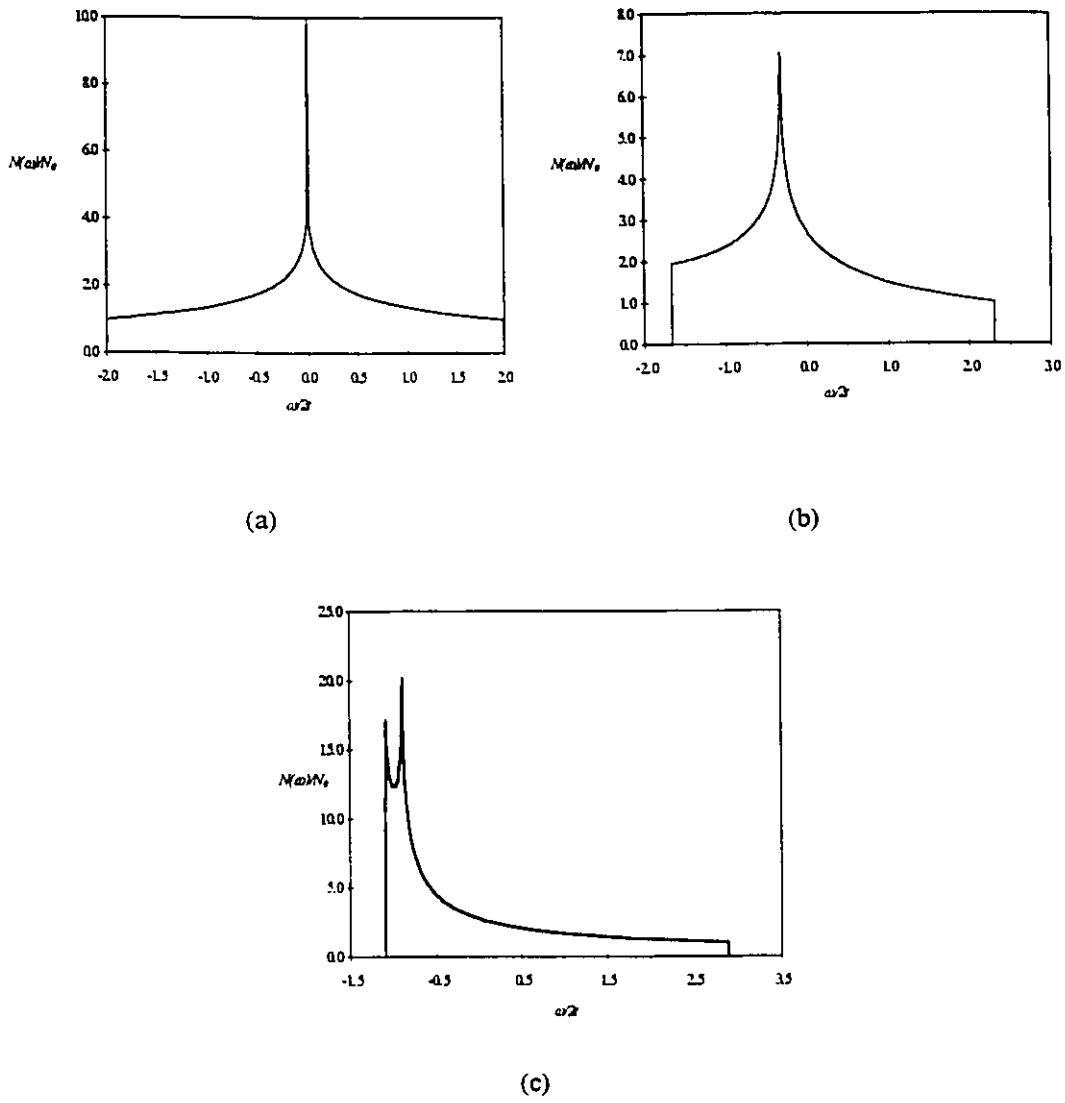

Figure 2.2 **Electronic density of states for the tight-binding dispersion. (a) *B=0*; (b) *B=0.16*; (c) *B=0.45*. In all three figures N_0 is the density of states taken at the upper band edge. The density of states is calculated by a direct summation over momentum: $N(\omega)=\Sigma_k \delta(\omega-\varepsilon_k)$.**

where $N(0)$ is the electronic density of states at the Fermi surface and $F(\varepsilon_k)$ is independent of the direction of **k**. For the case where $F(\varepsilon_k)$ can be separated into a

function that depends on energy and one that depends on the angle of k then one can integrate over the energy and angle separately by

$$\sum_{\mathbf{k}} F(\varepsilon_{\mathbf{k}}) \rightarrow \int d\varepsilon N(\varepsilon) \int \frac{d\hat{k}}{4\pi} F(\varepsilon, \hat{k}) \qquad : 2.9$$

and then a model density of states can be used to perform the integrations. For the case in this work, the summation over k is converted to an integral over k:

$$\sum_{\mathbf{k}} F(\mathbf{k}) \rightarrow \frac{1}{(2\pi)^2} \int_{-\pi}^{+\pi} dk_x \int_{-\pi}^{+\pi} dk_y F(\mathbf{k}) \qquad : 2.10$$

and it is these double integrals which will be carried out numerically. Thus the van Hove singularity in the density of states is accounted for fully.

2.2. *The Strong Coupling Theory of Superconductivity*

The strong coupling theory of superconductivity will now be discussed. Excellent derivations and discussions of strong coupling theory exist (Allen and Mitrovic, 1982; Schrieffer, 1964), hence a full derivation will not be repeated here, only the key elements will be discussed and the Eliashberg equations which follow.

The strong coupling theory is most easily derived using quantum field theoretic methods using Green's functions and Feynman diagrams. There are excellent texts on this method of perturbation theory (Fetter and Walecka, 1971; Mahan, 1981; Abrikosov *et al.*, 1963; Rickayzen, 1980; Doniach and Sondheimer,

1974) so a basic knowledge of Feynman-Dyson perturbation theory will be assumed. For the superconducting state it is convenient to use a two component field operator (Nambu, 1960):

$$\Psi_{\mathbf{k}} = \begin{pmatrix} c_{\mathbf{k}\uparrow} \\ c^{+}_{-\mathbf{k}\downarrow} \end{pmatrix} \qquad : 2.11$$
$$\Psi^{+}_{\mathbf{k}} = \begin{pmatrix} c^{+}_{-\mathbf{k}\downarrow} & c_{\mathbf{k}\uparrow} \end{pmatrix} \quad .$$

This representation equally well describes the normal state properties but is generally not used due to the complications introduced by the matrix algebra. With this representation the electron Green's function

$$G(\mathbf{k},\tau) = -\left\langle T_{\tau}\left(c_{\mathbf{k}\uparrow}(\tau)c^{+}_{\mathbf{k}\uparrow}(0)\right)\right\rangle \qquad : 2.12$$

the hole Green's function

$$\overline{G}(\mathbf{k},\tau) = -\left\langle T_{\tau}\left(c^{+}_{-\mathbf{k}\downarrow}(\tau)c_{-\mathbf{k}\downarrow}(0)\right)\right\rangle \qquad : 2.13$$

and Gor'kov's anomalous Green's function

$$F(\mathbf{k},\tau) = -\left\langle T_{\tau}\left(c_{\mathbf{k}\uparrow}(\tau)c_{-\mathbf{k}\downarrow}(0)\right)\right\rangle \qquad : 2.14$$

and

$$\overline{F}(\mathbf{k},\tau) = -\left\langle T_{\tau}\left(c^{+}_{-\mathbf{k}\downarrow}(\tau)c^{+}_{\mathbf{k}\uparrow}(0)\right)\right\rangle \qquad : 2.15$$

can be written in a condensed matrix notation:

$$\begin{aligned}\hat{G}(\mathbf{k},\tau) &= -\left\langle T_{\tau}\left(\Psi_{\mathbf{k}}(\tau)\Psi^{+}_{\mathbf{k}}(0)\right)\right\rangle \\ &= -\begin{pmatrix} \left\langle T_{\tau}\left(c_{\mathbf{k}\uparrow}(\tau)c^{+}_{\mathbf{k}\uparrow}(0)\right)\right\rangle & \left\langle T_{\tau}\left(c_{\mathbf{k}\uparrow}(\tau)c_{-\mathbf{k}\downarrow}(0)\right)\right\rangle \\ \left\langle T_{\tau}\left(c^{+}_{-\mathbf{k}\downarrow}(\tau)c^{+}_{\mathbf{k}\uparrow}(0)\right)\right\rangle & \left\langle T_{\tau}\left(c^{+}_{-\mathbf{k}\downarrow}(\tau)c_{-\mathbf{k}\downarrow}(0)\right)\right\rangle \end{pmatrix} \quad .\end{aligned} \qquad : 2.16$$

Here the operators are in the Heisenberg representation,

$$c_{\mathbf{k}\sigma}(\tau) = e^{H\tau} c_{\mathbf{k}\sigma} e^{-H\tau}$$
$$c^{+}_{\mathbf{k}\sigma}(\tau) = e^{-H\tau} c^{+}_{\mathbf{k}\sigma} e^{H\tau} \qquad : 2.17$$

and

$$\langle A \rangle = \frac{1}{tr\left\{e^{-\beta H}\right\}} tr\left\{e^{-\beta H} A\right\} \qquad : 2.18$$

is the grand canonical average for the operator A, $\beta=1/T$, $tr\{A\}$ is the trace and the Hamiltonian implicitly includes the term $-\mu N$, where μ is the chemical potential and N is the number of particles and T_τ is Wick's time ordering operator. Wick's time ordering operator orders operators in increasing values of τ, i.e. for a product of operators (of boson or fermion type) a_n:

$$T_\tau(a_1(\tau_1)a_2(\tau_2)\cdots a_m(\tau_m)) = (-1)^p a_{p_1}(\tau_{p_1}) a_{p_2}(\tau_{p_2}) \cdots a_{p_m}(\tau_{p_m}) \qquad : 2.19$$

where

$$\tau_{p_1} > \tau_{p_2} > \cdots > \tau_{p_m} \qquad : 2.20$$

and p is the parity of permutation of fermion operators such that 2.20 is satisfied.

It can be shown that in the range $-\beta<\tau<\beta$ that

$$\hat{G}(\mathbf{k}, \tau+\beta) = -\hat{G}(\mathbf{k}, \tau) \qquad : 2.21$$

This property is used for defining the Green's function outside the range $\tau\in(-\beta,\beta)$ and hence one can write a Fourier representation of the Green's function:

$$\hat{G}(\mathbf{k}, \tau) = \frac{1}{\beta} \sum_{n=-\infty}^{+\infty} e^{-i\omega_n \tau} \hat{G}(\mathbf{k}, i\omega_n) \qquad : 2.22$$

where $\omega_n=(2n+1)\pi/\beta$, $n\in\mathbf{Z}$ are the so called fermion Matsubara frequencies. The Fourier coefficients are given by

$$\hat{G}(\mathbf{k},i\omega_n)=\frac{1}{2}\int_{-\beta}^{+\beta}d\tau e^{i\omega_n\tau}\hat{G}(\mathbf{k},\tau) \quad . \qquad : 2.23$$

Similarly one can define a boson Green's function

$$D_\sigma(\mathbf{k},\tau)=-\left\langle T_\tau\left(b_{\mathbf{k}\sigma}(\tau)b^+_{\mathbf{k}\sigma}(0)\right)\right\rangle \qquad : 2.24$$

where $b_{k\sigma}$ and $b^{\dagger}_{k\sigma}$ are boson operators. The Fourier representation is

$$D_\sigma(\mathbf{k},\tau)=\frac{1}{\beta}\sum_{n=-\infty}^{+\infty}e^{-i\nu_n\tau}D_\sigma(\mathbf{k},i\nu_n) \qquad : 2.25$$

where $\nu_n=2\pi n/\beta$, $n\in\mathbf{Z}$ are the so called boson Matsubara frequencies. Once the Green's function is known one can calculate the physical properties of the system.

A simple case is the system of non-interacting electrons. The Hamiltonian is

$$H=\sum_{\mathbf{k}\sigma}\varepsilon_{\mathbf{k}\sigma}c^+_{\mathbf{k}\sigma}c_{\mathbf{k}\sigma} \qquad : 2.26$$

and then the Green's function is

$$G_\sigma(\mathbf{k},i\omega_n)=\frac{1}{i\omega_n-\varepsilon_{\mathbf{k}\sigma}} \quad . \qquad : 2.27$$

The electronic density of states is given by

$$N_\sigma(\omega)=-\frac{1}{\pi}\sum_{\mathbf{k}}\mathrm{Im}G_\sigma(\mathbf{k},\omega+i0^+) \qquad : 2.28$$

where 0^+ is a positive infinitesimal number. By using Dirac's identity

$$\frac{1}{\omega - x \pm i0^{+}} = \wp\frac{1}{\omega - x} \mp i\pi\delta(\omega - x) \qquad : 2.29$$

where $\omega, x \in \boldsymbol{R}$, $\wp$ denotes the principal part and $\delta(x)$ is the Dirac delta function.

Hence

$$N_{\sigma}(\omega) = \sum_{\mathbf{k}} \delta(\omega - \varepsilon_{\mathbf{k}\sigma}) \qquad : 2.30$$

and by definition this is the density of states.

The superconducting state is conceptually no more difficult. The difference is that the Green's function is generalized and is a 2×2 matrix. It can be represented diagrammatically as shown in Figure 2.3.

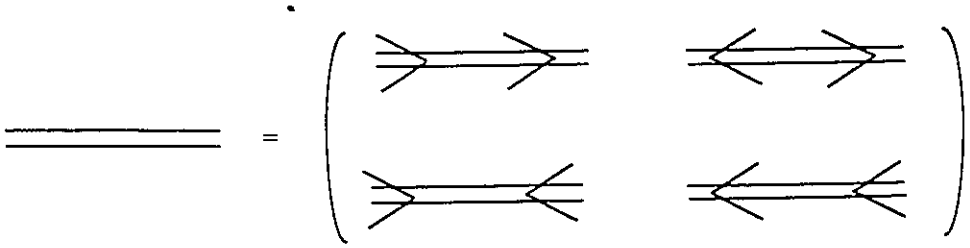

Figure 2.3 Feynman Diagram representation of the superconducting Green's function 2.16 as a 2×2 matrix using the Nambu representation, where the arrows signify the direction in time of the electron.

The Dyson equation for the Green's function is given by

$$\hat{G}^{-1}(\mathbf{k}, i\omega_{n}) = \hat{G}_{0}^{-1}(\mathbf{k}, i\omega_{n}) - \hat{\Sigma}(\mathbf{k}, i\omega_{n}) \qquad : 2.31$$

where $\hat{\Sigma}(\mathbf{k}, i\omega_{n})$ is the self-energy and $\hat{G}_{0}(\mathbf{k}, i\omega_{n})$ is the Green's function calculated in the normal state.

$$\hat{G}_0(\mathbf{k},i\omega_n) = \begin{pmatrix} \dfrac{1}{i\omega_n - \varepsilon_{\mathbf{k}}} & 0 \\ 0 & \dfrac{1}{i\omega_n + \varepsilon_{\mathbf{k}}} \end{pmatrix}$$
$$= \frac{1}{i\omega_n \hat{\tau}_0 - \varepsilon_{\mathbf{k}} \hat{\tau}_3} \qquad : 2.32$$
$$= -\frac{i\omega_n \hat{\tau}_0 + \varepsilon_{\mathbf{k}} \hat{\tau}_3}{\varepsilon_{\mathbf{k}}^2 + \omega_n^2}$$

where the Pauli matrices have been introduced:

$$\hat{\tau}_0 = \begin{pmatrix} 1 & 0 \\ 0 & 1 \end{pmatrix} \quad \hat{\tau}_1 = \begin{pmatrix} 0 & 1 \\ 1 & 0 \end{pmatrix}$$
$$\hat{\tau}_2 = \begin{pmatrix} 0 & -i \\ i & 0 \end{pmatrix} \quad \hat{\tau}_3 = \begin{pmatrix} 1 & 0 \\ 0 & -1 \end{pmatrix} \qquad : 2.33$$

The most general form for the self-energy is

$$\hat{\Sigma}(\mathbf{k},i\omega_n) = i\omega_n\big(1 - Z(\mathbf{k},i\omega_n)\big)\hat{\tau}_0 + \chi(\mathbf{k},i\omega_n)\hat{\tau}_3 + \phi(\mathbf{k},i\omega_n)\hat{\tau}_1 + \overline{\phi}(\mathbf{k},i\omega_n)\hat{\tau}_2 \qquad : 2.34$$

where $Z, \chi, \phi, \overline{\phi}$ are four independent functions to be determined later. Then from the Dyson equation the Green's function can be written

$$\hat{G}^{-1}(\mathbf{k},i\omega_n) = i\omega_n Z(\mathbf{k},i\omega_n)\hat{\tau}_0 - \big(\varepsilon_{\mathbf{k}} + \chi(\mathbf{k},i\omega_n)\big)\hat{\tau}_3 - \phi(\mathbf{k},i\omega_n)\hat{\tau}_1 - \overline{\phi}(\mathbf{k},i\omega_n)\hat{\tau}_2 \qquad : 2.35$$

and hence

$$\hat{G}(\mathbf{k},i\omega_n) = -\frac{i\omega_n Z(\mathbf{k},i\omega_n)\hat{\tau}_0 + \big(\varepsilon_{\mathbf{k}} + \chi(\mathbf{k},i\omega_n)\big)\hat{\tau}_3 + \phi(\mathbf{k},i\omega_n)\hat{\tau}_1 + \overline{\phi}(\mathbf{k},i\omega_n)\hat{\tau}_2}{\big(\omega_n Z(\mathbf{k},i\omega_n)\big)^2 + \big(\varepsilon_{\mathbf{k}} + \chi(\mathbf{k},i\omega_n)\big)^2 + \phi^2(\mathbf{k},i\omega_n) + \overline{\phi}^2(\mathbf{k},i\omega_n)} \qquad : 2.36$$

Since the Green's function is diagonal in the normal state, then ϕ and $\overline{\phi}$ must vanish. It will turn out that ϕ is proportional to the superconducting gap. Also

note that with $\phi = \overline{\phi} = 0$ that the normal state Green's function is obtained if one solves for Z and χ in the normal state.

Now the self-energy can be evaluated and hence $Z, \chi, \phi, \overline{\phi}$ can be determined. Since χ has the effect of renormalizing the energy ε_k, it will be implicitly included in the chemical potential and will be dropped from here on. Also ϕ and $\overline{\phi}$ will satisfy identical equations, thus ϕ and $\overline{\phi}$ are equal up to a proportionality factor and any solution that preserves $\phi^2 + \overline{\phi}^2$ will be valid. Hence there are solutions $(\phi, \overline{\phi}) = (\phi_0 \cos 2\alpha, \phi_0 \sin 2\alpha)$, where 2α is an arbitrary phase. Since physical observables can't depend on the phase and since BCS theory breaks gauge symmetry, α can be set equal to zero and hence $\overline{\phi} = 0$.

2.2.1. The Electron-Boson Interaction

The most important contribution to the self-energy is the electron-boson interaction since this is the driving mechanism for superconductivity. For conventional superconductors the bosons which mediate the superconductivity are phonons. For a superconducting state stabilized by anti-ferromagnetic spin fluctuations, the electron-boson interaction is given by (Millis *et al.*, 1988; Monthoux *et al.*, 1991 and 1992; Monthoux and Pines, 1993)

$$H_{sf} = \sum_{\mathbf{kk'}} V_{\mathbf{kk}} \left[S_z(\mathbf{k}-\mathbf{k}')\Psi^+_{\mathbf{k}'}\hat{\tau}_0\Psi_{\mathbf{k}} + S_+(\mathbf{k}-\mathbf{k}')\Psi^+_{\mathbf{k}'}\hat{\tau}_-\Psi_{\mathbf{k}} + S_+(\mathbf{k}-\mathbf{k}')\Psi^+_{\mathbf{k}'}\hat{\tau}_+\Psi_{\mathbf{k}} \right] \quad : 2.37$$

where S(q) is the spin fluctuation operator ($S_\pm(\mathbf{q}) = S_x(\mathbf{q}) \pm i\, S_y(\mathbf{q})$) with components ($S_x$, S_y, S_z) and whose properties are determined by the spin-spin correlation function $\chi_{ij}(\mathbf{q},\omega)$, $\hat{\tau}_\pm = \frac{1}{2}\left(\hat{\tau}_1 \pm i\hat{\tau}_2\right)$ and $V_{\mathbf{kk}}$ is the interaction matrix element.

For conventional superconductors the electron-phonon interaction is given by

$$H_{e-p} = \sum_{\mathbf{kq}\sigma\alpha} \left\langle \mathbf{k}+\mathbf{q}|\vec{\nabla}_\alpha V|\mathbf{k}\right\rangle u_{\mathbf{q}\alpha}\Psi^+_{\mathbf{k}+\mathbf{q}}\hat{\tau}_3\Psi_{\mathbf{k}} \quad : 2.38$$

where $\left\langle \mathbf{k}+\mathbf{q}|\vec{\nabla}_\alpha V|\mathbf{k}\right\rangle$ is the matrix element scattering electrons from an atom displaced by an infinitesimal amount, and

$$u_{\mathbf{q}\alpha} = \sum_i \left(2NM\omega_{\mathbf{q}i}\right)^{-1/2} \varepsilon_{\mathbf{q}i}\left(b_{\mathbf{q}i} + b^+_{\mathbf{q}i}\right) \quad : 2.39$$

is the displacement operator, with N= the number of atoms, M is the mass of the atom, $\omega_{\mathbf{q}i}$ is the phonon dispersion of branch i, $\varepsilon_{\mathbf{q}i}$ is the polarization and $b_{\mathbf{q}i}$ ($b^*_{\mathbf{q}i}$) destroys (creates) a phonon with momentum q in branch i. This system of electrons interacting with phonons (Frölich, 1952) is the basis for conventional superconductivity for both the BCS and Eliashberg theories. Migdal (1958) showed that the dominant contribution to the electronic self-energy due to phonons comes from the lowest order Feynman diagram (Figure 2.4) where the wavy line is the phonon propagator and the solid line is the electron propagator.

Figure 2.4 Lowest order contribution the electronic self-energy from the electron-phonon interaction. The wavy line is the phonon propagator and the solid line is the electron propagator.

This is due to the fact that the ions in a crystal are much more massive than the electrons and hence the response of the ions to the electrons is very small and this leads to an electron-phonon interaction that is of the order of $(m/M)^{1/2}$ where m is the electron mass and M is the ion mass. This ratio is small and hence in higher orders of perturbation the contribution is smaller and smaller and hence the lowest order term is dominant. In systems where the dimension is less than three it is possible that Migdal's theorem breaks down (Kostur and Mitrovic, 1993; Hirsch and Fradkin, 1982; Allen and Mitrovic, 1982) and hence it is not reasonable to retain only the lowest order contribution. There is no corresponding theorem to Migdal's for electron-spin fluctuation interactions, however it will be assumed that there is a similar result and only the lowest order diagram will be calculated and retained.

Within this approximation, the lowest order electronic self-energy due to the interactions with spin-fluctuations is

$$\hat{\Sigma}_{sf}(\mathbf{k},i\omega_n) = T\sum_{\mathbf{k}m}\int_0^\infty d\Omega \frac{I^2\chi(\mathbf{k},\mathbf{k}';\Omega)}{N(4t)}\frac{2\Omega}{\nu_m^2+\Omega^2}\hat{\tau}_0\hat{G}(\mathbf{k}',i\omega_n-i\nu_m)\hat{\tau}_0 \qquad : 2.40$$

where I is an interaction constant and $N(4t)=(4\pi t)^{-1/2}$ is the density of states at the band edge.

2.2.2. The Coulomb Interaction

There is a Coulomb interaction between electrons. Due to the absence of any small parameter it is not possible to deal with this interaction in a perturbative manner satisfactorily. This Hamiltonian is given by

$$H_C = \sum_{\mathbf{k}\mathbf{k}'} \frac{4\pi e^2}{(\mathbf{k}-\mathbf{k}')^2} \rho^+_{\mathbf{k}+\mathbf{k}'} \rho_{\mathbf{k}+\mathbf{k}'} \qquad : 2.41$$

where $\rho_{\mathbf{k}}$ is the Fourier transform of the electron density operator,

$$\rho_{\mathbf{k}} = \sum_{\mathbf{q}\mathbf{q}'} \langle \mathbf{q}' | e^{-i\mathbf{k}\cdot\mathbf{r}} | \mathbf{q} \rangle \Psi^+_{\mathbf{q}'} \hat{\tau}_3 \Psi_{\mathbf{q}} \quad . \qquad : 2.42$$

The Coulomb interaction is repulsive and thus inhibits the formation of the superconducting state. As long as it does not overcome the attractive electron-boson interaction then the superconducting state will form and the Coulomb interaction is less important. This is due to the formation of a condensate of Cooper pairs and thus the electrons in a pair do not come in close contact with one another. Within the Hartree-Fock approximation the contribution to the electronic self-energy in the superconducting state can be written

$$\hat{\Sigma}_C(\mathbf{k}, i\omega_n) = -T \sum_{\mathbf{k}\mathbf{k}'n'} \mu^*_{\mathbf{k}\mathbf{k}'}(\omega_c)\theta(\omega_c - |\omega_{n'}|)\hat{\tau}_3 \hat{G}^{od}(\mathbf{k}', i\omega_{n'})\hat{\tau}_3 \qquad : 2.43$$

where $\theta(x)$ is the Heaviside step function

$$\theta(x) = \begin{cases} 1 & x \geq 0 \\ 0 & x < 0 \end{cases} , \qquad : 2.44$$

$\hat{G}^{od}$ is the Green's function with the diagonal terms set equal to zero and μ^* is a parameter representing the Coulomb interaction. μ^* is called the Coulomb (or Morel-Anderson) pseudopotential. In the constant density of states approximation, ignoring any anisotropy,

$$\mu^*(\omega_c) = \frac{\mu_c(E_F)}{1 + \mu_c(E_F) \ln \frac{E_F}{\omega_c}} \qquad : 2.45$$

where $\mu_c(E_F)$ is an average Coulomb repulsion for electrons at the Fermi surface and ω_c is a cutoff frequency typically of the order of the maximum boson frequency. It is then possible to fit the parameter $\mu_c(E_F)$ to experiment by tunneling (Galkin *et al.*, 1974; McMillan and Rowell, 1969).

2.2.3. The Impurity Scattering Interaction

Electron Scattering from impurities can also be included. Here only scattering from nonmagnetic (normal) impurities will be considered. The Hamiltonian in Nambu notation is

$$H_I = n_I \sum_{\mathbf{k}\mathbf{k}'} \langle \mathbf{k}' | V_I | \mathbf{k} \rangle \Psi_{\mathbf{k}'}^{\dagger} \hat{\tau}_3 \Psi_{\mathbf{k}} \qquad : 2.46$$

where V_I is the interaction strength and n_I is the concentration of impurities. The electronic self-energy will be calculated in the T-matrix expansion (Hirschfeld *et al.*, 1986 and 1988). The self-energy for the single impurity site approximation is given by

$$\hat{\Sigma}_I(\mathbf{k},i\omega_n) = n_I \hat{T}(\mathbf{k},\mathbf{k};i\omega_n) \qquad : 2.47$$

where $\hat{T}(\mathbf{k},\mathbf{k}';i\omega_n)$ is the T-matrix which obeys the equation

$$\hat{T}(\mathbf{k},\mathbf{k}';i\omega_n) = V_I(\mathbf{k},\mathbf{k}')\hat{\tau}_3 + \sum_{\mathbf{k}''} V_I(\mathbf{k},\mathbf{k}'')\hat{\tau}_3 \hat{G}(\mathbf{k}'',i\omega_n)\hat{T}(\mathbf{k}'',\mathbf{k}';i\omega_n) \qquad : 2.48$$

where $V_I(\mathbf{k},\mathbf{k}') = \langle \mathbf{k}'|V_I|\mathbf{k}\rangle$. The T-matrix expansion is shown diagrammatically in Figure 2.5.

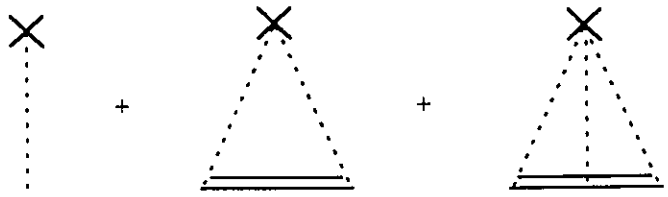

Figure 2.5 Feynman diagrams for the T-matrix expansion. Here the dashed line is the interaction with the impurity.

By taking $V_I(\mathbf{k},\mathbf{k}')$ to be constant, $V_I = V_I(\mathbf{k},\mathbf{k}')$, then the T-matrix is independent of momentum, hence

$$\hat{T}(i\omega_n) = V_I\hat{\tau}_3 + V_I\hat{\tau}_3 \sum_{\mathbf{k}} \hat{G}(\mathbf{k},i\omega_n)\hat{T}(i\omega_n) \qquad : 2.49$$

or

$$\left(\hat{\tau}_0 - V_I \hat{\tau}_3 \hat{\overline{G}}(i\omega_n)\right)\hat{T}(i\omega_n) = V_I \hat{\tau}_3 \qquad : 2.50$$

where

$$\hat{\overline{G}}(i\omega_n) = \sum_{\mathbf{k}} \hat{G}(\mathbf{k}, i\omega_n) \quad . \qquad : 2.51$$

Solving for the T-matrix then gives

$$\hat{T}(i\omega_n) = \frac{V_I}{\left[1 - V_I \overline{G}_{11}(i\omega_n)\right]\left[1 + V_I \overline{G}_{22}(i\omega_n)\right] + V_I^2 \overline{G}_{21}(i\omega_n)\overline{G}_{12}(i\omega_n)} \times \begin{pmatrix} 1 + V_I \overline{G}_{22}(i\omega_n) & -V_I \overline{G}_{12}(i\omega_n) \\ -V_I \overline{G}_{21}(i\omega_n) & -1 + V_I \overline{G}_{11}(i\omega_n) \end{pmatrix} \qquad : 2.52$$

where $\overline{G}_{ij}(i\omega_n)$ denotes the ijth element of $\hat{\overline{G}}(i\omega_n)$. By symmetry of the Green's function (eq:2.36):

$$\hat{T}(i\omega_n) = \frac{-i\Omega(i\omega_n)\hat{\tau}_0 + D(i\omega_n)\hat{\tau}_1}{V_I^{-2} + \Omega^2(i\omega_n) + D^2(i\omega_n)} \qquad : 2.53$$

where

$$\Omega(i\omega_n) = \sum_{\mathbf{k}} \frac{\tilde{\omega}_{\mathbf{k}}(i\omega_n)}{\varepsilon_{\mathbf{k}}^2 + \tilde{\omega}_{\mathbf{k}}^2(i\omega_n) + \phi_{\mathbf{k}}^2(i\omega_n)} \qquad : 2.54$$

$$D(i\omega_n) = \sum_{\mathbf{k}} \frac{\phi_{\mathbf{k}}(i\omega_n)}{\varepsilon_{\mathbf{k}}^2 + \tilde{\omega}_{\mathbf{k}}^2(i\omega_n) + \phi_{\mathbf{k}}^2(i\omega_n)} \qquad : 2.55$$

and where the renormalized Matsubara frequencies have been introduced,

$$\tilde{\omega}_{\mathbf{k}}(i\omega_n) = \omega_n Z(i\omega_n) \quad . \qquad : 2.56$$

The term proportional to $\hat{\tau}_3$ has been absorbed into χ and hence absorbed into the chemical potential. The electronic self-energy due to scattering from impurities is

$$\hat{\Sigma}_I(i\omega_n) = n_I \frac{-i\Omega(i\omega_n)\hat{\tau}_0 + D(i\omega_n)\hat{\tau}_1}{V_I^{-2} + \Omega^2(i\omega_n) + D^2(i\omega_n)} \quad . \qquad : 2.57$$

Impurity scattering in the Born approximation can be found by taking the limit of weak scattering ($V_I \to 0$) in 2.57. The electron self-energy in the Born approximation is

$$\hat{\Sigma}_I^{(Born)}(i\omega_n) = n_I V_I^2 \left(-i\Omega(i\omega_n)\hat{\tau}_0 + D(i\omega_n)\hat{\tau}_1\right) \quad . \qquad : 2.58$$

For unitary scattering one takes the opposite limit of the strongest possible scattering ($V_I \to \infty$) thus giving

$$\hat{\Sigma}_I^{(unitary)}(i\omega_n) = n_I \frac{-i\Omega(i\omega_n)\hat{\tau}_0 + D(i\omega_n)\hat{\tau}_1}{\Omega^2(i\omega_n) + D^2(i\omega_n)} \quad . \qquad : 2.59$$

2.2.4. The Eliashberg Equations

Summarizing each contribution to the electron self-energy (eq's: 2.40, 2.43, 2.57):

$$\hat{\Sigma}_{sf}(\mathbf{k}, i\omega_n) = T\sum_{\mathbf{k}n'} \lambda_{\mathbf{k}\mathbf{k}'}(\omega_n - \omega_{n'})\hat{\tau}_0 \hat{G}(\mathbf{k}', i\omega_{n'})\hat{\tau}_0 \qquad : 2.60$$

$$\hat{\Sigma}_C(\mathbf{k}, i\omega_n) = -T\sum_{\mathbf{k}\mathbf{k}'n'} \mu^*_{\mathbf{k}\mathbf{k}'}(\omega_c)\theta(\omega_c - |\omega_{n'}|)\hat{\tau}_3 \hat{G}^{od}(\mathbf{k}', i\omega_{n'})\hat{\tau}_3 \qquad : 2.61$$

$$\hat{\Sigma}_I(i\omega_n) = n_I \frac{-i\Omega(i\omega_n)\hat{\tau}_0 + D(i\omega_n)\hat{\tau}_1}{\Omega^2(i\omega_n) + D^2(i\omega_n)} \qquad : 2.62$$

thus giving the total self-energy,

$$\hat{\Sigma}(\mathbf{k}, i\omega_n) = \hat{\Sigma}_{sf}(\mathbf{k}, i\omega_n) + \hat{\Sigma}_C(\mathbf{k}, i\omega_n) + \hat{\Sigma}_I(\mathbf{k}, i\omega_n) \qquad : 2.63$$

where

$$\lambda_{\mathbf{k}\mathbf{k}'}(\nu_m) = \frac{1}{N(4t)} \int_0^\infty d\Omega \frac{2\Omega I^2 \chi(\mathbf{k},\mathbf{k}';\Omega)}{\nu_m^2 + \Omega^2} \quad . \qquad : 2.64$$

With $\hat{G}(\mathbf{k}, i\omega_n)$ given by 2.36 and by comparing eq's 2.60, 2.61, 2.62, 2.63 with 2.34 then expressions for Z and ϕ can be extracted by examining the coefficients of $\hat{\tau}_0$ and $\hat{\tau}_1$ respectively:

$$\tilde{\omega}_{\mathbf{k}}(\omega_n) = \omega_n + T\sum_{\mathbf{k}'n'} \lambda_{\mathbf{k}\mathbf{k}'}(\omega_n - \omega_{n'})\Omega_{\mathbf{k}'}(\omega_{n'}) + n_I \frac{\Omega(\omega_n)}{V_I^{-2} + \Omega^2(\omega_n) + D^2(\omega_n)} \qquad : 2.65$$

$$\phi_{\mathbf{k}}(\omega_n) = -T\sum_{\mathbf{k}'n'} \left[\lambda_{\mathbf{k}\mathbf{k}'}(\omega_n - \omega_{n'}) + \mu^*(\omega_c)\theta(\omega_c - |\omega_m|)\right] D_{\mathbf{k}'}(\omega_{n'}) + n_I \frac{D(\omega_n)}{V_I^{-2} + \Omega^2(\omega_n) + D^2(\omega_n)} \qquad : 2.66$$

where

$$\Omega_{\mathbf{k}}(\omega_n) = \frac{\tilde{\omega}_{\mathbf{k}}(\omega_n)}{\varepsilon_{\mathbf{k}}^2 + \tilde{\omega}_{\mathbf{k}}^2(\omega_n) + \phi_{\mathbf{k}}^2(\omega_n)} \qquad : 2.67$$

$$D_{\mathbf{k}}(\omega_n) = \frac{\phi_{\mathbf{k}}(\omega_n)}{\varepsilon_{\mathbf{k}}^2 + \tilde{\omega}_{\mathbf{k}}^2(\omega_n) + \phi_{\mathbf{k}}^2(\omega_n)} \qquad : 2.68$$

$$\Omega(\omega_n) = \sum_{\mathbf{k}} \Omega_{\mathbf{k}}(\omega_n) \qquad : 2.69$$

$$D(\omega_n) = \sum_{\mathbf{k}} D_{\mathbf{k}}(\omega_n) \quad . \qquad : 2.70$$

The eq`s 2.65 and 2.66 are the Eliashberg equations for a superconductor stabilized by anti-ferromagnetic spin fluctuations. They are a pair of coupled integral equations describing the superconducting state which is characterized by

$Z(\mathbf{k},i\omega_n)$ the renormaliztion and the superconducting gap $\Delta(\mathbf{k},i\omega_n)=$ $Z(\mathbf{k},i\omega_n)\phi(\mathbf{k},i\omega_n)$. In deriving these equations the usual approximation of a constant density of states has been avoided and thus the effect of different band structures along with the details of the band structure can be examined and thus the van Hove singularity in the density of states can be accounted for fully. Also note that these equations are valid for arbitrary momentum dependence of the electronic interactions and thus this effect can also be studied.

2.2.5. The Padé Approximation

Equations 2.65 and 2.66 are the Eliashberg equations defined on the imaginary frequency axis. The two quantities $Z(\mathbf{k},i\omega_n)$ and $\phi(\mathbf{k},i\omega_n)$ are real functions defined at the points $i\omega_n$. For thermodynamic properties it is sufficient to have knowledge of $Z(\mathbf{k},i\omega_n)$ and $\phi(\mathbf{k},i\omega_n)$ defined on the imaginary axis, thus solution of 2.65 and 2.66 determines the thermodynamic properties. Some properties, such as transport properties require knowledge of $Z(\mathbf{k},i\omega_n)$ and $\phi(\mathbf{k},i\omega_n)$ defined on the real frequency axis. This can be accomplished by analytically continuing $Z(\mathbf{k},i\omega_n)$ and $\phi(\mathbf{k},i\omega_n)$ to the real axis by taking $i\omega_n \rightarrow \omega+i0^+$ after the Matsubara frequency summations have been performed. This is guaranteed to be the correct continuation by the Baym-Mermin Theorem(1961).

Then one obtains a pair of coupled integral equations for the now complex functions $Z(\mathbf{k},\omega)$ and $\phi(\mathbf{k},\omega)$. These equations involve principal part integrations and hence are much more difficult to solve than the imaginary axis equations. It is possible to perform the principal part integration analytically (Marsiglio *et al.*, 1988) but one is still left with more complex equations than the imaginary axis equations. One still needs to know the solution of the imaginary axis equations.

Another possibility of acquiring the solutions of $Z(\mathbf{k},i\omega_n)$ and $\phi(\mathbf{k},i\omega_n)$ on the real frequency axis is by means of Padé approximants (Vidberg and Serene, 1977; Leavens and Richie, 1985; Blashke and Blocksdorf, 1982). The Padé approximation continues a function known on a discrete set of points to one known on a continuous set. The algorithm for the approximation is as follows. Given a function with values u_i at N complex points z_i ($i=1,\ldots,N$), define the continued fraction

$$C_N(z) = \cfrac{a_1}{1+\cfrac{a_2(z-z_1)}{1+\cfrac{a_3(z-z_3)}{\vdots \\ 1+\cfrac{a_n(z-z_n)}{1}}}} \qquad : 2.71$$

where the coefficients a_i are determined such that

$$C_N(z_i) = u_i \quad i = 1,\ldots,N \quad . \qquad : 2.72$$

Then the coefficients are given by the recursion relation

$$a_i = g_i(z_i)\ ,\ \ g_1(z_i) = u_i\ ,\ \ i = 1,\ldots,N\ ,$$

$$g_p(z) = \frac{g_{p-1}(z_{p-1}) - g_{p-1}(z)}{(z - z_{p-1})g_{p-1}(z)}\ ,\ \ p \geq 2 \quad . \qquad : 2.73$$

This gives

$$C_N(z) = \frac{A_N(z)}{B_N(z)} \qquad : 2.74$$

where $A_N(z)$ and $B_N(z)$ are given by the recursion relations

$$A_{n+1}(z) = A_n(z) + (z - z_n)a_n A_{n-1}(z)$$

$$B_{n+1}(z) = B_n(z) + (z - z_n)a_n B_{n-1}(z) \qquad : 2.75$$

$$A_0 = 0\ ,\ \ A_1 = a_1\ ,\ \ B_0 = B_1 = 1 \quad .$$

This gives an N-point Padé approximation to the function u. The Padé approximation technique is most reliable when the frequency and temperature are small, i.e. in the region $\omega << \Omega_{max}$ and $T << T_c$ where Ω_{max} is the maximum boson frequency. In this region there is excellent agreement between the Padé approximation to the imaginary axis solutions and numerical solutions of the real axis Eliashberg equations. The advantage is that the Padé approximation combined with the solution of the imaginary axis Eliashberg equations is much faster than a direct solution of the real axis Eliashberg equations. The disadvantage is that this is an approximation and the effect of this will be discussed later.

2.2.6. The T_c Equations

The critical temperature T_c, can be found from the Eliashberg equations. Since in the normal state $\phi=0$ and below T_c, $\phi\neq 0$, then just below T_c one linearizes the Eliashberg equations to first order in ϕ. This gives

$$\tilde{\omega}_{\mathbf{k}}(\omega_n) = \omega_n + T\sum_{\mathbf{k}'n'} \lambda_{\mathbf{k}\mathbf{k}'}(\omega_n - \omega_{n'})\Omega_{\mathbf{k}'}(\omega_{n'})\big|_{T_c} + n_I \frac{\Omega(\omega_n)\big|_{T_c}}{V_I^{-2} + \Omega^2(\omega_n)\big|_{T_c}} \qquad : 2.76$$

$$\phi_{\mathbf{k}}(\omega_n) = -T\sum_{\mathbf{k}'n'}\left[\lambda_{\mathbf{k}\mathbf{k}'}(\omega_n - \omega_{n'}) + \mu^*(\omega_c)\theta(\omega_c - |\omega_m|)\right]D_{\mathbf{k}'}(\omega_{n'})\big|_{T_c} + n_I \frac{D(\omega_n)\big|_{T_c}}{V_I^{-2} + \Omega^2(\omega_n)\big|_{T_c}} \qquad : 2.77$$

where

$$\Omega_{\mathbf{k}}(\omega_n)\big|_{T_c} = \frac{\tilde{\omega}_{\mathbf{k}}(\omega_n)}{\varepsilon_{\mathbf{k}}^2 + \tilde{\omega}_{\mathbf{k}}^2(\omega_n)} \qquad : 2.78$$

$$D_{\mathbf{k}}(\omega_n)\big|_{T_c} = \frac{\phi_{\mathbf{k}}(\omega_n)}{\varepsilon_{\mathbf{k}}^2 + \tilde{\omega}_{\mathbf{k}}^2(\omega_n)} \qquad : 2.79$$

and similar definitions to 2-69 and 2-79 for $\Omega(\omega_n)\,|_{T_c}$ and $D(\omega_n)\,|_{T_c}$. All temperatures are at $T=T_c$. Once T_c has been calcuiated, Z and ϕ can be calculated (and hence the Green's function) for any temperature below T_c. The superconducting state is then, in principle, completely characterized. The catch is that the equations all must be solved numerically except for the very simplest of cases.

A solution of the Eliashberg equations always exists. It is a solution with $\phi(\mathbf{k}, i\omega_n)=0$ and thus describes the normal state. With $\phi=0$ the equation describing the normal state is

$$\tilde{\omega}_{\mathbf{k}}^{N}(\omega_n) = \omega_n + T\sum_{\mathbf{k}'n'} \lambda_{\mathbf{k}\mathbf{k}'}(\omega_n - \omega_{n'})\Omega_{\mathbf{k}'}^{N}(\omega_{n'}) + n_I \frac{\Omega^N(\omega_n)}{V_I^{-2} + \Omega^{N^2}(\omega_n)} \qquad : 2.80$$

where

$$\Omega^N(\omega_n) = \sum_{\mathbf{k}} \Omega_{\mathbf{k}}^{N}(\omega_n) = \sum_{\mathbf{k}} \frac{\tilde{\omega}_{\mathbf{k}}^{N}(\omega_n)}{\varepsilon^2 + \tilde{\omega}_{\mathbf{k}}^{N^2}(\omega_n)} \quad . \qquad : 2.81$$

Thus the normal state is described by this single integral equation, where the superscript N signifies that the quantity is calculated in the normal state.

2.3. *The d-wave Eliashberg Equations*

2.3.1. The Boson Spectrum

If one knows the form of the boson spectrum $I^2\chi(\mathbf{k},\mathbf{k}';\Omega)$, and hence $\lambda_{\mathbf{k}\mathbf{k}'}$, T_c can be calculated from a completely microscopic basis. For the electron-phonon interaction it is possible to calculate the phonon spectrum (called $\alpha^2F(\mathbf{k},\mathbf{k}';\Omega)$ for the case of phonons) from first principles (Grimvall, 1981). Excellent agreement

between the calculation and the experimentally determined phonon spectrum is obtained (Carbotte, 1990). A more fruitful method of obtaining the phonon spectrum is by so called tunneling inversion (McMillan and Rowell, 1965 and 1969). This involves choosing an initial guess for $\alpha^2F(\mathbf{k},\mathbf{k}';\Omega)$ and $\mu^*_{\mathbf{k}\mathbf{k}'}$, then solving the real axis Eliashberg equations at zero temperature and calculating the superconducting density of states. This is then compared to the density of states obtained by tunneling experiments and then a second guess of $\alpha^2F(\mathbf{k},\mathbf{k}';\Omega)$ and $\mu^*_{\mathbf{k}\mathbf{k}'}$ is found and the density of states is recalculated from scratch. This is continued until the choice of $\alpha^2F(\mathbf{k},\mathbf{k}';\Omega)$ and $\mu^*_{\mathbf{k}\mathbf{k}'}$ lead to a density of states which matches with the experimentally found density of states. This method gives both the phonon spectrum and the Coulomb pseudopotential, and then all the other properties for a specific material can be calculated.

As of yet for the electron-spin fluctuation interaction there is no satisfactory method to calculate the spin fluctuation spectrum $I^2\chi(\mathbf{k},\mathbf{k}';\Omega)$. Millis, Monien and Pines (1990) have developed a phenomenological model for $I^2\chi(\mathbf{k},\mathbf{k}';\Omega)$ based on NMR data. Solution of the superconducting state in the weak coupling limit leads directly to a gap with $d_{x^2-y^2}$ symmetry (Monthoux *et al.*, 1992). Here $d_{x^2-y^2}$ symmetry signifies a superconducting state with spin singlet pairing (as in BCS theory) and a symmetry such that the gap changes sign as one travels along the Fermi surface. For example Monthoux *et al.* (1992) find a gap of the form

$$\Delta(\mathbf{k}) = \Delta_0\left(\cos k_x - \cos k_y\right) \quad . \qquad : 2.82$$

The key feature of this gap is that it goes to zero along the lines $k_x = \pm k_y$. Thus the gap goes to zero at four points on the Fermi surface which leads to excitations of infinitesimally small energy as opposed to a gap which is positive everywhere and thus there is a gap in the excitation spectrum in all directions in k-space. This leads to a power law temperature dependence of properties which depend on the quasi-particle energy as opposed to exponentially activated behavior as in BCS theory at low temperatures. Examples include the electronic specific heat which goes as $e^{-\gamma T}$ for BCS superconductors and as T^2 for superconductors in which the gap goes to zero at points on the Fermi surface (Schachinger and Carbotte, 1991), and a power law temperature dependence is also seen for the London penetration depth (Prohammer and Carbotte, 1991). These d-wave calculations have been done for a constant density of states and a spherical Fermi surface in relevance to the heavy fermion superconductors.

2.3.2. The $d_{x^2-y^2}$ Symmetry Expansion

The interest in the present work is not in the microscopic basis of the electron-spin fluctuation interaction but in the consequences of a gap with $d_{x^2-y^2}$

symmetry within this 2-dimensional model. For simplicity a separable model (Clem, 1966) in momentum and frequency is taken for $I^2\chi(\mathbf{k},\mathbf{k}';\Omega)$,i.e.

$$I^2\chi(\mathbf{k},\mathbf{k}';\Omega) = I^2\chi_0(\mathbf{k},\mathbf{k}')\Phi(\Omega) \quad . \qquad : 2.83$$

Now the momentum dependence comes in via the separate function $\chi_0(\mathbf{k},\mathbf{k}')$. To examine the momentum dependence $\chi_0(\mathbf{k},\mathbf{k}')$ is expanded as

$$\chi_0(\mathbf{k},\mathbf{k}') = \chi_0\left(1 - g\eta(\mathbf{k})\eta(\mathbf{k}')\right) \qquad : 2.84$$

where all the momentum dependence is in the functions $\eta(\mathbf{k})$ which have $d_{x^2-y^2}$ symmetry, g is a parameter representing the strength of the d-wave superconductivity ($g=0$ is no d-wave superconductivity and $g=1$ is pure d-wave superconductivity, no s-wave contribution). A complete representation of a gap with $d_{x^2-y^2}$ symmetry relevant to the high T_c oxides has been enumerated by Wenger and Östlund (1993) using group theoretical techniques. The result for two dimensions is

$$\Delta_{\mathbf{k}} = \sum_{r_1=1}^{\infty}\sum_{r_2=0}^{r_1-1} a_{r_1 r_2}\left(\cos k_x r_1 \cos k_y r_2 - \cos k_x r_2 \cos k_y r_1\right) \qquad : 2.85$$

where $a_{r_1 r_2}$ are arbitrary constants. Thus in general for $\eta(\mathbf{k})$ choose:

$$\eta(\mathbf{k}) = \sum_{r_1=1}^{\infty}\sum_{r_2=0}^{r_1-1} a_{r_1 r_2}\left(\cos k_x r_1 \cos k_y r_2 - \cos k_x r_2 \cos k_y r_1\right) \qquad : 2.86$$

with the coefficients chosen such that $\eta(\mathbf{k})$ is normalized to unity. Equation 2.86 can be rewritten as

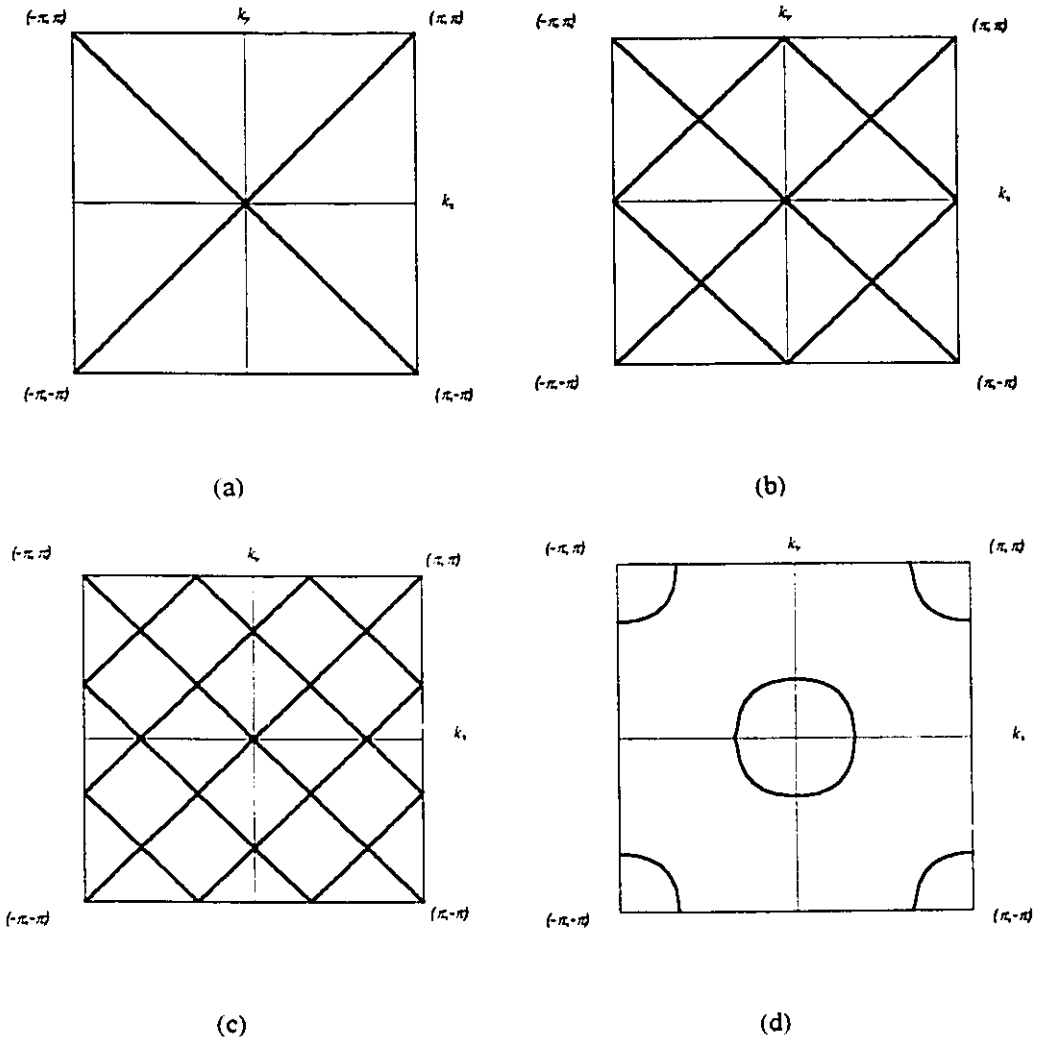

Figure 2.6 The zeros (dark solid lines) in the first Brillouin zone of the first few terms in the $d_{x^2-y^2}$ expansion for the superconducting gap. Solution of (a) $\eta_{10}(k)=0$; (b) $\eta_{20}(k)=0$;(c) $\eta_{30}(k)=0$;(d) $\eta_{21}(k)=0$.

$$\eta(\mathbf{k}) = \sum_{r_1=1}^{\infty}\sum_{r_2=0}^{r_1-1} a_{r_1 r_2}\eta_{r_1 r_2}(\mathbf{k}) \qquad : 2.87$$

$$\eta_{pq}(\mathbf{k}) = \cos pk_x \cos qk_y - \cos qk_x \cos pk_y \quad .$$

It is interesting to examine the first few terms of 2.87 to determine where in the Brillouin zone they go to zero, and how and where they cross the Fermi surface. This information will give the temperature dependence in the observed properties:

$$\eta_{10}(\mathbf{k}) = \cos k_x - \cos k_y \qquad : 2.88$$

$$\eta_{20}(\mathbf{k}) = \cos 2k_x - \cos 2k_y = 2\left(\cos k_x + \cos k_y\right)\left(\cos k_x - \cos k_y\right) \qquad : 2.89$$

$$\eta_{21}(\mathbf{k}) = \cos 2k_x \cos k_y - \cos k_x \cos 2k_y \qquad : 2.90$$

$$\eta_{30}(\mathbf{k}) = \cos 3k_x - \cos 3k_y \qquad : 2.91$$

$$\eta_{31}(\mathbf{k}) = \cos 3k_x \cos k_y - \cos k_x \cos 3k_y \qquad : 2.92$$

$$\eta_{32}(\mathbf{k}) = \cos 3k_x \cos 2k_y - \cos 2k_x \cos 3k_y \qquad : 2.93$$

$$\eta_{40}(\mathbf{k}) = \cos 4k_x - \cos 4k_y \qquad : 2.94$$

and so on. η_{10} is the usual term taken for a gap with $d_{x^2-y^2}$ symmetry in the literature. It has zeros along $k_x=\pm k_y$ as shown in Figure 2.6. Comparing this with the Fermi surfaces in Figure 2.1 it can be seen that the gap goes to zero at points on the Fermi surface for any values of μ and B. η_{20} has zeros as shown in Figure 2.6. The point here is that for the special case of $B=0$ and $\mu=0$ the gap is zero everywhere on the Fermi surface and goes to zero at points for any other values of μ and B. Shown in Figure 2.6 are the zeros of η_{30} and again as with η_{10} the gap goes to zero at points on the Fermi surface however it goes to zero at more points. Shown in Figure 2.6 are the zeros of η_{21}. Here the gap will go to zero only at

points on the Fermi surface with the exception that it is everywhere on the Fermi surface when the lines of zero coincide with Fermi surface for a particular μ and B. This type of behavior continues for each term in the expansion 2.87; i.e. η_{pq} has zeros at points on the Fermi surface when p is an odd integer and has zeros also at points on the Fermi surface when p is an even integer with the possibility of being zero everywhere on the Fermi surface for a particular choice of the chemical potential and next nearest neighbor hopping strength. In both cases the number of points where the zeros of η_{pq} cross the Fermi surface increases as p increases.

2.3.3. The $d_{x^2-y^2}$ Eliashberg Equations

Once the expansion for the spin fluctuation spectrum has been made as in 2.84, it can be substituted into the Eliashberg equations 2.65 and 2.66, hence obtaining the Eliashberg equations appropriate for a d-wave superconductor:

$$\tilde{\omega}_0(\omega_n) = \omega_n + T\sum_{n'} \lambda(\omega_n - \omega_{n'})\Omega_0(\omega_{n'}) + n_I \frac{\Omega_0(\omega_n)}{V_I^{-2} + \Omega_0^2(\omega_n) + D_0^2(\omega_n)} \qquad : 2.95$$

$$\tilde{\omega}_j(\omega_n) = -gT\sum_{n'} \lambda(\omega_n - \omega_{n'})\Omega_j(\omega_{n'}) \ , \ j > 0 \qquad : 2.96$$

$$\phi_0(\omega_n) = -T\sum_{n'}\left[\lambda(\omega_n - \omega_{n'}) + \mu^*(\omega_c)\theta(\omega_c - |\omega_{n'}|)\right]D_0(\omega_{n'}) + n_I \frac{D_0(\omega_n)}{V_I^{-2} + \Omega_0^2(\omega_n) + D_0^2(\omega_n)} \qquad : 2.97$$

$$\phi_j(\omega_n) = gT\sum_{n'} \lambda(\omega_n - \omega_{n'})D_j(\omega_{n'}) \ , \ j > 0 \quad . \qquad : 2.98$$

Here the functions have been expanded in terms of $\eta(\mathbf{k})$ as

$$\begin{aligned} \tilde{\omega}_{\mathbf{k}}(\omega_n) &= \sum_j \tilde{\omega}_j(\omega_n)\eta_j(\mathbf{k}) \\ \phi_{\mathbf{k}}(\omega_n) &= \sum_j \phi_j(\omega_n)\eta_j(\mathbf{k}) \end{aligned} \qquad : 2.99$$

and $\mu^*_{kk'}$ has been taken to be isotropic ($=\mu^*$),

$$\begin{aligned} \Omega_j(\omega_n) &= \sum_{\mathbf{k}} \frac{\tilde{\omega}_{\mathbf{k}}(\omega_n)\eta_j(\mathbf{k})}{\varepsilon_{\mathbf{k}}^2 + \tilde{\omega}_{\mathbf{k}}^2(\omega_n) + \phi_{\mathbf{k}}^2(\omega_n)} \\ D_j(\omega_n) &= \sum_{\mathbf{k}} \frac{\phi_{\mathbf{k}}(\omega_n)\eta_j(\mathbf{k})}{\varepsilon_{\mathbf{k}}^2 + \tilde{\omega}_{\mathbf{k}}^2(\omega_n) + \phi_{\mathbf{k}}^2(\omega_n)} \end{aligned} \qquad : 2.100$$

and with

$$\lambda(\nu_m) = \int_0^\infty d\Omega \frac{2\Omega\Phi(\Omega)}{\nu_m^2 + \Omega^2} \qquad : 2.101$$

where the constant $I^2\chi_0$ has been absorbed into $\Phi(\Omega)$ and $\eta_0(\mathbf{k})=1$ and $\eta_j(\mathbf{k})$ for $j>0$ are the terms in 2-87. The usual model takes only the $j=1$ term, with

$$\eta_j(\mathbf{k}) = \cos k_x - \cos k_y \quad . \qquad : 2.102$$

Then by symmetry the equations 2.95 to 2.98 reduce to

$$\tilde{\omega}_0(\omega_n) = \omega_n + T\sum_{n'} \lambda(\omega_n - \omega_{n'})\Omega_0(\omega_{n'}) + n_I \frac{\Omega_0(\omega_n)}{V_I^{-2} + \Omega_0^2(\omega_n) + D_0^2(\omega_n)} \qquad : 2.103$$

$$\phi_1(\omega_n) = gT\sum_{n'} \lambda(\omega_n - \omega_{n'})D_1(\omega_{n'}) \qquad : 2.104$$

with

$$\tilde{\omega}_{\mathbf{k}}(\omega_n) = \tilde{\omega}_0$$
$$\phi_{\mathbf{k}}(\omega_n) = \phi_{\mathbf{k}}(\omega_n)\eta(\mathbf{k}) \quad . \qquad : 2.105$$

The equations for critical temperature now become:

$$\tilde{\omega}_0(\omega_n) = \omega_n\big|_{T_c} + T_c\sum_{n'}\lambda(\omega_n - \omega_{n'})\Omega_0(\omega_{n'})\big|_{T_c} + n_I\frac{\Omega_0(\omega_n)\big|_{T_c}}{V_I^{-2} + \Omega_0^2(\omega_n)\big|_{T_c} + D_0^2(\omega_n)\big|_{T_c}} \qquad : 2.106$$

$$\phi_1(\omega_n) = gT_c\sum_{n'}\lambda(\omega_n - \omega_{n'})D_1(\omega_{n'})\big|_{T_c} \qquad : 2.107$$

where

$$\Omega_j(\omega_n)\big|_{T_c} = \sum_{\mathbf{k}}\frac{\tilde{\omega}_{\mathbf{k}}(\omega_n)\eta_j(\mathbf{k})}{\varepsilon_{\mathbf{k}}^2 + \tilde{\omega}_{\mathbf{k}}^2(\omega_n)}$$
$$D_j(\omega_n)\big|_{T_c} = \sum_{\mathbf{k}}\frac{\phi_{\mathbf{k}}(\omega_n)\eta_j(\mathbf{k})}{\varepsilon_{\mathbf{k}}^2 + \tilde{\omega}_{\mathbf{k}}^2(\omega_n)} \qquad : 2.108$$

with all temperature taken at $T=T_c$.

These equations will be the ones used throughout this work. At times another term will be taken from 2.87 but only one term at a time will be taken (i.e.; the coefficient of $cos2k_x$-$cos2k_y$ will be taken to be nonzero and all other coefficients will be zero). The effect of different terms from 2.87 will be seen in the next chapter on the London penetration depth.

2.4. Solutions for T_c

The solution of the Eliashberg equations requires that a choice be made for the kernel or equivalently $\Phi(\Omega)$ from 2.83. Also a choice of the other parameters t,B,μ from the electron dispersion; g the ratio of d-wave to s-wave superconductivity; n_I, V_I the impurity concentration and the impurity scattering strength. Once these parameters have been fixed then the equations for T_c are solved numerically by iteration for the critical temperature. The equations 2.103 and 2.104 for the superconducting state are then solved numerically by iteration for Z and ϕ at temperatures below T_c. The normal state is always given by 2.80 (a single equation to be solved by iteration) for any temperature.

The results of the calculation for T_c as a function of μ are shown in Figure 2.7. The choice of parameters are $t=100\ meV$, $B=0$, $g=1$, $n_I=0$ and $\Phi(\Omega)=A\,\delta(\Omega-\omega_E)$, an Einstein spectrum with Einstein frequency $\omega_E=100\ meV$ and the amplitude A chosen such that $T_c(\mu=0)\approx 127\ K$. It can be seen that T_c has a maximum value at $\mu=0$ with a sharp decrease as $|\mu|$ increases. Also note that the curve is symmetric around $\mu=0$ as this is due to particle-hole symmetry in this model. If one includes next nearest neighbor hopping then T_c is also reduced from the case when there is no next nearest neighbor hopping. This is shown in Figure 2.7 where the parameters haven't changed except for the chemical potential has been fixed at $25\ meV$ and now $T_c\approx 115\ K$. A sharp drop-off in T_c from $B=0$ is observed as B is

increased. For B=0.16 T_c has been reduced to 80% of its maximum and for B=0.45 T_c has been reduced to 30% of its maximum. Hence the maximum value of the critical temperature occurs at half-filling ($\mu=0$)with no next nearest neighbor hopping and the value of T_c is very sensitive to changes in both the chemical potential and the strength of next nearest neighbor hopping.

T_c has also been calculated as a function of impurity scattering. The results are shown in Figure 2.8 for $t=100meV$, $\mu=25\ meV$, $B=0$, $g=1$ and $\Phi(\Omega)=A\delta(\Omega-\omega_E)$, with $\omega_E=100\ meV$ and the amplitude A chosen such that $T_c(n_I=0)\approx 115\ K$ (Arberg and Carbotte, 1995). T_c has been plotted against the impurity term from 2.106

$$n_I \frac{\Omega_0(\omega_n)\big|_{T_c}}{V_I^{-2}+\Omega_0^2(\omega_n)\big|_{T_c}} \quad . \qquad : 2.109$$

For Born scattering ($V_I \to 0$) this becomes

$$\Gamma^{(Born)}(\omega_n) = n_I V_I^2 \Omega_0(\omega_n)\big|_{T_c} \qquad : 2.110$$

and for unitary scattering ($V_I \to \infty$),

$$\Gamma^{(unitary)}(\omega_n) = n_I \frac{1}{\Omega_0(\omega_n)\big|_{T_c}} \quad . \qquad : 2.111$$

For the case of constant density of states and an infinite band, these expressions reduce to the more familiar terms (Prohammer and Carbotte, 1991),

$$\Gamma^{(Born)} = \pi N(0) n_I V_I^2 \,\mathrm{sgn}(\omega_n)$$

$$\Gamma^{(unitary)} = \frac{n_I}{\pi N(0)} \mathrm{sgn}(\omega_n) \qquad : 2.112$$

which have a simple dependence on ω_n (namely through the sign of ω_n). For the case here, due to the more complicated density of states containing a van Hove

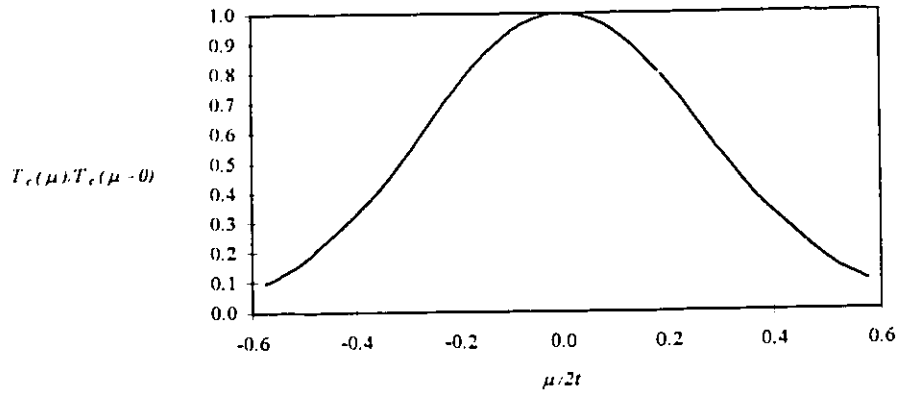

(a)

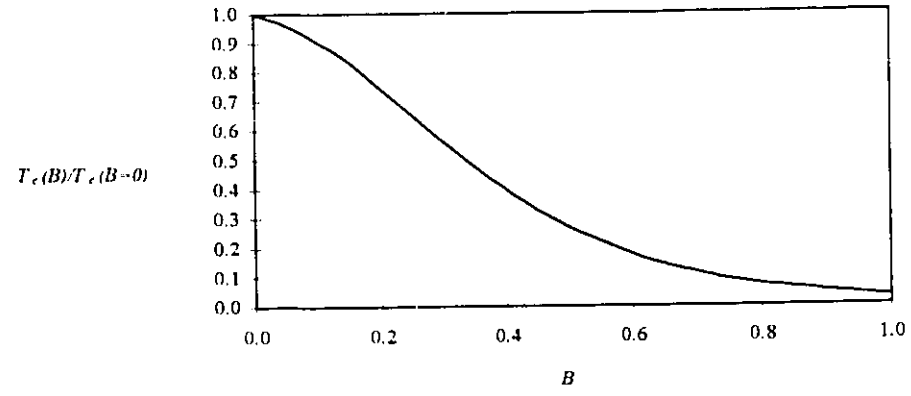

(b)

Figure 2.7 The dependence of T_c on band structure. The parameters are $t=100\ meV$, $B=0$ and μ varied for (a) and $\mu=25\ meV$ and B varied for (b), $g=1$, $n_I=0$ and $\Phi(\Omega)=A\delta(\Omega-\omega_E)$, with $\omega_E=100\ meV$ and the amplitude A chosen such that $T_c(\mu=0)\approx 127\ K$ in (a) and $T_c(B=0)\approx 115\ K$ in (b). Figure (a) shows the dependence on the chemical potential and (b) shows the dependence on the strength of next nearest neighbor hopping. The bandwidth is $8t=800\ meV$.

singularity, the dependence on ω_n of the scattering strength is much more complicated. Hence for a measure of the scattering strength, 2.109 will be evaluated only at the first Matsubara frequency, $n=0$ and this is the quantity T_c is plotted against in Figure 2.8. This decrease of T_c as a function of impurity strength is in direct contrast to the case of conventional (s-wave) superconductors. Conventional superconductors for the isotropic case have no dependence of T_c on normal impurity scattering, but scattering from magnetic impurities does reduce T_c (Abrikosov and Gorkov, 1960 and 1961). Here in d-wave superconductivity T_c is reduced by scattering from normal impurities and thus normal impurities act as Cooper pair breakers as do magnetic impurities in conventional superconductivity.

The main difference between the conventional constant density of states approximation and the work here is that now there is a difference with scattering in the Born approximation and the unitary limit. This can be seen by writing 2.112 which is the constant density of states limit as

$$\Gamma^{(Born)} = \tau \,\mathrm{sgn}(\omega_n)$$
$$\Gamma^{(unitary)} = \tau' \,\mathrm{sgn}(\omega_n) \qquad : 2.113$$

With this approximation there is a single parameter (τ (τ') for Born (unitary) scattering (compare with 2.112) but basically one measurable parameter - the scattering time due to impurities) describing the impurity scattering strength and hence the two types of scattering cannot be distinguished. However in the present work the scattering terms in the two limits are given by 2.110 and 2.111. There is

now a non-trivial difference in these two terms that cannot be ignored: The Born scattering term has

a $\Omega_0(\omega_n)$ in the numerator while the unitary scattering term has it in the denominator. Hence these two limits of impurity scattering strength are indeed different.

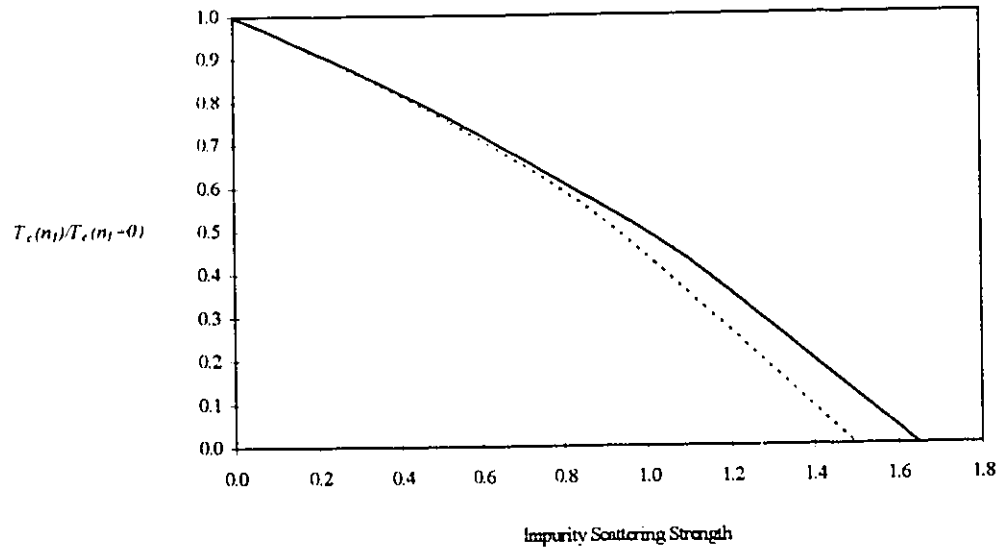

Figure 2.8 The change in the critical temperature as the scattering strength from impurities is increased in both the Born and unitary limits. The parameters are $t=100\ meV$, $\mu=25\ meV$, $B=0$, $g=1$ and $\Phi(\Omega)=A\,\delta(\Omega-\omega_E)$, with $\omega_E=100\ meV$ and the amplitude A chosen such that $T_c(n_I=0)\approx 115\ K$, and n_I varied to reduce the critical temperature. The solid curve is for Born scattering and T_c is plotted against $n_I V_I^2 \Omega_0(\omega_n)$ evaluated at T_c as in 2.110. The dotted curve is for unitary scattering and T_c is plotted against $n_I/\Omega_0(\omega_n)$ evaluated at T_c as in 2.111. This shows that for d-wave superconductivity, normal impurities act as pair breakers whereas in conventional superconductors they have no effect. One can say that they are analogous to magnetic impurities in conventional superconductors.

2.5. *Summary*

In summary, the strong-coupling theory of superconductivity and the tight-binding Hubbard model in 2-dimensions has been discussed. Eliashberg equations for a 2-dimensional superconductor with $d_{x^2-y^2}$ symmetry with representations derived via group theory have been derived. Within this model, the van Hove singularity in the electronic density of states has been accounted for fully by performing integrations in k-space over the entire Brillouin zone and not assuming any model for the electronic density of states. This is evidenced in the strong dependence of T_c on the chemical potential and the next nearest neighbor hopping strength. It is also seen that for d-wave superconductors that pair-breaking can occur when normal (nonmagnetic) impurities are included. The next chapters use the solutions of the Eliashberg equations to calculate some physical properties of 2-dimensional d-wave superconductors.

3. Magnetic Penetration Depth

The London penetration depth can now be calculated within the model developed in chapter 2. This involves calculating the solution of the Eliashberg equations and then calculating the current-current response function. In conventional superconductors where the gap Δ, is positive everywhere on the Fermi surface, there are no excitations with energy less than Δ. This leads to exponentially activated behavior in properties which depend on the population of excited states such as the London penetration depth (which is related to the number of condensed electrons in the superconducting state),

$\lambda(T) \sim \left(1 - e^{-\Delta/T}\right)^{-1/2}$ for $T << T_c$, usually written as $\left(\lambda(0)/\lambda(T)\right)^2 \sim 1 - e^{-\Delta/T}$ and this is proportional to the number of electrons in the superconducting state. However if the gap goes to zero at points on the Fermi surface there are

excitations at infinitesimal energies, thus the population of excited states is proportional to the temperature and a power law temperature dependence is seen in the London penetration depth, $(\lambda(0)/\lambda(T))^2 \sim 1-T$. This linear dependence in the penetration depth is exactly the behavior seen experimentally for $T \leq T_c$ in the High-T_c superconductors (Hardy *et al.*, 1993). A power law dependence has also been identified in the penetration depth of the heavy fermion superconductors (Einzel *et al.*, 1986; Gross *et al.*, 1988) and calculated for a d-wave superconductor with cubic symmetry ,constant density of states and infinite bandwidth (Prohammer and Carbotte, 1991). Now a general expression for the London penetration depth will be derived.

3.1. The Current-Current Correlation Function

To calculate the penetration depth one needs to know the current-current correlation function $K_{\mu\nu}(\mathbf{q},\omega)$ where $\mu\nu$ run over the spatial indices. Following Nam (1967a, 1967b), the current operator in the presence of a vector potential $\mathbf{A}(\mathbf{q},\omega)$ is

$$J_\mu(\mathbf{q},\omega) = -\frac{1}{4\pi} K_{\mu\nu}(\mathbf{q},\omega) A^\nu(\mathbf{q},\omega) \quad . \qquad : 3.1$$

$K_{\mu\nu}$ is the sum of the paramagnetic response and the diamagnetic response,

$$K_{\mu\nu}(\mathbf{q},\omega) = K^{(p)}_{\mu\nu}(\mathbf{q},\omega) + K^{(d)}_{\mu\nu} \qquad : 3.2$$

where the diamagnetic part $K^{(d)}{}_{\mu\nu}$ is proportional to the density of electrons and thus is a constant independent of whether or not the system is superconducting. Since in the normal state there is no induced current by a static field,

$$K^{N}_{\mu\nu}(\mathbf{q},0) = K^{(p)^{N}}_{\mu\nu}(\mathbf{q},0) + K^{(d)}_{\mu\nu} = 0 \qquad : 3.3$$

or

$$K^{(d)}_{\mu\nu} = -K^{(p)^{N}}_{\mu\nu}(\mathbf{q},0) \quad . \qquad : 3.4$$

Then in the superconducting state

$$J_{\mu}(\mathbf{q},\omega) = -\frac{1}{4\pi}\left\{K^{(p)^{S}}_{\mu\nu}(\mathbf{q},\omega) - K^{(p)^{N}}_{\mu\nu}(\mathbf{q},0)\right\}A^{\nu}(\mathbf{q},\omega) \qquad : 3.5$$

where the superscripts $S(N)$ refer to the quantity taken in the superconducting (normal) state. The current-current correlation function is given by

$$K_{\mu\nu}(\mathbf{q},\tau) = 4\pi\left\langle T_{\tau}\left(j^{(p)}_{\mu}(\mathbf{q},\tau)j^{(p)}_{\nu}(\mathbf{q},0)\right)\right\rangle \qquad : 3.6$$

where $\mathbf{j}^{(p)}(\mathbf{q},\tau)$ is the paramagnetic current operator given by

$$j^{(p)}_{\mu}(\mathbf{q}) = -e\sum_{\mathbf{k}}\Psi^{+}_{\mathbf{k}}\hat{\gamma}_{\mu}(\mathbf{k}+\tfrac{1}{2}\mathbf{q})\Psi^{+}_{\mathbf{k}+\mathbf{q}} \qquad : 3.7$$

where

$$\hat{\gamma}_{\mu}(\mathbf{k}) = \hat{\tau}_{0}\frac{\partial\varepsilon_{\mathbf{k}}}{\partial k_{\mu}} \qquad : 3.8$$

is the bare vertex function. Then one can write

$$K_{\mu\nu}^{(p)}(\mathbf{q},iv_m) = 4\pi e^2 T \sum_{\mathbf{k}i\omega_n} tr\left\{\hat{\gamma}_\mu\left(\mathbf{k}+\tfrac{1}{2}\mathbf{q}\right)\hat{G}\left(\mathbf{k}+\tfrac{1}{2}\mathbf{q},i\omega_n+iv_n\right)\hat{\Gamma}_\nu\left(\mathbf{k}-\tfrac{1}{2}\mathbf{q}\right)\hat{G}\left(\mathbf{k}+\tfrac{1}{2}\mathbf{q},i\omega_n\right)\right\} \quad : 3.9$$

where this expression is shown graphically in Figure 3.1.

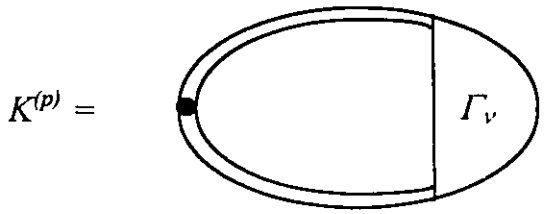

Figure 3.1 **Feynman diagram for the current-current correlation function where the solid dot represents the bare vertex γ.**

$\hat{\Gamma}_\nu(\mathbf{k})$ is the dressed vertex function shown graphically in Figure 3.2.

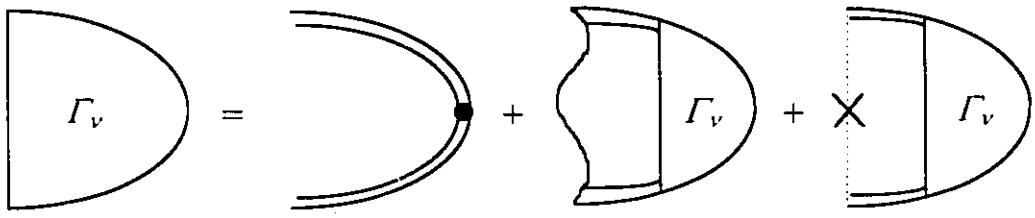

Figure 3.2 **Expansion of the full vertex function with phonon and impurity interactions.**

The electron-phonon interaction vertex corrections have the effect of renormalizing the electron-phonon interaction α^2F to a transport electron-phonon interaction, $\alpha^2_{tr}F$. This does not change the essential physics of the current-current correlation function, hence the electron-phonon vertex will be ignored. As for the

impurity corrections, they are too complicated to include fully in a self-consistent manner. However it is sufficient for most purposes to ignore them as the important physics is contained within the lowest order term, the bare vertex (Rickayzen, 1980: For example if one includes the so called ladder diagrams, this has the effect renormalizing the electron scattering rate from impurities. Hence one can use an effective scattering rate and drop these diagrams). For a first approximation then take $\hat{\Gamma}(\mathbf{k}) = \hat{\gamma}(\mathbf{k})$, then

$$K_{\mu\nu}^{(p)}(\mathbf{q}, iv_m) = 4\pi e^2 T \sum_{\mathbf{k}i\omega_n} tr\left\{\hat{\gamma}_\mu\left(\mathbf{k}+\tfrac{1}{2}\mathbf{q}\right)\hat{G}\left(\mathbf{k}+\tfrac{1}{2}\mathbf{q}, i\omega_n + iv_n\right) \times \hat{\gamma}_\nu\left(\mathbf{k}-\tfrac{1}{2}\mathbf{q}\right)\hat{G}\left(\mathbf{k}+\tfrac{1}{2}\mathbf{q}, i\omega_n\right)\right\} \quad . \qquad : 3.10$$

The London penetration depth is given by (Nam, 1967b)

$$\lambda_{\mu\nu}(T) = \frac{2}{\pi}\int_0^\infty dq \frac{1}{q^2 + K_{\mu\nu}(0,0)} \qquad : 3.11$$

where the temperature dependence has been shown explicitly. Hence

$$\lambda_{\mu\nu}(T) = K_{\mu\nu}^{-\frac{1}{2}}(0,0) \quad . \qquad : 3.12$$

Since the current-current response function contains the two terms from the paramagnetic and diamagnetic response, 3.12 becomes by using 3.15

$$\lambda_{\mu\nu}(T) = \left[K_{\mu\nu}^{S}(0,0) - K_{\mu\nu}^{N}(0,0)\right]^{-\frac{1}{2}} \quad . \qquad : 3.13$$

Hence the general expression for the London penetration depth is (Arberg *et al.*, 1993a, 1993b)

$$\lambda_{\mu\nu}(T)=\left\{4\pi e^2 T\sum_{\mathbf{k}i\omega_n}\left[\frac{\partial\varepsilon_{\mathbf{k}}}{\partial k_\mu}\frac{\partial\varepsilon_{\mathbf{k}}}{\partial k_\nu}\left(tr\left\{\hat{G}^S(\mathbf{k},i\omega_n)\hat{G}^S(\mathbf{k},i\omega_n)\right\}-tr\left\{\hat{G}^N(\mathbf{k},i\omega_n)\hat{G}^N(\mathbf{k},i\omega_n)\right\}\right)\right]\right\}^{-\frac{1}{2}}$$

where $\hat{G}^S(\mathbf{k},i\omega_n)$ is given by

$$\hat{G}^S(\mathbf{k},i\omega_n)=-\frac{i\tilde{\omega}_{\mathbf{k}}(\omega_n)\hat{\tau}_0+\varepsilon_{\mathbf{k}}\hat{\tau}_3+\phi_{\mathbf{k}}(\omega_n)\hat{\tau}_1}{\varepsilon_{\mathbf{k}}^2+\tilde{\omega}_{\mathbf{k}}^2(\omega_n)+\phi_{\mathbf{k}}^2(\omega_n)} \qquad : 3.14$$

and

$$\hat{G}^N(\mathbf{k},i\omega_n)=-\frac{i\tilde{\omega}_{\mathbf{k}}^N(\omega_n)\hat{\tau}_0+\varepsilon_{\mathbf{k}}\hat{\tau}_3}{\varepsilon_{\mathbf{k}}^2+\tilde{\omega}_{\mathbf{k}}^{N^2}(\omega_n)} \qquad : 3.15$$

Hence

$$\lambda_{\mu\nu}(T)=\left\{8\pi e^2 T\sum_{\mathbf{k}i\omega_n}\frac{\partial\varepsilon_{\mathbf{k}}}{\partial k_\mu}\frac{\partial\varepsilon_{\mathbf{k}}}{\partial k_\nu}\left[\frac{\varepsilon_{\mathbf{k}}^2+\phi_{\mathbf{k}}^2(\omega_n)-\tilde{\omega}_{\mathbf{k}}^2(\omega_n)}{\left(\varepsilon_{\mathbf{k}}^2+\tilde{\omega}_{\mathbf{k}}^2(\omega_n)+\phi_{\mathbf{k}}^2(\omega_n)\right)^2}-\frac{\varepsilon_{\mathbf{k}}^2-\tilde{\omega}_{\mathbf{k}}^{N^2}(\omega_n)}{\left(\varepsilon_{\mathbf{k}}^2+\tilde{\omega}_{\mathbf{k}}^{N^2}(\omega_n)\right)^2}\right]\right\}^{-\frac{1}{2}} \qquad : 3.16$$

where the superscript N refers to the quantity to be calculated in the normal state as according to 2.80. With $\varepsilon_{\mathbf{k}}$ given by 2.7, then

$$\frac{\partial\varepsilon_{\mathbf{k}}}{\partial k_x}=2t\left(1-2B\cos k_y\right)\sin k_x$$
$$\frac{\partial\varepsilon_{\mathbf{k}}}{\partial k_y}=2t\left(1-2B\cos k_x\right)\sin k_y \qquad : 3.17$$

From symmetry, then

$$\lambda_{xx}(T)=\lambda_{yy}(T)=\lambda(T) \quad ,$$
$$\lambda_{xy}(T)=\lambda_{yx}(T)=0 \quad . \qquad : 3.18$$

The equation 3.16 is a completely general expression for the London penetration depth and thus any band structure and symmetry of the electron-boson interaction

can be substituted along with any boson spectrum required to solve the Eliashberg equations for the renormalization function and the gap.

One can calculate the penetration depth from a knowledge of the renormalization function and the gap which are obtained from the solution of the Eliashberg equations. Now results will be shown for the penetration depth and its dependence on temperature, impurity scattering and band structure will be seen. It is also calculated with different $d_{x^2-y^2}$ symmetry functions from the expansion 2.87.

3.2. *Strong Coupling Effects*

One can calculate the penetration depth from a knowledge of the renormalization function and the gap which are obtained by solution of the Eliashberg equations. Results will be shown for the penetration depth and its dependence on temperature, impurity scattering, coupling strength and band structure through the chemical potential μ, and the next nearest neighbor hopping strength B. The nearest neighbor hopping strength t, and the ratio of d-wave to s-wave superconductivity g, do not change the qualitative behavior of any quantity, they do however change the magnitude of various properties (such as the critical temperature) and hence will be considered as fixed parameters throughout. Unless stated otherwise the hopping integral will be taken as $t=100\ meV$ and the d-wave

strength will be taken to be $g=1$ (a pure d-wave superconductor). The penetration depth has also been calculated with different $d_{x^2-y^2}$ symmetry functions from the expansion in 2.87.

The penetration depth is calculated for different coupling strengths. Until the section where different terms of the $d_{x^2-y^2}$ symmetry expansion are examined the interaction is taken to have the standard momentum dependence of only the first term,

$$\eta_{10}(\mathbf{k}) = \cos k_x - \cos k_y \qquad : 3.19$$

and hence the gap has the form

$$\begin{aligned} \Delta_{\mathbf{k}}(\omega) &= \Delta(\omega)\eta_{10}(\mathbf{k}) \\ &= \Delta(\omega)\left(\cos k_x - \cos k_y\right) \end{aligned} \qquad : 3.20$$

where $\Delta(\omega)$ is independent of momentum. The parameters used are $t=100\ meV$, $\mu=25\ meV$, $B=0$, $g=1$, $n_I=0$, and a Einstein spectrum for the boson interaction.

T_c/ω_E	$2\Delta_0/T_c$
0.1	3.68
0.2	6.79
0.3	14.7
0.4	46.8

Table 3-1 Δ_0 **is the gap edge defined by** $\Delta_0 = Re\Delta(\Delta_0)$.

$\Phi(\Omega)=A\,\delta(\Omega-\omega_E)$ with $\omega_E=100\ meV$ and the values of A chosen such that $T_c/\omega_E=0.1,\ 0.2,\ 0.3,\ 0.4$. The ratio of the gap to the critical temperature are shown in Table 3-1, and the results for the temperature dependence of the penetration depth for the different coupling strengths are shown in Figure 3.3.

The low temperature dependence of $\lambda^{-2}(T)$ is seen to be linear in temperature as expected for a d-wave superconductor. For all coupling but the strongest shown, $\lambda^{-2}(T)$ is also linear near the critical temperature. Also note that as the coupling strength is increased, the slope of $\lambda^{-2}(T)$ reaches a maximum and then decreases again. This same behavior of the slope increasing and then decreasing as the

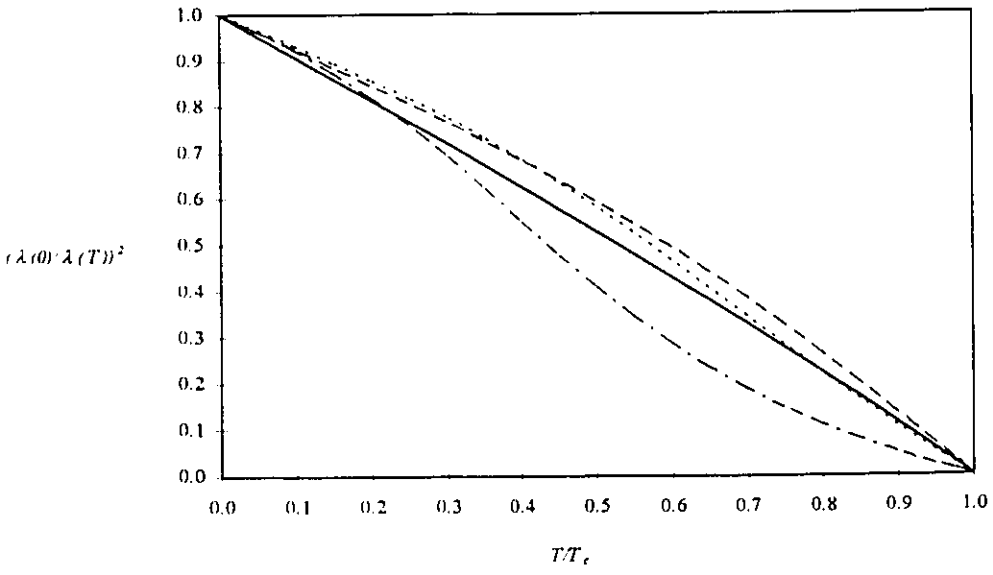

Figure 3.3 **Effect of coupling strengths on the penetration depth. The solid line is for $T_c/\omega_E=0.1$; the dashed line is for $T_c/\omega_E=0.2$; the dotted line is for $T_c/\omega_E=0.3$; and the dash-dash-dotted line is for $T_c/\omega_E=0.4$.**

coupling strength is increased is also seen in electron-phonon theory for conventional superconductors (Carbotte, 1990).

Comparing the curves in Figure 3.3 with the experiment of Hardy *et al.* (1993) it is seen that weaker coupling strengths ($T_c/\omega_E \leq 0.3$) give a more adequate agreement between theory and experiment, and strong coupling ($T_c/\omega_E = 0.4$) is in complete disagreement with experiment. Examining the weakest coupling curve ($T_c/\omega_E = 0.1$), the agreement between theory and experiment is best at low temperatures ($T \leq \frac{1}{2} T_c$) where the slope of $\lambda^{-2}(T)$ is near -1 while at higher temperature ($T \geq \frac{1}{2} T_c$) the theory underestimates the slope by about a factor of two. Therefore a reasonable set of parameters has $t = 100\ meV$, $\mu = 25\ meV$, $B = 0$, $g = 1$, $n_I = 0$, $\Phi(\Omega) = A\,\delta(\Omega - \omega_E)$ with $\omega_E = 100\ meV$ and the values of A chosen such that $T_c/\omega_E = 0.1$ or $T_c \approx 115\ K$. The discrepancy at high temperatures (near T_c) between the experimental results and the results here could be due to the fact that near the critical temperature one must include fluctuations off the mean field (Inderhees *et al.*, 1988, 1991; Annet and Goldenfeld, 1992; Liang *et al.*, 1992; Loram *et al.*, 1992; Ghiron *et al.*, 1993; Ernst *et al.*, 1993).

3.3. Band Structure Effects

The effect of band structure can also be examined within this model. This is possible since the usual approximations of an infinite band and constant density of states has not been made, hence the details of the band structure including any van Hove singularities can be studied. First how variations in the chemical potential affects the temperature dependence of the penetration depth will be seen.

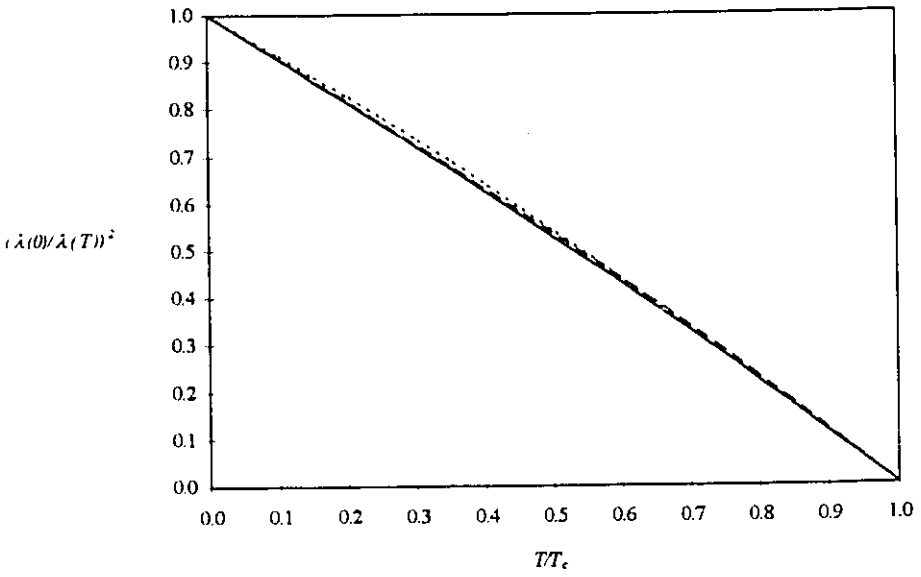

Figure 3.4 **Effect of band structure on the penetration depth. The solid line is for μ=25 meV (μ=0.125 in units of 2t); the dashed line is for μ=0 meV (μ=0 in units of 2t); and the dotted line is for μ=110 meV (μ=0.55 in units of 2t).**

The calculation has been done with no next nearest neighbor hopping ($B=0$), no impurity scattering ($n_I=0$) and $\Phi(\Omega)=A\,\delta(\Omega-\omega_E)$ with $\omega_E=100\ meV$ and A chosen such that $T_c(\mu=0)\approx 127\ K$. Recall that the dependence of the critical temperature

on the chemical potential is shown in Figure 2.7 and now in Figure 3.4 the temperature dependence of $\lambda(T)$ for three different chemical potentials (μ=*0, 25, 110 meV* or $\mu/2t$=*0, 0.125, 0.55*) are shown.

The linear temperature dependence is quite apparent over the entire temperature range with $\lambda^{-2}(T) \propto 1-T$. This behavior is not influenced greatly as the chemical potential changes. This is in contrast to the large dependence of T_c on μ (Figure 2.7) where small changes in the chemical potential can affect great changes in T_c and eventually destroying the superconducting state. The dependence of the magnitude or zero temperature penetration depth on μ is shown in Figure 3.5. As can be seen, $\lambda(0)$ exhibits a small dependence on chemical potential (*~5%* over the range of chemical potentials for which it is calculated: μ=*0,..., 110 meV*). However when the chemical potential becomes large enough such that T_c=*0*, then the penetration depth becomes infinite (as the material is no longer superconducting) and this behavior is seen in Figure 3.5 as the sharp increase as T_c decreases.

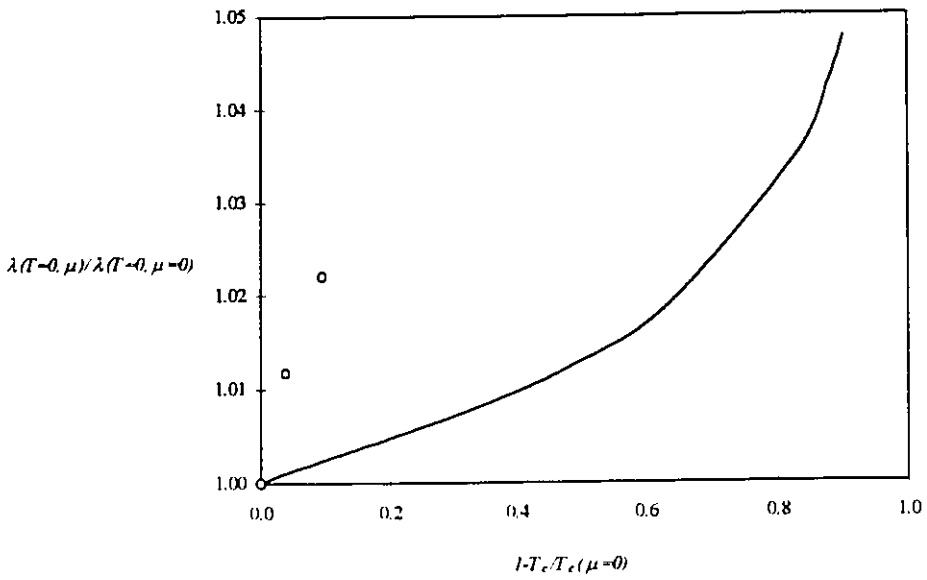

Figure 3.5 **Effect of varying the chemical potential on the magnitude of the penetration depth. The zero temperature penetration depth is plotted against the change in the critical temperature as a function of the chemical potential for the solid line, and the open circles is the zero temperature penetration depth for the three physical values of next nearest neighbor hopping (*B=0,0.16,0.45*).**

The dependence of $\lambda(T)$ on B, the next nearest neighbor hopping strength is shown in Figure 3.6. The parameters have been kept the same with the exception that μ has been fixed at $25\ meV$, and the amplitude of the delta function boson spectrum has been chosen such that $T_c(B=0) \approx 235\ K$ (This last change is for computational simplicity due to the length of time required to run the computer programs at lower temperatures), and $B=0,\ 0.16,\ 0.45,\ 1.0$. The $B=0$ curve is with no next nearest neighbor hopping; $B=0.16$ is believed to be the next nearest neighbor hopping strength in the La-Sr-Cu-O compounds; $B=0.45$ is believed to be the relevant hopping strength in the Y-Ba-Cu-O compounds; and $B=1.0$ is

unphysical but is included to push the limits on the effect of next nearest neighbor hopping. Within this set of values for B, $\lambda^{-2}(T)$ remains linear in temperature but the slope is increased over the entire temperature range. However for a reasonable choice of next nearest neighbor hopping ($B \leq 0.45$), the penetration depth does not exhibit large deviations from the simplest case of no next nearest neighbor hopping. The effect of next nearest neighbor hopping on the magnitude of the zero temperature penetration depth is also small (~2% for reasonable values of B) as seen in Figure 3.5 whereas the value of T_c has decreased substantially over this range of values (see Figure 2.7).

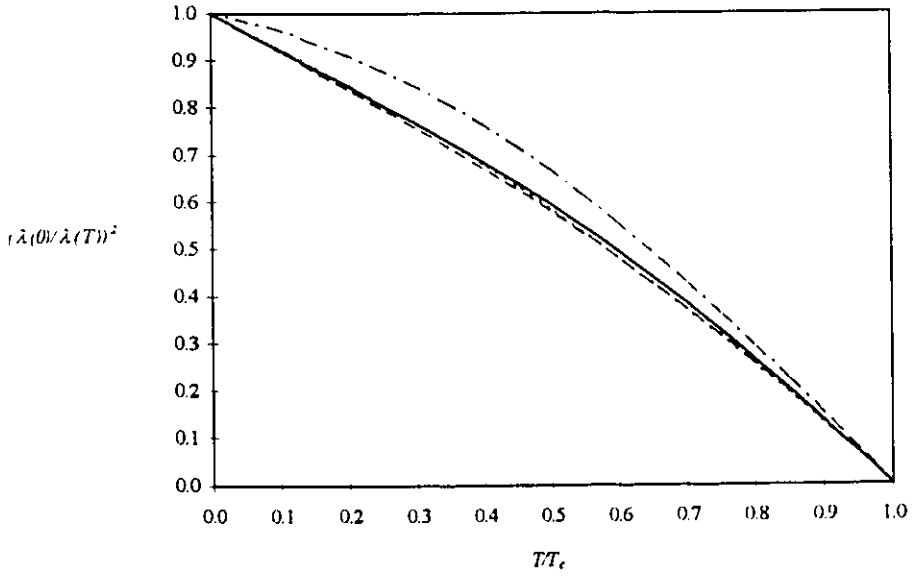

Figure 3.6 Effect of next nearest neighbor hopping. The solid curve is for $B=0$; the dashed curve is for $B=0.16$; the dotted curve is for $B=0.45$; and the dash-dash-dotted curve is for $B=1.0$.

3.4. Impurity Scattering Effects

Deviations from linearity in temperature of the penetration depth can be caused by introducing impurity scattering. This effect can be seen in experiments on the high T_c superconductors where small concentrations of Zn and Ni which act as impurities are introduced into the pure samples and thus can change the temperature dependence of the penetration depth to quadratic in temperature(Lee *et al.*, 1993). First the case of scattering in the Born approximation is considered. This is weak scattering ($V_I \to 0$) and then the appropriate impurity term to be included in the Eliashberg equations is given by 2.110. The results for the temperature dependence of the penetration depth are shown in Figure 3.7 for the standard set of parameters now with the relevant parameter for Born scattering $n_I V_I^2$ varied from $n_I=0$ (pure case), 0.16, 0.64, 0.75 with V_I fixed at $50\ meV$.

A more lucid measure of the impurity scattering is the ratio T_c/T^0_c where T^0_c is the critical temperature with no impurity scattering and T_c is the critical temperature for a given scattering strength. Then as the amount of impurity scattering increases the ratio T_c/T^0_c decreases until it reaches zero for a sufficient amount of impurity scattering and the superconducting state is destroyed. As can be seen from Figure 2.8 and Figure 3.7 Born scattering can have a large effect on the critical temperature but a much smaller effect on $(\lambda(0)/\lambda(T))^2$. This is evidenced by the fact that a drop in T_c to almost half of T^0_c ($T_c/T^0_c=0.52$) produces

almost no change in $(\lambda(0)/\lambda(T))^2$ and hence remains linear at low enough temperatures. Only at very high concentrations of Born scattering centres does $(\lambda(0)/\lambda(T))^2$ begin to show a T^2 dependence at low temperatures. For T near T_c the temperature dependence remains linear with an almost constant slope. The dependence of $\lambda(T=0)$ as a function of Born scattering strength (or reduction of T_c from the pure value) is shown in Figure 3.8 as the solid line. As impurity concentration increases (T_c/T^0_c decreases) $\lambda(T=0)$ increases and will approach infinity when the superconducting state is destroyed by the impurity scattering.

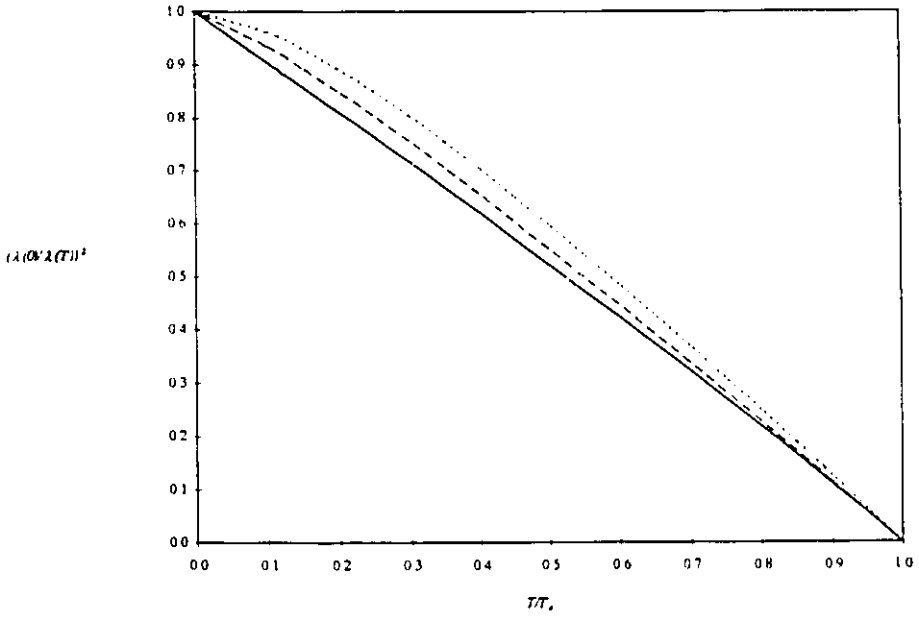

Figure 3.7 **Effect of impurity scattering in the Born limit on the penetration depth. The solid curve is for $T_c/T^0_c=0.90$; the dashed curve is for $T_c/T^0_c=0.52$; and the dotted curve is for $T_c/T^0_c=0.40$. Here T^0_c is the critical temperature in the absence of any impurity scattering and T_c is the critical temperature in the presence of impurity scattering. Hence the ratio T_c/T^0_c is a measure of the amount of impurity scattering: i.e. As the amount of impurity scattering increases, the critical temperature is reduced and hence the ratio T_c/T^0_c decreases.**

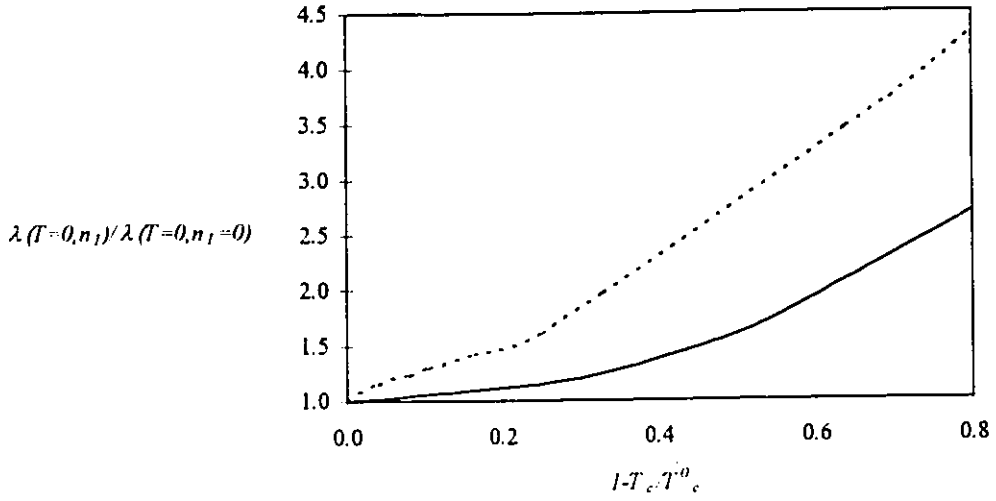

Figure 3.8 The effect of impurity scattering on the magnitude of the penetration depth. The zero temperature penetration depth is plotted against the reduction from one of the ratio T_c/T^0_c due to impurity scattering both in the Born limit (solid line) and the unitary limit (dotted line).

The inclusion of strong scattering or resonant scattering in the unitary limit ($V_I \rightarrow \infty$) has a much larger effect on the penetration depth. The appropriate scattering term to be included in the Eliashberg equations is given by 2.111. The penetration depth for the usual set of parameters with $n_I=0$, *0.005*, *0.13*, *0.03* is shown on Figure 3.9. Now a *4%* reduction in T_c from the clean limit gives a low temperature behavior of T^2 in $(\lambda(0)/\lambda(T))^2$. As the impurity concentration increases the T^2 dependence occurs over an increasing temperature range until a linear dependence can no longer be identified (T_c/T^0_c) for any range of temperature. Shown as the dotted curve in Figure 3.8 is the dependence of $\lambda(T=0)$ as a function of impurity concentration in the unitary limit. This shows qualitatively the same behavior as the effect of scattering in the Born limit but $\lambda(T=0)$ has a sharper

increase due to the larger strength of impurity scattering in the unitary limit over the Born limit.

These results can be compared with experimental results (Lee *et al.*, 1993).

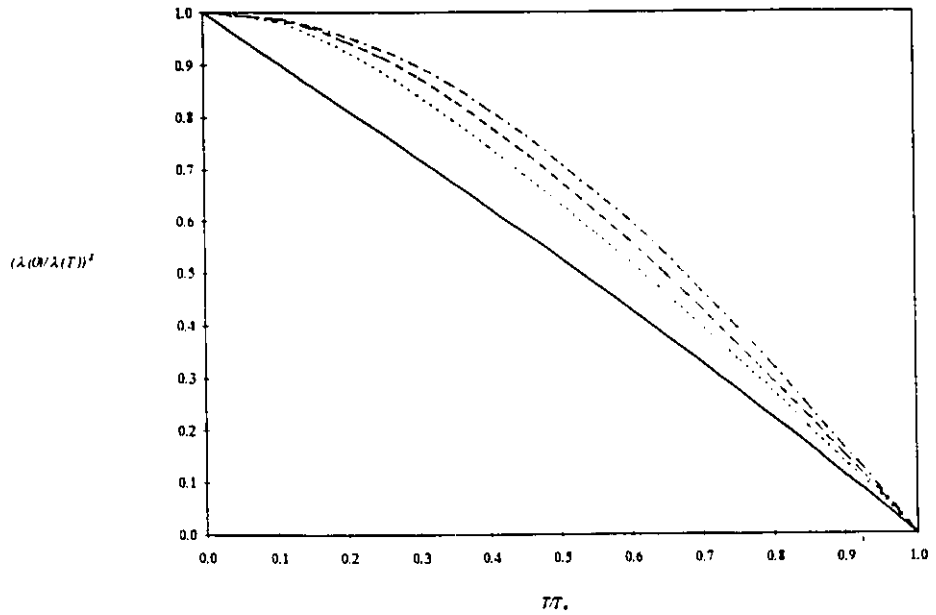

Figure 3.9 **The effect of scattering in the unitary limit on the penetration depth. The solid line is for $T_c/T^0_c=1.0$; the dotted line is for $T_c/T^0_c=0.96$; the dashed line is for $T_c/T^0_c=0.90$; and the dash-dash-dotted line is for $T_c/T^0_c=0.75$. Here T_c is the critical temperature calculated in the presence of impurity scattering in the unitary limit.**

The square of the ratio of the penetration depth at zero temperature and no impurity scattering to the finite temperature and finite impurity scattering, $(\lambda(T=0,n_I=0)/\lambda(T,n_I))^2$ as a function of temperature is shown in Figure 3.10 for $n_I=0$, 0.01, 0.02 (or $T_c/T^0_c=1.0$, 0.92, 0.84). Lee *et al.* have performed experiments on thin films of $YBa_2Cu_3O_{7-\delta}$ with $\delta=0$ (their sample A or B) with $T_c/T^0_c\approx0.92$ (where T^0_c is the critical temperature of single crystal $YBa_2Cu_3O_{7-\delta}$) and oxygen depleted ($\delta>0$ and chosen such that $T_c/T^0_c=0.85$), their sample A′.

The penetration depth for the films are both quadratic in temperature where the pure (single crystal) penetration depth is linear at low temperatures. This can be compared directly with Figure 3.10 where the quadratic behavior is seen for small concentrations of impurity scattering. Additionally the value for $(\lambda(T=0,n_I=0)/\lambda(T,n_I=0.01))^2$ is ≈ 0.66 from the theory here and ≈ 0.64 from the experiment. $(\lambda(T=0,n_I=0)/\lambda(T,n_I=0.02))^2$ is ≈ 0.50 from the theory and ≈ 0.32 from the experiment. Hence the theory and experiment are in excellent qualitative agreement and very good quantitative agreement (Arberg and Carbotte, 1995). It should be noted that changing the oxygen content of the sample changes the chemical potential and thus the dotted line should be calculated with a modified chemical potential. However it was seen earlier that $\lambda(T=0)$ does not have a strong dependence on the chemical potential (Figure 3.4) and thus over the range of critical temperatures considered by Lee *et al.*, the dependence of $\lambda(T=0)$ on μ can be ignored within this model since for small changes in critical temperature due to changes in μ implies that μ changes very little (Figure 2.7). The experiments of Ulm *et al.* (1993a, 1993b) performing Al, Ni and Zn substitutions for Cu in Y-Ba-Cu-O shows that $\lambda(T=0)$ for different impurity concentrations are always larger (up to a factor of two) than the theoretical results presented here, however the qualitative behavior is in agreement between the experiments and the theory.

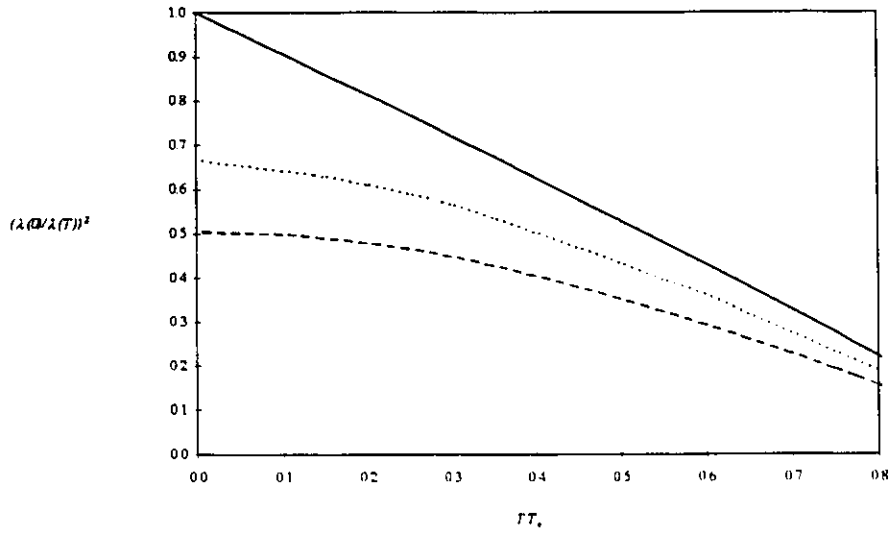

Figure 3.10 **Effect of impurity scattering in the unitary limit on the magnitude and temperature dependence of the penetration depth. The solid line is for $T_c/T^0_c=1.0$ (or $n_I=0$); the dotted line is for $T_c/T^0_c=0.92$ (or $n_I=0.01$); and the dashed line is for $T_c/T^0_c=0.84$ (or $n_I=0.02$). This graph is compared directly with experimental results of Lee *et al.*, 1993 and their samples A(or B) with $T_c/T^0_c=0.92$; sample A' with $T_c/T^0_c=0.92$; and a single crystal of $YBa_2Cu_3O_7$ with $T_c/T^0_c=1.0$. See the text for a full comparison.**

The behavior of the penetration depth as one goes from weak to strong scattering is shown in Figure 3.11. Here the impurity concentration has been adjusted such that T_c/T^0_c remains fixed at *0 90* while the scattering potential V_I, has been varied from *0* (Born approximation) to ∞ (unitary scattering). The temperature dependence of $(\lambda(0)/\lambda(T))^2$ begins linear for small values of V_I and then quickly becomes a T^2 dependence as V_I is increased. Thus the behavior (T^2) that characterizes scattering in the unitary limit ($V_I \rightarrow \infty$) is reached for rather modest scattering strengths. The T^2 dependence at low temperatures is readily seen in Figure 3.11 for $V_I=500\ meV$ while linear behavior can still be seen for

V_I=200 meV. Hence if the scattering is anything but very weak, it will make itself readily apparent in the temperature dependence of the penetration depth.

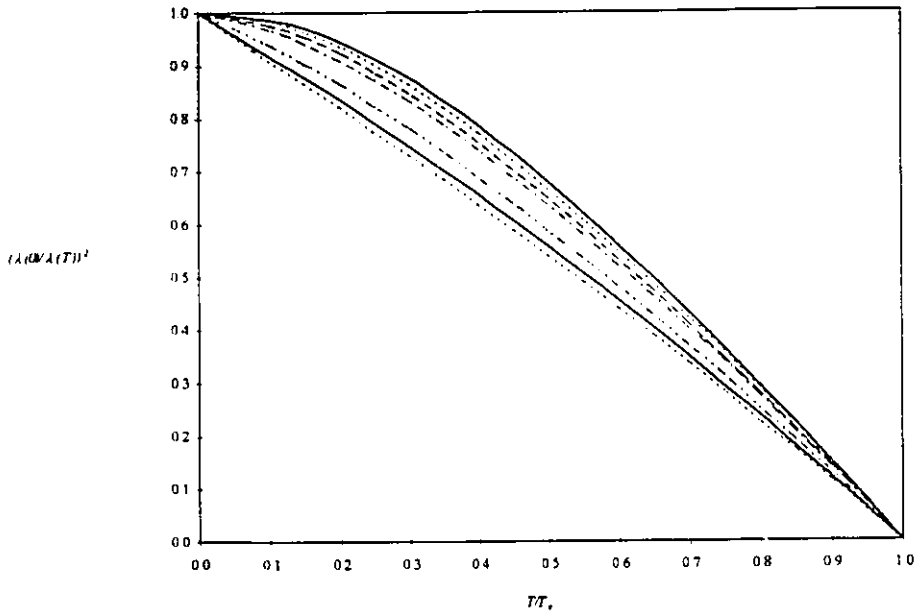

Figure 3.11 Effect of the strength of impurity scattering on the penetration depth and the crossover from strong to weak scattering. In each curve the ratio T_c/T^0_c has been fixed at *0.9* and the strength of the scattering potential V_I, has been varied. The top solid curve has $V_I \to \infty$ *meV* (unitary scattering limit); the highest dotted curve has V_I=*1000.0 meV*; the dashed curve has V_I=*667.7 meV*; the dash-dash-dotted curve has V_I=*500.0 meV*; the dash-dotted curve has V_I=*333.3 meV*; the lower solid curve has V_I=*250.0 meV*; and the lower dotted curve has V_I=*200.0 meV*.

3.5. *Interaction Symmetry Effects*

The dependence of the penetration depth on the band structure and impurity scattering in both weak and strong limits and intermediate values has been

calculated. All of this has been done for a gap with momentum dependence $cosk_x$-$cosk_y$. This is only one term ($\eta_{10}(\mathbf{k})$) in the expansion of a gap with $d_{x^2-y^2}$ symmetry. In principal one may take N terms of the series however then N pairs of Eliashberg equations must be solved simultaneously, and hence quickly becomes prohibitively long to solve as N increases. This is the general case but one can take individual terms of the expansion which are still equally good functions to use for a $d_{x^2-y^2}$ symmetry. This is exactly the procedure used to obtain results for the single $cosk_x$-$cosk_y$ function. The effect of each term can be seen without mixing this term with the other terms of the expansion. The Eliashberg equations will now be solved and the penetration depth calculated for some different $d_{x^2-y^2}$ symmetry functions.

The general expansion of a gap with $d_{x^2-y^2}$ symmetry is from equation 2.85 $\Delta(\mathbf{k},\omega)=\Delta(\omega)\,\eta(\mathbf{k})$ where

$$\eta(\mathbf{k}) = \sum_{n_1=1}^{\infty}\sum_{n_2=0}^{n_1-1} a_{n_1 n_2}\,\eta_{n_1 n_2}(\mathbf{k}) \qquad : 3.21$$

where

$$\eta_{mn}(\mathbf{k}) = \cos mk_x \cos nk_y - \cos nk_x \cos mk_y \quad . \qquad : 3.22$$

As $\eta_{10}(\mathbf{k})$ has been explored, consider the next term

$$\nu_{20}(\mathbf{k}) = \cos 2k_x - \cos 2k_y \qquad : 3.23$$

and expand $\chi_0(\mathbf{k},\mathbf{k}')$ as in 2.84 with $\eta_{20}(\mathbf{k})$ in the place of $\eta_{10}(\mathbf{k})$. This then leads to a gap of the form

$$\Delta(\mathbf{k},\omega) = \Delta(\omega)\eta_{20}(\mathbf{k}) \quad . \qquad : 3.24$$

This gap has zeros along the lines shown in Figure 2.6. The gap goes to zero at points on the Fermi surface (as with a gap with $\eta_{10}(\mathbf{k})$ momentum dependence) but also has zeros everywhere on the Fermi surface at half-filling ($\mu=0$) with no next nearest neighbor hopping ($B=0$). Also note that not only does the gap go to zero at these points, so also does the interaction $\chi_0(\mathbf{k},\mathbf{k}')$ and this is actually the origin of the zeros in the gap function. The penetration depth is shown in Figure 3.12 for different chemical potentials. The parameters used are $t=100\ meV$, $B=0$, $g=1$, $n_i=0$, $\Phi(\Omega)=A\,\delta(\Omega-\omega_E)$ with $\omega_E=100\ meV$ and A chosen such that $T_c\approx 167\ K$ for $\mu=100\ meV$ and μ is varied throughout the values $35,\ 40,\ 50,\ 60,\ 75,\ 100\ meV$. Far away from half-filling, $\mu/2t=0.5$, corresponding to the top solid curve in Figure 3.12, the penetration depth is linear in temperature and not too different from the $\eta_{10}(\mathbf{k})$ calculations with no impurity scattering. This is just as expected since the gap goes to zero at points on the Fermi surface as shown in Figure 3.13. As $\mu=0$ is approached the gap still goes to zero at points on the Fermi surface, but the magnitude of the gap on the Fermi surface is decreasing as the Fermi surface is becoming closer to the half-filling case, where the gap is identically zero everywhere on the Fermi surface. Since the magnitude of the gap is now smaller at the Fermi surface and hence the gap in the excitation spectrum, it becomes easier to excite electrons out of the superconducting state. This effect is seen in the penetration depth since it can be shown (Fetter and Walcka, 1971) that

$(\lambda(0)/\lambda(T))^2$ is proportional to the number of electrons in the superconducting state. This is evidenced by the fact that $(\lambda(0)/\lambda(T))^2$ shows a more rapid decrease near $T=0$ as $\mu \to 0$. However it was not possible to solve the Eliashberg equations and hence compute the penetration depth at $\mu=0$ for this model with a reasonable amount of computer time.

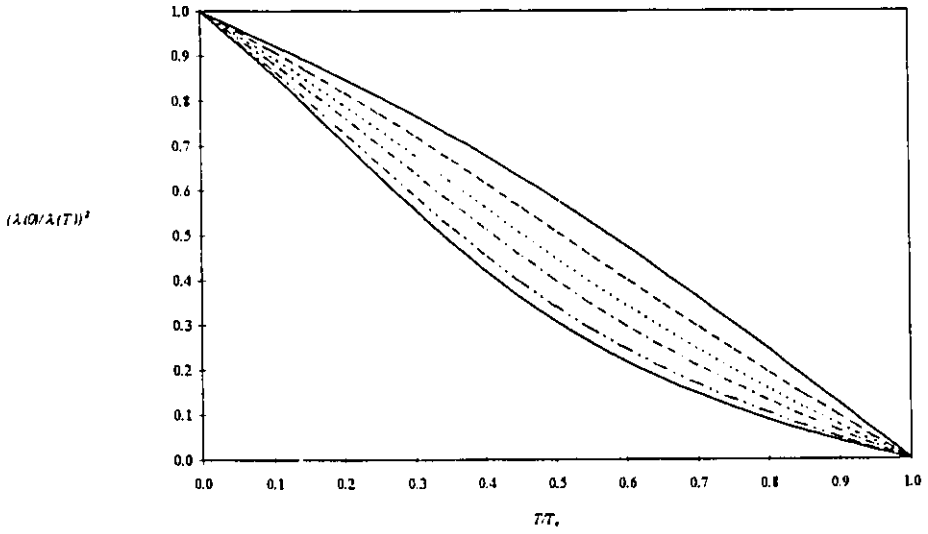

Figure 3.12 Temperature dependent penetration depth for different chemical potentials with the $\eta_{20}(\mathbf{k})$ function. The top solid line is $\mu=100$ meV; the dashed line is $\mu=75$ meV; the dotted line is $\mu=60$ meV; the dot-dashed line is $\mu=50$ meV; the dot-dot-dashed line is $\mu=40$ meV; and the lower solid line is $\mu=35$ meV, or $\mu/2t=0.5, 0.375, 0.3, 0.25, 0.2, 0.175$ respectively.

A range of $d_{x^2-y^2}$ symmetry functions has been examined. The penetration depth is shown in Figure 3.14 for the $d_{x^2-y^2}$ symmetry functions $\eta_{10}(\mathbf{k})$ (shown for comparison), $\eta_{30}(\mathbf{k})$, $\eta_{40}(\mathbf{k})$, $\eta_{50}(\mathbf{k})$, $\eta_{70}(\mathbf{k})$, $\eta_{90}(\mathbf{k})$. All *even*(*odd*) harmonics (where *even*(*odd*) will refer to the function $\eta_{mn}(\mathbf{k})$ where m is an even(odd) integer) have lines of zeros crossing the Fermi surface at points. However the

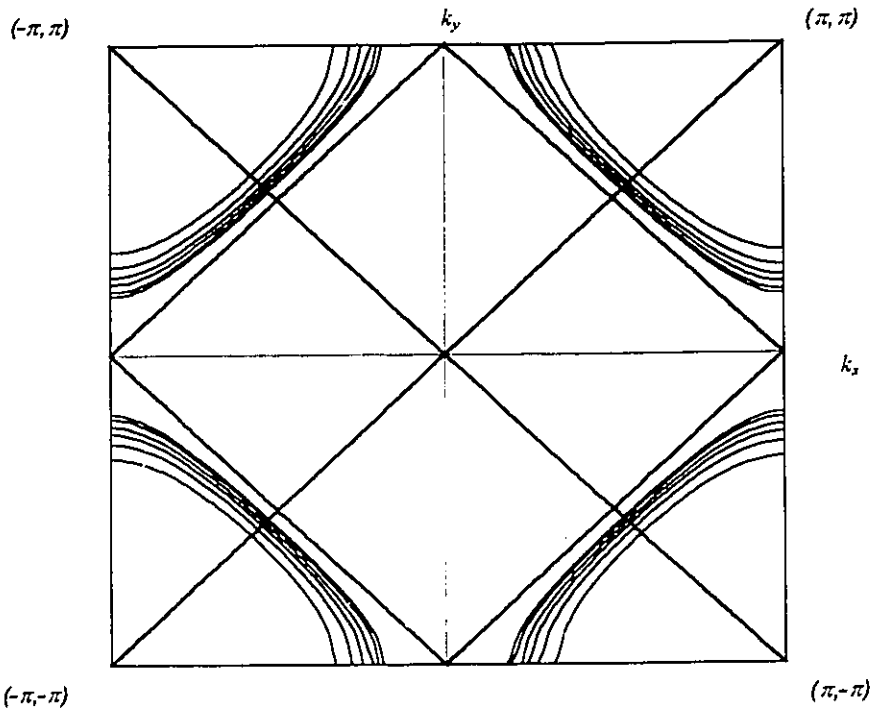

Figure 3.13 Zeros of $\eta_{20}(k)$ (heavy solid lines) in the first Brillouin zone and the Fermi surfaces (lighter solid lines) for the six chemical potentials: $\mu/2t=0.5, 0.375, 0.3, 0.25, 0.2, 0.175$ from the outside line to the inside line. As the magnitude of the chemical potential decreases the Fermi surfaces approach the line of zeros of $\eta_{20}(k)$. As the Fermi surface approaches the zeros, the magnitude of the gap is also decreasing and hence it becomes easier to excite quasiparticles out of the condensate and hence the decrease in the number of electrons in the superconducting state.

even harmonics also have zeros along the Fermi surface when $\mu=0$ and $B=0$ just as in the case for the zeros of $\eta_{20}(\mathbf{k})$. This is effect is seen in the penetration depth as near half-filling (here $\mu=25\ meV = t/4 = 8t/32$, where $8t$ is the band width and hence very closer to half-filling) for the even harmonics the magnitude of the gap is small on the Fermi surface which leads to a small gap in the excitation spectrum and hence $(\lambda(0)/\lambda(T))^2$ decreases more quickly from $T=0$, while remaining linear since the gap still goes to zero at points on the Fermi surface.

There is however a competing effect. As the order of the harmonic increases (i.e. m increases in $\eta_{mn}(\mathbf{k})$) the number of points at which the gap goes to zero on the Fermi surface also increases and so does the slope of the gap increase at these points. Hence the gap becomes larger more quickly away from the Fermi surface and hence it becomes more difficult to excite the quasiparticles and the slope of $(\lambda(0)/\lambda(T))^2$ is driven back towards -1. This is seen in Figure 3.14 as the penetration depth for $\eta_{60}(\mathbf{k})$ is closer to linear than the $\eta_{40}(\mathbf{k})$ case (and $\eta_{20}(\mathbf{k})$ from Figure 3.12).

A similar effect of the competition between the number of points at which the gap goes to zero on the Fermi surface and the increase in the slope of the gap where it crosses the Fermi surface is also seen in the odd harmonics. The odd harmonics have zeros on the Fermi surface only at points for all values of μ and B, and hence the slope of $(\lambda(0)/\lambda(T))^2$ will remain linear in temperature for all of the odd harmonics. This is seen in Figure 3.14 that $(\lambda(0)/\lambda(T))^2$ is linear with slope -1 for $\eta_{10}(\mathbf{k})$ but decreases in slope for $\eta_{10}(\mathbf{k})$ and then increases in slope approaching -1 for $\eta_{50}(\mathbf{k})$, $\eta_{70}(\mathbf{k})$, $\eta_{90}(\mathbf{k})$. The behavior of the penetration depth with the odd harmonics should be relatively stable to small changes in μ and B since the gap will always and only have zeros at points on the Fermi surface. This can be seen for the case of $\eta_{10}(\mathbf{k})$ in Figure 3.4 where the penetration depth is shown for different values of chemical potential and in Figure 3.6 for different values of next nearest

neighbor hopping. In both figures the change in the penetration depth is noticeable but the effects are small and the qualitative behavior has not changed.

The effect of band structure on the penetration depth for the higher order odd harmonics are shown in Figure 3.15 and Figure 3.16. Also shown is a second term from the $d_{x^2-y^2}$ symmetry expansion,

$$\eta_{52}(\mathbf{k}) = \cos 5k_x \cos 2k_y - \cos 2k_x \cos 5k_y \quad . \qquad : 3.25$$

Adding next nearest neighbor hopping has changed the slope of $(\lambda(0)/\lambda(T))^2$. While remaining linear at both high and low temperatures the curve has shifted closer to complete linearity over the entire temperature range as B is increased.

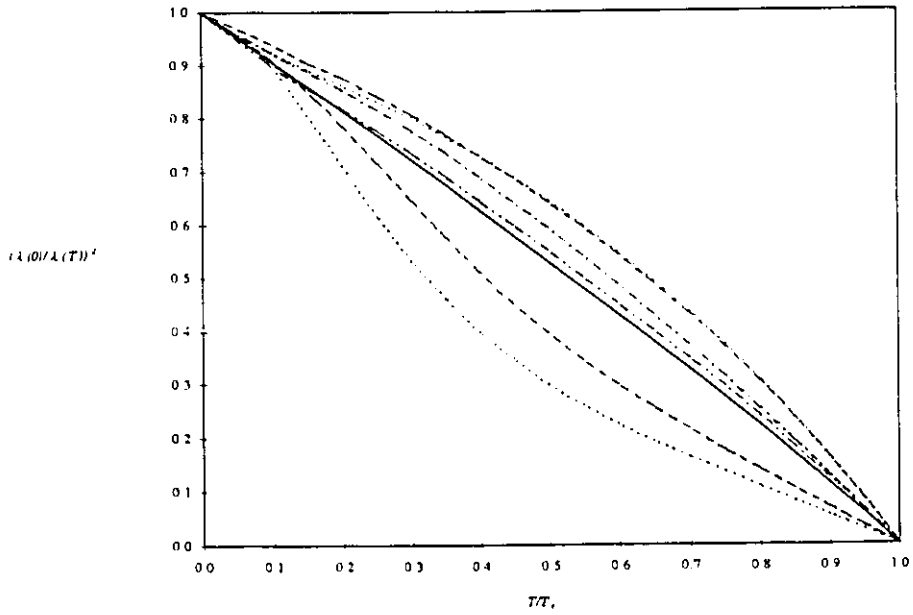

Figure 3.14 The penetration depth for different $d_{x^2-y^2}$ symmetry functions $\eta_{mn}(k)$. The solid curve is for $\eta_{10}(k)$; the top dashed curve is for $\eta_{30}(k)$; the top dotted curve is for $\eta_{50}(k)$; the dot-dashed curve is for $\eta_{70}(k)$; the dot-dot-dashed curve is for $\eta_{90}(k)$; the lower dotted curve is for $\eta_{40}(k)$; and the lower dashed curve is for $\eta_{10}(k)$. Note that all the even harmonics fall below the $\eta_{10}(k)$ line while all the odd harmonics are above the $\eta_{10}(k)$ curve.

For the mixed term $\eta_{52}(\mathbf{k})$, the low temperature behavior of $(\lambda(0)/\lambda(T))^2$ has curved in the opposite direction compared with the $\eta_{50}(\mathbf{k})$ case. The effect of band structure on an even harmonic is shown in Figure 3.16. Changing the next nearest neighbor hopping from $B=0$ to $B=0.45$ has the effect of moving the Fermi surface (Figure 2.1) away from the zeros of the gap (and areas where the gap is small), such that the gap now goes to zero only at points on the Fermi surface. This is seen in $(\lambda(0)/\lambda(T))^2$ as it is almost linear over the entire temperature range. Also shown in Figure 3.16 is the penetration depth for the mixed term

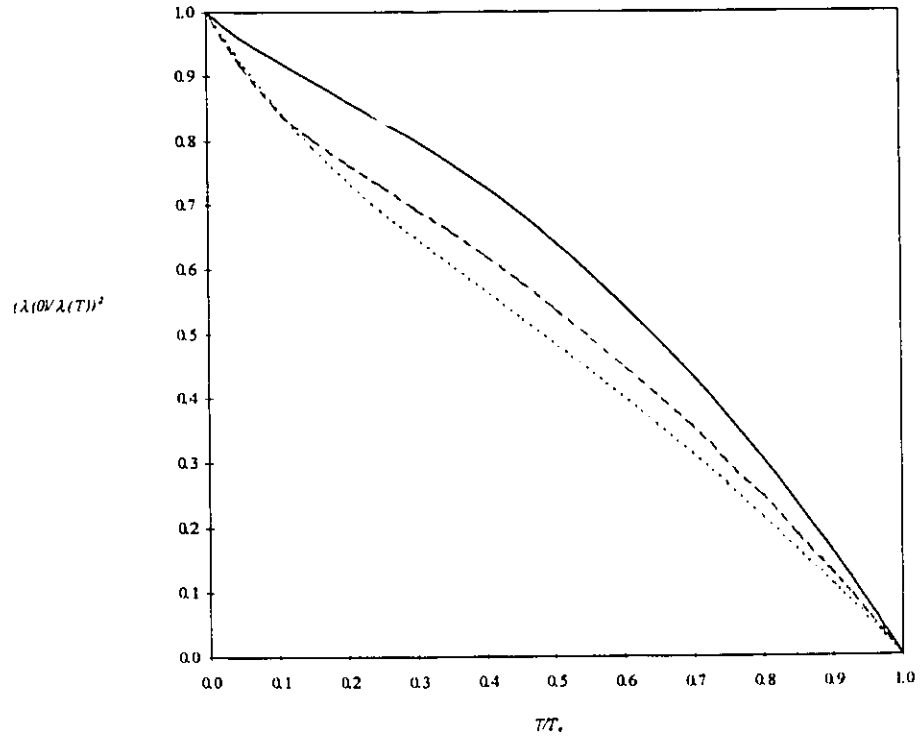

Figure 3.15 Penetration depth with the $\eta_{50}(k)$ harmonic with next nearest neighbor hopping. The solid curve has $B=0$; the dashed curve has $B=0.45$; and the dotted curve is for $\eta_{52}(k)$ with $B=0$.

$$\eta_{61}(\mathbf{k}) = \cos 6k_x \cos k_y - \cos k_x \cos 6k_y \quad . \qquad : 3.26$$

This curve has the same shape as the $\eta_{60}(\mathbf{k})$ case but is much more curved. It is seen that band structure has a much larger effect on $(\lambda(0)/\lambda(T))^2$ with the higher harmonics than with the lowest order one, $\eta_{10}(\mathbf{k})$.

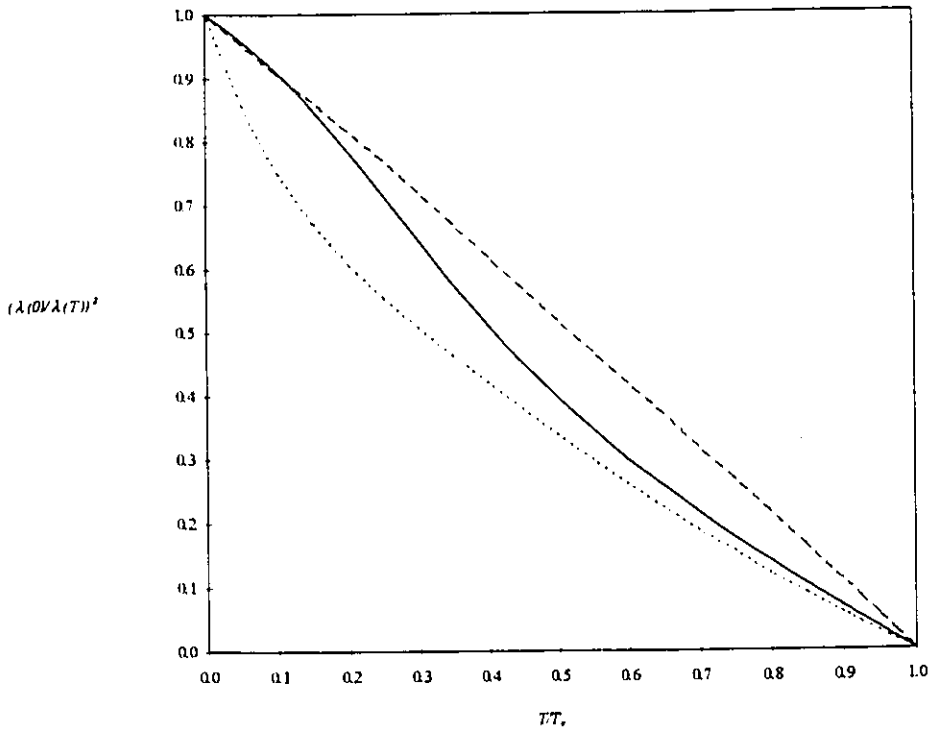

Figure 3.16 Penetration depth with the $\eta_{60}(\mathbf{k})$ harmonic with next nearest neighbor hopping. The solid curve has $B=0$; the dashed curve has $B=0.45$; the dotted curve has $B=1.0$; and the dotted curve is for $\eta_{61}(\mathbf{k})$ with $B=0$.

3.6. Summary

In conclusion, the penetration depth for a $d_{x^2-y^2}$ symmetry gap has been calculated and $\lambda^{-2}(T)$ is found to be linear in temperature and can be modeled satisfactorily by only the lowest order term $\eta_{10}(\mathbf{k}) = \cos k_x - \cos k_y$ of the entire expansion in $d_{x^2-y^2}$ functions, $\eta_{mn}(\mathbf{k})$. With an electron-boson interaction having this momentum dependence, the penetration depth both the temperature dependence and the magnitude are stable to changes in the band structure (within the limits that the superconducting state is well developed) but the effects are noticeable, with more drastic differences occurring in the higher order harmonic expansions. This is in contrast to conventional superconductors where the details of the band structure have no effect on the penetration depth. However the even order terms do not at all represent the experimentally measured penetration depth (Hardy *et al.*, 1993). The odd order harmonics (with no mixed terms, i.e., only including terms of the form $\eta_{m0}(\mathbf{k})$ where m is an odd integer) do represent the experimental results well with the best agreement coming at lower temperatures ($T \leq T_c$). Still the qualitative behavior of the penetration depth is described well by the lowest order harmonic $\eta_{10}(\mathbf{k})$, hence the addition of other terms can be, for the moment, regarded as fine tuning to the model.

The inclusion of impurity scattering has a large effect on the penetration depth both in the temperature dependence and the magnitude. Born scattering has

the smaller effect as the scattering has to reduce the critical temperature by half of the pure value in order to have noticeable deviations in $\lambda^{-2}(T)$ from linear to quadratic in temperatures near $T=0$. However, when scattering in the unitary limit ($V_I \to \infty$) is considered significant deviations in the low temperature penetration depth are already observed for a *4%* reduction in the critical temperature. This change in the penetration depth is seen long before the actual limit of $V_I \to \infty$ reached, hence even for small amounts of impurity scattering the temperature dependence of $\lambda^{-2}(T)$ will be noticeably different from linear behavior of the pure behavior. That is to say that Born scattering ($V_I \to 0$) is a special case not likely to make itself readily apparent. As discussed earlier the theoretical results agree quite well with the experimentally measured quantities.

The described model of a 2-dimensional $d_{x^2-y^2}$ symmetry superconductor with a gap of the form

$$\begin{aligned} \Delta(\mathbf{k}, i\omega) &= \Delta(\omega)\eta_{10}(\mathbf{k}) \\ &= \Delta(\omega)\left(\cos k_x - \cos k_y\right) \end{aligned} \qquad : 3.27$$

exhibits the same qualitative behavior for the penetration depth as seen in the high-T_c superconductors. Moreover, in the model studied here it is found that details of the momentum dependence of the electron-boson interaction can be seen in the penetration depth along with the details of the electronic band structure including the van Hove singularity in the density of states and the effect of impurity scattering in the range of the weakest possible scattering to the strongest possible

scattering. The main features which are indicative of a $d_{x^2-y^2}$ symmetry in the gap is that at low temperatures $\lambda^{-2}(T)$ is linear in temperature for the pure case and has a quadratic temperature dependence when impurity scattering is present.

4. Optical Conductivity

The optical conductivity within this 2-dimensional $d_{x^2-y^2}$ symmetry superconductor model will now be calculated. The optical conductivity at zero temperature in conventional superconductors has a delta function peak at zero frequency (this is the zero dc resistance of a superconductor) and then as frequency increases there is no optical conductivity (or optical absorption) until the frequency reaches a value of $2\Delta_0$, where Δ_0 is the superconducting gap (Schrieffer, 1963). Then there is a rise to a local maximum and then a drop-off as the frequency is further increased. At high enough frequencies the optical conductivity in the superconducting state will asymptotically approach the optical conductivity of the normal state. This gap of width $2\Delta_0$ in the optical conductivity spectrum is due to the gap Δ_0 in the electronic excitation spectrum. The gap in the optical

spectrum is $2\Delta_0$ since an electron-hole pair must be created in order for the photon to be absorbed, hence there is one Δ_0 energy required for the electron and one for the hole.

This gap in the optical absorption spectrum is not the behavior when excitations with energies less than Δ_0 are possible. Then the optical absorption will begin at a frequency which scales with the minimum positive value of the gap. Thus for a d-wave superconductor in which the gap goes to zero on the Fermi surface the optical conductivity will be finite for all frequencies since excitations of infinitely small energies are possible. Within this scenario it is not possible to pin down the value of the gap as one half of the energy at which the optical absorption begins. This type of behavior is observed in the high T_c superconductors (Sumner *et al.*, 1993; Kim *et al.*, 1993a, 1993b, 1993c; Basov *et al.* 1994, 1995; Zhang *et al.* 1994).

Once again as with any property of a strong coupling superconductor the Eliashberg equations must be solved. The optical conductivity also requires knowledge of the current-current correlation function which was introduced in the last chapter on the London penetration depth. However for the case of the optical conductivity one requires knowledge of the current-current correlation function on the real frequency axis. Recall that the penetration depth only needed the current-current correlation function at zero frequency, and hence a direct substitution of $Z(\mathbf{k},i\omega_n)$ and $\phi(\mathbf{k},i\omega_n)$ obtained from the Eliashberg equations could be performed.

For the optical conductivity this is not the case. Thus there are two options to obtain the optical conductivity. The first is to solve the Eliashberg equations on the real axis for the complex functions $Z(\mathbf{k},\omega)$ and $\phi(\mathbf{k},\omega)$, hence obtaining the Green's function on the real frequency axis and thus computing the current-current correlation function. For the case of isotropic superconductors the solution of the Eliashberg equations on the real axis for $Z(\omega)$ and $\phi(\omega)$ can be accomplished with a reasonable amount of computer time. However this is not possible for superconductors with more complicated symmetries. Another possibility is to solve the Eliashberg equations on the imaginary axis and then to calculate the current-current correlation function on the imaginary axis. Once the current-current correlation function is known on the imaginary frequency axis it can be analytically continued to the real frequency axis by the Padé approximation (Bickers, *et al.*, 1990). This method does have the disadvantage of failing at high temperatures and/or high frequencies but at low temperatures and frequencies it has the advantage that results can be obtained quicker than a real axis solution. These results do give excellent agreement with the real axis solutions (see Nicol *et al.*, 1991 for a comparison). The real axis solution in principle can give results at any temperature and frequency however in all but the simplest symmetries the solution will take an extraordinary amount of computer time (Jiang, 1992). Due to the complicated symmetry of the superconducting state and van Hove singularity in the 2-dimensional $d_{x^2-y^2}$ symmetry model considered here it is the second

technique of analytically continuing the current-current correlation function which will be followed.

4.1. The Optical Conductivity

The optical conductivity is the response of a material to an external electromagnetic field just as the magnetic penetration depth seen in the previous chapter. The difference is that the penetration depth is the response to a static electromagnetic field and the optical conductivity is the response to a time varying electromagnetic field. An expression for the optical conductivity will now be derived.

From eq.'s 3.2 and 3.4 the total response function is

$$K_{\mu\nu}(\mathbf{q},i\nu_m) = K^{(p)}_{\mu\nu}(\mathbf{q},i\nu_m) - K^{(p)^N}_{\mu\nu}(\mathbf{q},0) \qquad : 4.1$$

where $K_{\mu\nu}(\mathbf{q},i\nu_m)$ is given by eq. 3.10. Again since the Green's function is peaked about the Fermi surface and the fact that the momentum of optical photons is much less than the Fermi momentum one takes $\mathbf{q}\to 0$, thus giving

$$K_{\mu\nu}(i\nu_m) = K^{(p)}_{\mu\nu}(i\nu_m) - K^{(p)^N}_{\mu\nu}(0) \quad , \qquad : 4.2$$

and

$$K^{(p)}{}_{\mu\nu}(i\nu_m) = 8\pi e^2 T \sum_{\mathbf{k},i\omega_n} tr\left\{\hat{\gamma}_\mu(\mathbf{k})\hat{G}(\mathbf{k},i\omega_n + i\nu_m)\hat{\gamma}_\nu(\mathbf{k})\hat{G}(\mathbf{k},i\omega_n)\right\}$$

$$= 8\pi e^2 T \sum_{\mathbf{k},i\omega_n} \frac{\partial\varepsilon_\mathbf{k}}{\partial k_\mu}\frac{\partial\varepsilon_\mathbf{k}}{\partial k_\nu} \frac{\varepsilon_\mathbf{k}^2 - \tilde{\omega}_\mathbf{k}(\omega_n)\tilde{\omega}_\mathbf{k}(\omega_n+\nu_m) + \phi_\mathbf{k}(\omega_n)\phi_\mathbf{k}(\omega_n+\nu_m)}{\left[\varepsilon_\mathbf{k}^2 + \tilde{\omega}_\mathbf{k}^2(\omega_n) + \phi_\mathbf{k}^2(\omega_n)\right]\left[\varepsilon_\mathbf{k}^2 + \tilde{\omega}_\mathbf{k}^2(\omega_n+\nu_m) + \phi_\mathbf{k}^2(\omega_n+\nu_m)\right]} \quad :4.3$$

where all references to $\mathbf{q}\to 0$ have been dropped. The conductivity is given by (Nam, 1967a)

$$\sigma_{\mu\nu}(\omega) = \frac{i}{4\pi\omega} K_{\mu\nu}(i\nu_m \to \omega + i0^+) \quad :4.4$$

where ω is the frequency and $\sigma_{\mu\nu}(\omega)$ is the optical conductivity, and $K_{\mu\nu}(i\nu_m\to\omega+i0^+)$ is the analytic continuation of $K_{\mu\nu}(i\nu_m)$ from here on written simply as $K_{\mu\nu}(\omega)$.

This is the point at which one chooses to calculate $K_{\mu\nu}(\omega)$ directly from Z and ϕ found by solution of the real axis Eliashberg equations or to calculate $K_{\mu\nu}(i\nu_m)$ and analytically continue this function to the real axis by Padé approximation. The latter is the method used here.

Since $K_{\mu\nu}(\omega)$ is a complex function $\sigma_{\mu\nu}(\omega)$ is also complex and can be written as

$$\sigma_{\mu\nu}(\omega) = -\frac{1}{4\pi\omega}\operatorname{Im}K_{\mu\nu}(\omega) + \frac{i}{4\pi\omega}\operatorname{Re}K_{\mu\nu}(\omega) \quad . \quad :4.5$$

From 4.2 and the fact that $K^{(p)^N}_{\mu\nu}(0)$ is a real function:

$$\sigma_{\mu\nu}(\omega) = -\frac{1}{4\pi\omega}\operatorname{Im}K^{(p)}_{\mu\nu}(\omega) + \frac{i}{4\pi\omega}\left[\operatorname{Re}K^{(p)}_{\mu\nu}(\omega) - K^{(p)^N}_{\mu\nu}(0)\right] \quad . \quad :4.6$$

From 4.3 and 3.18 and by symmetry then

$$\sigma_{xx}(\omega) = \sigma_{yy}(\omega) = \sigma(\omega)$$
$$\sigma_{xy}(\omega) = \sigma_{yx}(\omega) = 0 \quad . \qquad : 4.7$$

The expression 4.6 for the optical conductivity along with 4.3 is a completely general expression that can be applied to calculate the conductivity for any band structure and any symmetry of the electron-boson interaction and any boson spectrum used in the solution of the Eliashberg equations for Z and ϕ. It can also be used to calculate the optical conductivity in the normal state and in the superconducting state, depending on whether or not one substitutes Z and ϕ from solution of the Eliashberg equations or takes $\phi=0$ and calculates Z in the normal state.

If one chooses to calculate $\sigma(\omega)$ on the real axis directly, rather than to calculate it on the imaginary axis and obtain the conductivity by a Padé approximation, the spectral representation of the Green's function must be used. The solutions to the Eliashberg equations on the real axis $Z(\mathbf{k},\omega)$ and $\phi(\mathbf{k},\omega)$, which are both complex functions, are also needed. The Green's function is then known on the real axis and one can perform the Matsubara frequency summation in 4.3 by using the spectral representation:

$$\hat{G}(\mathbf{k},i\omega_n) = \int_{-\infty}^{+\infty} dx \frac{\hat{A}(\mathbf{k},\omega)}{i\omega_n - x} \quad . \qquad : 4.8$$

Here $\hat{A}(\mathbf{k},i\omega_n)$ is the spectral function defined by

$$\hat{A}(\mathbf{k},\omega) = -\frac{1}{\pi}\mathrm{Im}\,\hat{G}(\mathbf{k},\omega + i0^+) \quad . \qquad : 4.9$$

Then by using the identity (Fetter and Walecka, 1971)

$$\frac{1}{\beta}\sum_{i\omega_n}\frac{1}{i\omega_n - a} = f^-(a) \qquad : 4.10$$

where a is real number and $f^-(x)$ is the Fermi function given by

$$f^-(x) = \frac{1}{1+e^{\beta x}} \quad . \qquad : 4.11$$

The Matsubara frequency summation in 4.3 can be performed. This gives

$$K_{\mu\nu}^{(p)}(i\nu_m) = 8\pi e^2 \sum_{\mathbf{k}} \frac{\partial\varepsilon_{\mathbf{k}}}{\partial k_\mu}\frac{\partial\varepsilon_{\mathbf{k}}}{\partial k_\nu}\int_{-\infty}^{+\infty} dx f^-(x) tr\left\{\hat{A}(\mathbf{k},x)\left[\hat{G}(\mathbf{k},x+i\nu_m)+\hat{G}(\mathbf{k},x-i\nu_m)\right]\right\} \quad . \qquad : 4.12$$

This expression can be analytically continued directly giving

$$K_{\mu\nu}^{(p)}(\omega+i0^+) = 8\pi e^2 \sum_{\mathbf{k}} \frac{\partial\varepsilon_{\mathbf{k}}}{\partial k_\mu}\frac{\partial\varepsilon_{\mathbf{k}}}{\partial k_\nu}\int_{-\infty}^{+\infty} dx f^-(x) \times tr\left\{\hat{A}(\mathbf{k},x)\times\left[\hat{G}(\mathbf{k},x+\omega+i0^+)+\hat{G}(\mathbf{k},x-\omega-i0^+)\right]\right\} \qquad : 4.13$$

and hence giving the optical conductivity immediately

$$\sigma_{\mu\nu}(\omega) = \frac{i}{4\pi\omega}\left[K_{\mu\nu}^{(p)}(\omega+i0^+) - K_{\mu\nu}^{(p)^N}(0)\right] \quad . \qquad : 4.14$$

As can be seen, the gain of this method (namely that 4.13 is valid at any temperature and frequency) is overshadowed by other complications in all but the simplest cases. Comparing 4.13 with 4.3, the summation over Matsubara frequencies has been replaced by an integral over a continuous variable and the integrand is now a complex function where in 4.3 it is a real function. One now requires the solution of the real axis Eliashberg equations as opposed to the

simpler solution of the imaginary axis equations. The advantage of 4.13 over 4.3 is that when the momentum dependence of the integrand is simple or non-existent then the summation over **k** can be performed. A single integration can be evaluated to give the conductivity without the added complication of a Padé approximation at any stage. Hence, in this work, due to the complicated **k** dependence of both the band structure and the superconducting gap function, the response function will be calculated according to 4.3 and the optical conductivity will be obtained by a Padé approximation (applied to $K^{(p)}(i\nu_m)$ to give $K^{(p)}(\omega)$ and hence the optical conductivity $\sigma(\omega)$) as described in section 2.2.5.

Results for the optical conductivity will now be shown. Throughout this chapter the boson spectrum used is a truncated Lorentzian centred at ω_0 with width Γ_0 and truncation width Γ_c given by

$$\Phi(\Omega) = \begin{cases} A\left(\dfrac{1}{(\Omega-\omega_o)^2+\Gamma_o^2} - \dfrac{1}{\Gamma_c^2+\Gamma_o^2}\right), & |\Omega-\omega_o| < \Gamma_c \\ 0, & |\Omega-\omega_o| > \Gamma_c \end{cases} \qquad : 4.15$$

where ω_0=50 meV, Γ_0=5 meV, Γ_c =15 meV and is shown in Figure 4.1.

The parameters for the calculation are t=100 meV, B=0, g=1, and $\Phi(\Omega)$ from Figure 4.1 but with A chosen such that $T^0_c \approx 100$ K when μ=0 and n_I=0 and $T^0_c \approx 90$ K when μ=25 meV and n_I=0. The c-axis lattice parameter is taken to be 10^{-7} cm. The $\eta_{10}(\mathbf{k})$ symmetry function has been used throughout since this is the simplest $d_{x^2-y^2}$ symmetry function which incorporates all of the important features

of the model. It also gave the best results in regards to the penetration depth and hence will give the most consistent results between the conductivity and the penetration depth.

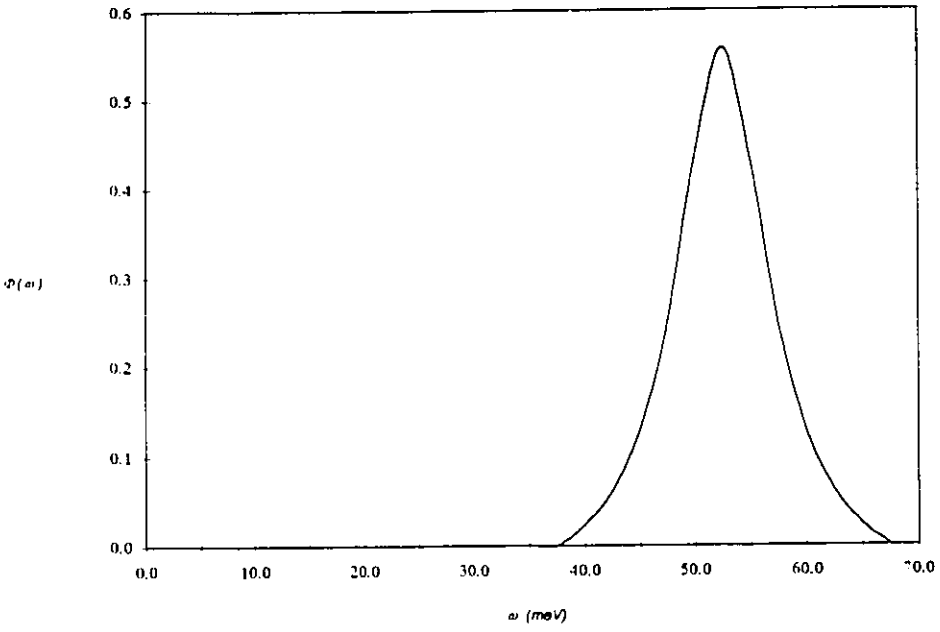

Figure 4.1 The boson spectrum as in 4.15 with $A=1$, $\omega_0=50$ *meV*, $\Gamma_0=5$ *meV*, $\Gamma_c=15$ *meV*.

The solution of the Eliashberg equations 2.95 to 2.98 give $Z(\mathbf{k},i\omega_n)$ and $\phi(\mathbf{k},i\omega_n)$, where ϕ is related to the gap function Δ by $\phi=Z\Delta$. These are directly substituted into 4.3 to calculate the response function on the imaginary axis which is then analytically continued to the real axis by the Padé approximation. Some general notes on the results of the Padé approximation will now be discussed. First since an N-point Padé approximation is given by a continued fraction (see equation 2.71) it is not always the case that choosing a larger N gives better

results. The Padé approximation should give the best results for frequencies $\omega << \nu_N = 2N\pi T$, the maximum boson frequency. Typically in the work here $N \sim 80$, $T \sim 0.7\ meV$ and hence the region where the Padé approximation should give the best results is $\omega << 350\ meV$.

The optical conductivity in the normal state is found to be stable (i.e., the shape and the magnitude does not change) over the entire frequency range considered to different Padé approximants. The optical conductivity in the superconducting state is stable for all frequencies with the exception of the low frequencies where changes in the magnitude are evident with different Padé approximants. Hence the optical conductivity in the superconducting state will be cutoff for frequencies less than $0.5\ meV$. This does not present a problem since this is a study of the optical conductivity and this region cannot be probed by far infrared experiments (Basov, 1995).

Also it was not possible to obtain results for the conductivity with no impurity scattering. This is due to the fact that with no impurity scattering to conserve momentum, then only phonons are left to conserve momentum. In the case here the minimum phonon energy is $35\ meV$ and the greatest number of phonons are centred around $50\ meV$ (see 4.15) and hence the photon energy will have to exceed this value in order to be absorbed.

Now results for different scattering strengths and concentrations and chemical potential will be shown. All calculations have been done at a temperature $T/T_c=0.1$ as the Padé approximation is best at low temperatures.

4.2. *Impurity Scattering Effects - Born Scattering*

The optical conductivity is shown first with the inclusion of impurity scattering in the Born approximation. The real part of the conductivity for three different scattering strengths ($T_c^{(Born)}/T_c^0=0.90,\ 0.80,\ 0.54$) is shown in Figure 4.2 for $\mu=0$. First concentrating on the normal state conductivity (Figure 4.2a) it is seen to be Drude like at low frequencies due to the electronic part of the system. For example a fit to a Drude conductivity,

$$\mathrm{Re}\,\sigma_{Drude}(\omega)=\frac{\sigma_0}{1+\omega^2\tau^2} \qquad : 4.16$$

where $\sigma_0\approx 23.47\times10^{14}\ s^{-1}$ is the dc conductivity and $\tau\approx 1.08\times10^{-13}\ s$ is the scattering time, is shown as a dot-dashed line for comparison with the solid line ($T_c^{(Born)}/T_c^0=0.90$) in Figure 4.2. The fit is excellent at low frequencies and less so at higher frequencies. This is due to the phonon assisted absorption (Dolgov *et al.*, 1990) at higher frequencies. Similar fits to the other two curves have been performed and the results are summarized in Table 4-1. The low frequency

behavior is that expected for a normal metal with the dc conductivity decreasing and the width of the peak increasing as the impurity concentration is increased.

$T_c^{(Born)}/T_c^0$	$\sigma_0\,(\times 10^{14}\,s^{-1})$	$\tau\,(\times 10^{13}\,s)$
0.90	*23.47*	*1.108*
0.89	*12.85*	*0.59*
0.54	*7.06*	*0.33*

Table 4-1 Parameters for the Drude conductivity fits to the normal state conductivity shown in Figure 4.2a.

The conductivity in the superconducting state (Figure 4.2b) has a much narrower peak at $\omega=0$ than in the normal state. This peak broadens as the impurity concentration is increased. There is no gap in the optical conductivity spectrum for any frequency. This is in contrast to an isotropic s-wave superconductor. For the boson spectrum under consideration (equation 4.15) a conventional superconductor has a gap in the optical absorption of twice the superconducting gap (Bickers *et al.*, 1990). Here there is obvious no evidence of superconductivity in the optical spectrum. This is not to say that superconductivity is not present since it is known before hand by the fact that the superconducting gap function is not zero everywhere in the Brillouin zone. It is to say that superconductivity is not present in the conventional sense (i.e., a gap of $2\Delta_0$ in the optical absorption spectrum).

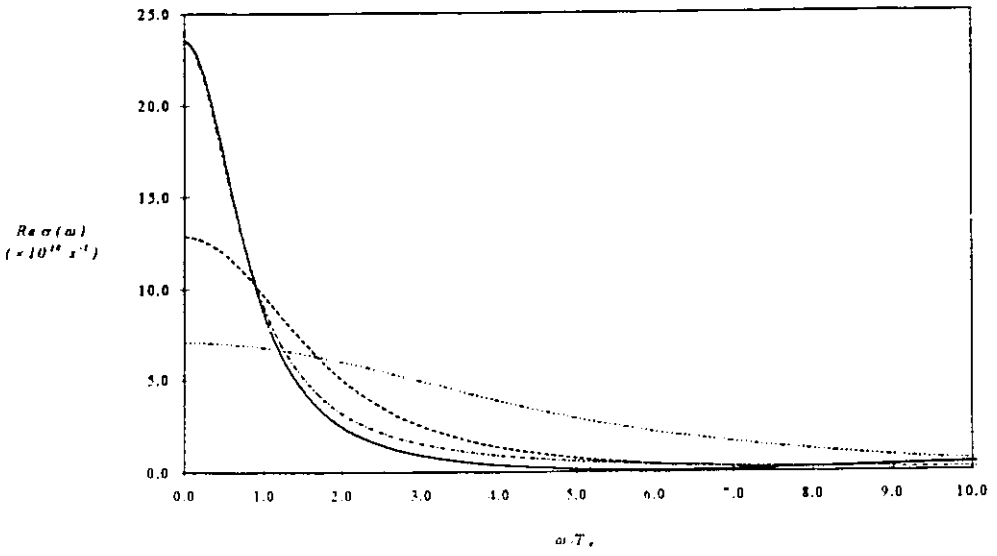

(a)

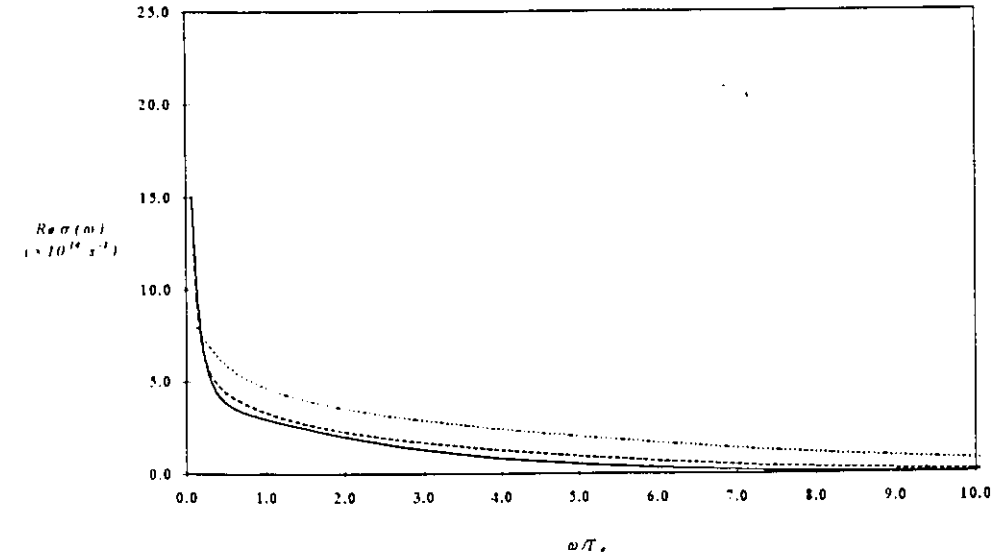

(b)

Figure 4.2 The real part of the conductivity in the normal state (a) and the superconducting state (b) for three different impurity concentrations in the Born approximation and $\mu=0$. The solid curve is $T_c/T_c^0=0.90$; the dashed curve is $T_c/T_c^0=0.79$; the dotted curve is $T_c/T_c^0=0.54$. The dot-dashed curve in (a) is A Drude conductivity fit to the $T_c/T_c^0=0.90$ curve with parameters $\sigma_0\approx 23.47\times10^{14}\ s^{-1}$ and $\tau\approx 1.08\times10^{-13}\ s$.

The phonon structure is seen at higher frequencies and is shown in Figure 4.3 for the single case of $T_c^{(Born)}/T_c^0=0.90$. There is an increase in the normal state conductivity at $\omega\approx\omega_0\approx 6.0T_c$ due to phonon assisted absorption. This increase has shifted in the superconducting state to a significantly higher frequency $\approx 10.0T_c$. A large shift such as this is seen for conventional superconductors and it is given by twice the superconducting gap. Such a large shift in the onset of phonon assisted absorption in a d-wave superconductor is not seen from a calculation of the conductivity on the real axis (Carbotte *et al.*, 1995) with a constant density of states. However this large shift is stable to different Padé approximants. Hence it is unlikely to be an artifact of the analytic continuation. Also a large shift is seen for all the impurity strengths, impurity concentrations and chemical potentials studied. Thus it appears to be a feature of this model. Since this large shift is always present it will only be shown for the single set of parameters here.

The ratio of the conductivity in the superconducting state to the normal state is shown in Figure 4.4. The features associated with the phonon assisted absorption are readily seen. There is a maximum at $\omega\approx 6.0T_c$ due to the onset of phonon assisted absorption in the normal state. There is a minimum at $\omega\approx 10.0T_c$ due to the onset of phonon assisted absorption in the superconducting state. At high enough energies the ratio will approach one. This is the only figure of the ratio as the features seen in it do not change significantly between the parameter sets.

The imaginary part of the conductivity for three different impurity concentrations is shown in Figure 4.6. The normal state (Figure 4.6a) is that expected for a Fermi liquid, increasing linearly from zero at $\omega=0$ and crossing over to a ω^{-1} behavior as ω increases. The position of the peak scales as the inverse of the scattering time and thus becomes broader as the impurity concentration is increased. The superconducting curve (Figure 4.2b) is much more sharply peaked and then approaches the normal state curve at higher frequencies. The imaginary

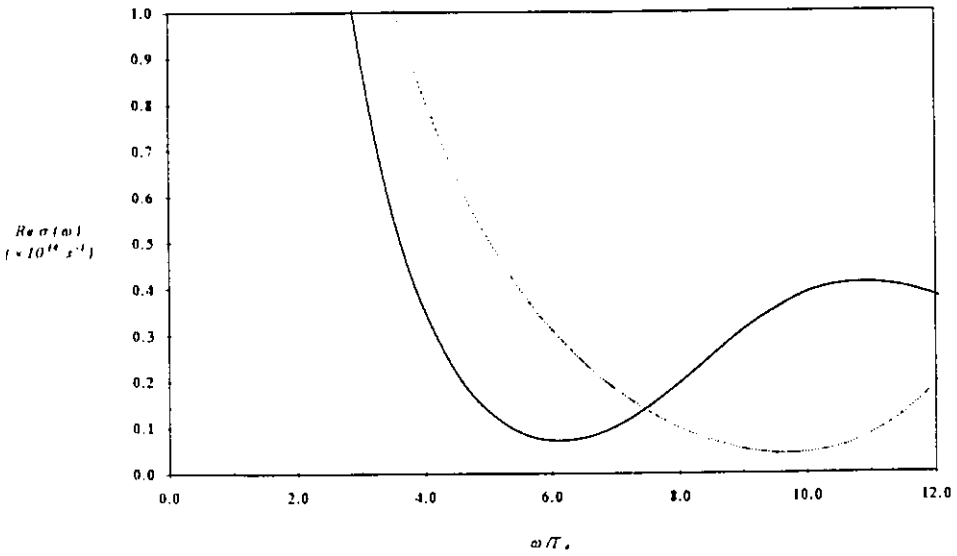

Figure 4.3 The real part of the conductivity in the normal state (solid line) and the superconducting state (dotted line) for $T_c/T_c^0=0.90$. The onset of phonon assisted absorption occurs at $\omega=\omega_0=50\ meV \approx 6.0T_c$ in the normal state and at $\omega \approx 10.0T_c$ in the superconducting state.

part of the conductivity will only be shown for the case here since it does not show any significant different behavior for the other sets of parameters.

The next figure shows the optical conductivity calculated with finite chemical potential (μ=*25 meV*) and three different impurity concentrations in the Born approximation ($T_c^{(Born)}/T_c^0$=*0.90, 0.77, 0.59*). The real part of the conductivity is shown in Figure 4.5a. Again the normal state conductivity is Drude like with parameters given in Table 4-2. Comparing the dc conductivities with those for μ=*0* (Table 4-1) it is seen that they have increased by ~*50%*. This is due to the increased number of carriers as one moves away from half-filling and the fact that the dc conductivity is proportional to this number.

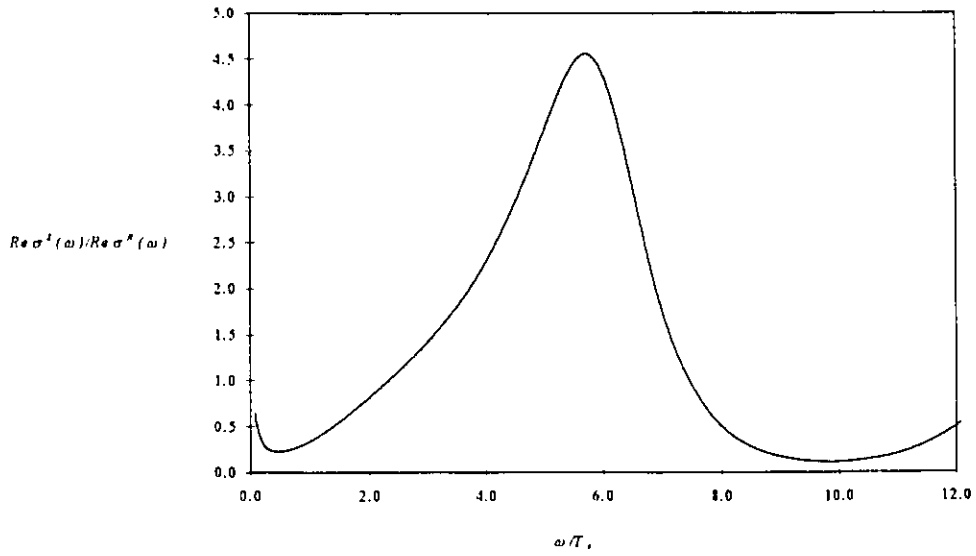

Figure 4.4 The ratio of the real part of the conductivity in the superconducting state to the normal state for T_c/T_c^0=*0.90*. Note the maximum at ≈*6.0* and minimum at ≈*10.0* due to the onset of phonon assisted absorption in the normal state and the superconducting state respectively.

$T_c^{(Born)}/T_c^0$	$\sigma_0 (\times 10^{14}\, s^{-1})$	$\tau (\times 10^{-13}\, s)$
0.90	38.26	1.94
0.77	17.82	0.90
0.59	10.70	0.54

Table 4-2 Parameters for the Drude conductivity fits to the normal state conductivity shown in Figure 4.5a.

There is a sharp peak at $\omega=0$ in the superconducting state (Figure 4.5b) as in the case with $\mu=0$. Also there is no evidence of the superconducting gap in the optical spectrum.

Other than the increase of the dc conductivity over that of the $\mu=0$ case there is little difference between the optical conductivity with $\mu=0$ and that with $\mu=25\ meV$. The normal state conductivity is Drude like for low frequencies and there is no evidence of superconductivity in the optical conductivity of the superconducting state.

The main feature to be seen in the conductivity is that there is no presence or indication of a gap in the optical spectrum. This is different from the case of a conventional superconductor where the superconducting gap can be obtained directly from the optical conductivity.

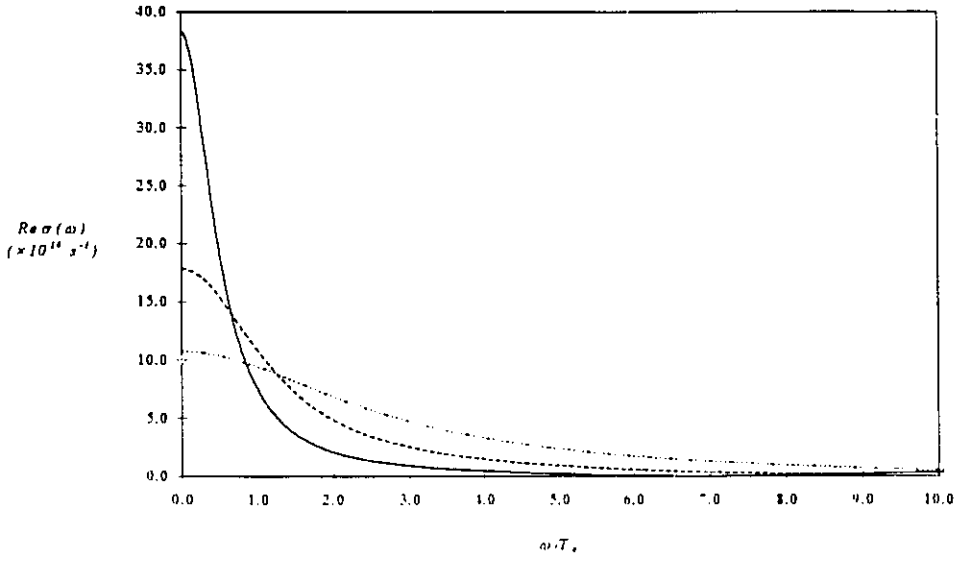

(a)

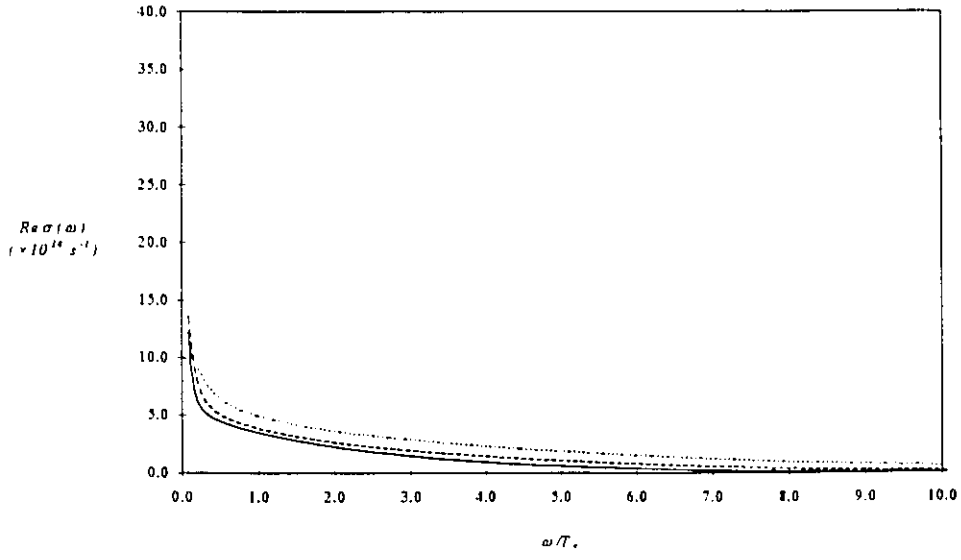

(b)

Figure 4.5 The real part of the conductivity in the normal state (a) and the superconducting state (b) for three different impurity concentrations in the Born approximation and finite chemical potential (μ=25 meV). The solid curve is T_c/T_c^0=0.90; the dashed curve is T_c/T_c^0=0.77; the dotted curve is T_c/T_c^0=0.59.

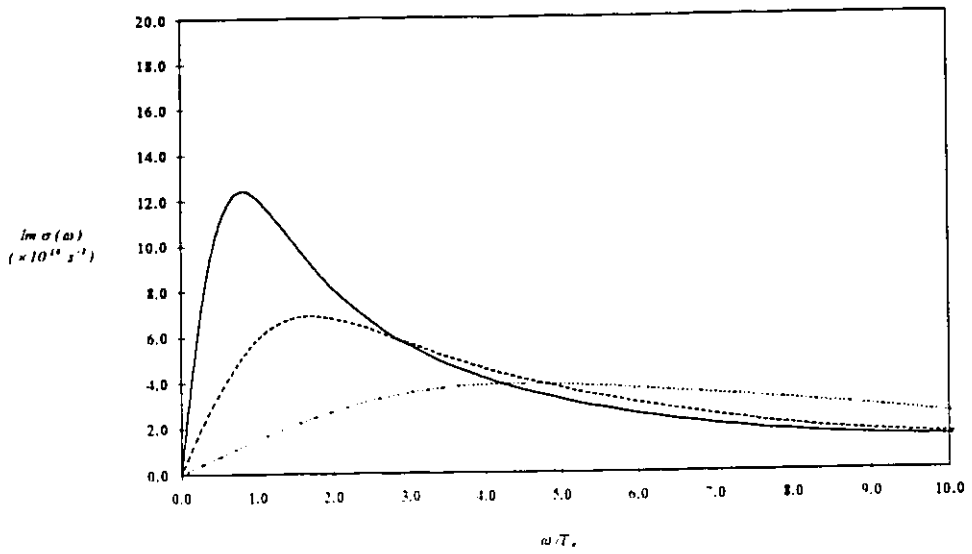

(a)

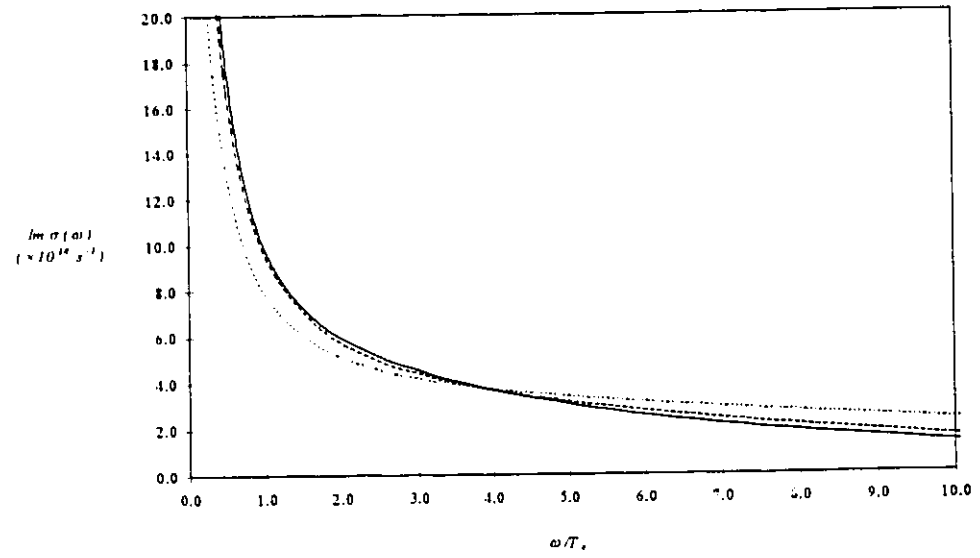

(b)

Figure 4.6 The imaginary part of the conductivity in the normal state (a) and the superconducting state (b) for three different impurity concentrations in the Born approximation and $\mu=0$. The solid curve is $T_c/T_c^0=0.90$; the dashed curve is $T_c/T_c^0=0.79$; the dotted curve is $T_c/T_c^0=0.54$.

4.3. Impurity Scattering Effects - Unitary Scattering

The optical conductivity is now calculated for three different impurity concentrations in the unitary limit. The real part of the conductivity is shown in Figure 4.7 for $\mu=0$ and a temperature and impurity concentration such that $T_c/T_c^0=0.90,\ 0.79,\ 0.71$. The normal state conductivity (Figure 4.7a) is Drude like at low frequencies with parameters as shown in Table 4-3. Also the peak at zero frequency is increasing in width and decreasing in magnitude as the impurity concentration is increased just as expected for a normal metal.

$T_c^{(unitary)}/T_c^0$	$\sigma_0\ (\times 10^{14}\ s^{-1})$	$\tau\ (\times 10^{-13}\ s)$
0.90	63.82	3.56
0.78	29.21	1.69
0.71	20.82	1.22

Table 4-3 Parameters for the Drude conductivity fits to the normal state conductivity shown in Figure 4.7a.

Note that for the same reduction in the critical temperature with unitary scattering and for Born scattering (compare Figure 4.2, Figure 4.7 and Table 4.1 and Table 4-3) that unitary scattering gives a less reduction of the dc conductivity and also has a substantially larger scattering time. This behavior is precisely that seen in experiments on Ni and Zn doped Y-Ba-Cu-O (Bonn, *et al.*, 1994). It is found that Ni provides as much scattering as Zn but has a much smaller effect on the critical

temperature. This is seen in both the penetration depth and the conductivity experiments. This same behavior is seen for the model under consideration in this work both in the conductivity presented here and in the penetration depth in the last chapter. This difference between Ni and Zn impurities stems from the fact that in this theory there is a non-trivial difference between Born scattering and unitary scattering (see sec. 2.4). This difference is not seen in the constant density of states approximation but it is seen here where no such approximation is made.

In the superconducting state (Figure 4.7b) the conductivity exhibits a shoulder whose magnitude is independent of impurity concentration for low frequencies and then a drop-off. This shoulder at low frequencies has been predicted for a $d_{x^2-y^2}$ symmetry d-wave superconductor with impurity scattering in the unitary limit (see Hirschfeld *et al.*, 1994). This feature can be taken as evidence of superconductivity if the superconductivity is accompanied by the presence of scattering centres in the unitary limit.

The optical conductivity with unitary scattering and finite chemical potential is now calculated. This is shown in Figure 4.8 for $\mu=25\ meV$ and the impurity concentrations such that $T_c/T_c^0=0.87,\ 0.82,\ 0.73$. The real part of the conductivity is shown in Figure 4.8a. The normal state again is Drude like with the parameters as shown in Table 4-4. The superconducting state (Figure 4.8b) exhibits a shoulder at low frequency characteristic of unitary scattering.

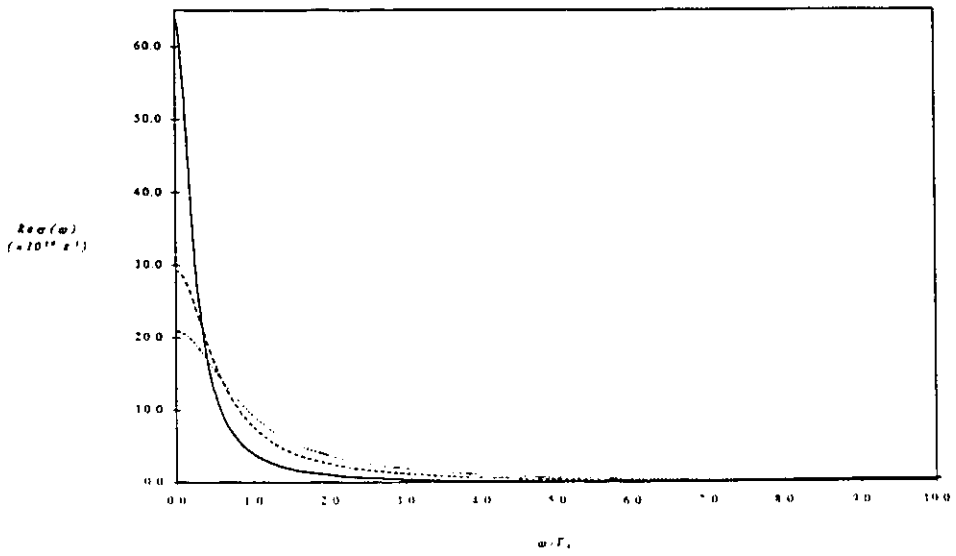

(a)

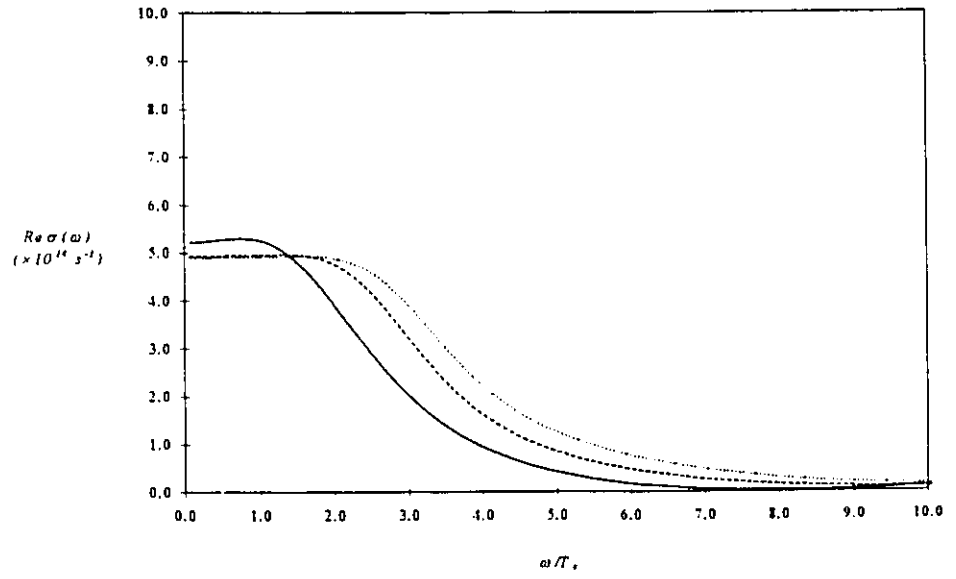

(b)

Figure 4.7 The real part of the conductivity in the normal state (a) and the superconducting state (b) for three different impurity concentrations in the unitary limit and $\mu=0$. The solid curve is $T_c/T_c^0=0.90$; the dashed curve is $T_c/T_c^0=0.79$; the dotted curve is $T_c/T_c^0=0.71$. Note the difference in the y-axis scales between the normal state, (a) and the superconducting state, (b).

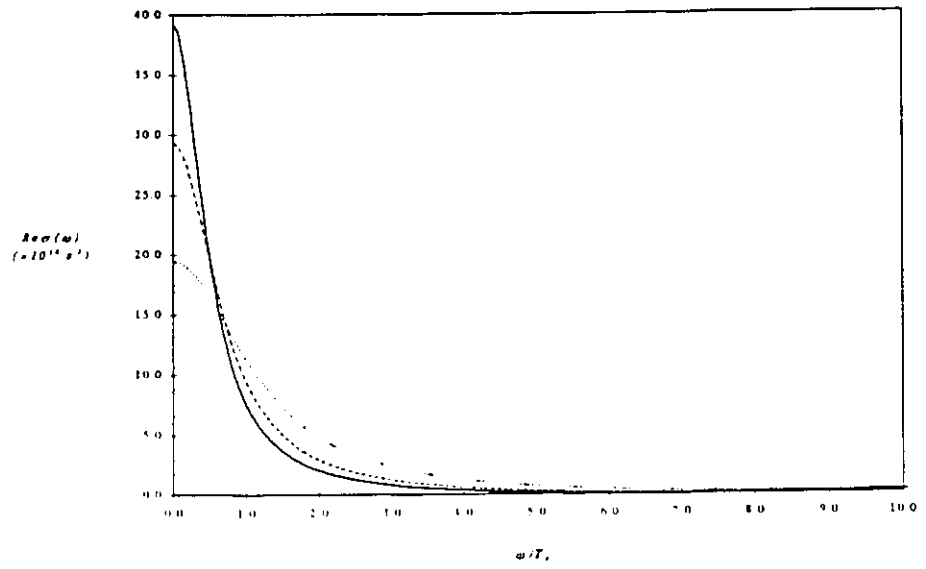

(a)

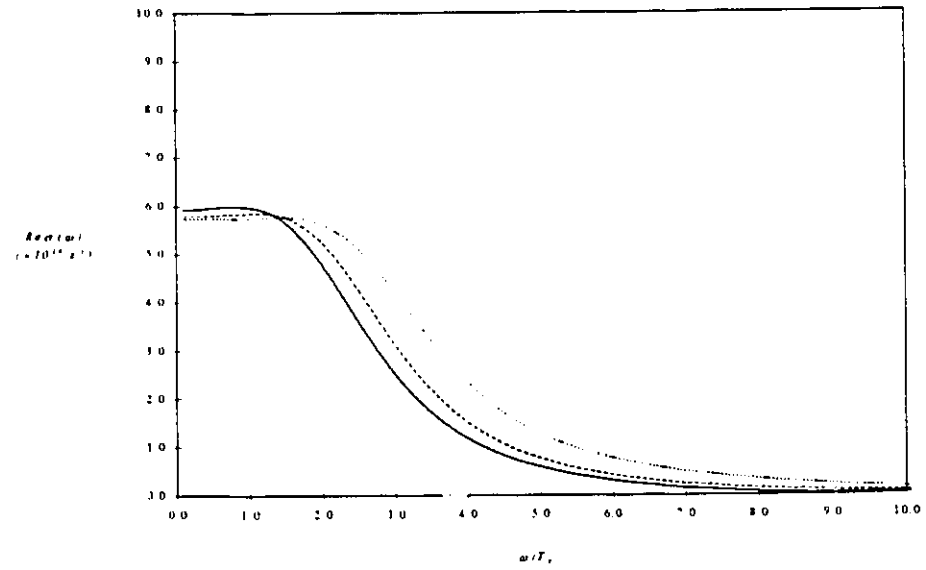

(b)

Figure 4.8 The real part of the conductivity in the normal state (a) and the superconducting state (b) for three different impurity concentrations in the unitary limit and μ=25 meV. The solid curve is T_c/T_c^0=0.87; the dashed curve is T_c/T_c^0=0.82; the dotted curve is T_c/T_c^0=0.73. Note the difference in the y-axis scales between the normal state, (a) and the superconducting state, (b).

$T_c^{(unitary)}/T_c^0$	σ_0 ($\times 10^{14}$ s^{-1})	τ ($\times 10^{-13}$ s)
0.87	*39.14*	*2.0*
0.82	*29.28*	*1.5*
0.73	*19.42*	*1.0*

Table 4-4 Parameters for the Drude conductivity fits to the normal state conductivity shown in Figure 4.8a.

The behavior of the optical conductivity with unitary scattering and finite chemical potential is not different from that with zero chemical potential. In both cases unitary scattering has a less drastic effect on the dc conductivity than Born scattering and now the presence of superconductivity is seen in the optical conductivity if there is also impurity scattering in the unitary limit present.

4.4. Impurity Scattering Effects - Arbitrary Strength

The behavior of the conductivity as going from weak to strong scattering is shown in Figure 4.9. Here the impurity concentration has been adjusted such that T_c/T_c^0 remains fixed at *0.90* while the scattering potential V_I, has been varied through *0* (Born scattering - see Figure 4.2), *20.0 meV*, *100 meV*, *1000 meV*, ∞ (unitary scattering - see Figure 4.7). The normal state conductivity is shown in Figure 4.9a for the three values of V_I. It is Drude like with the parameters as

shown in Table 4-5. From this table one can see the differences of scattering in the Born limit to that of unitary scattering both on the dc conductivity and on the scattering time. Note that unitary scattering has a less drastic effect on the dc conductivity and the scattering time than Born scattering for the same reduction in the critical temperature. Comparing the solid line of Figure 4.2 (Born scattering, $V_I \rightarrow 0$) with the dotted line of Figure 4.9 ($V_I = 20\ meV$), it is seen that these curves are both similar in shape and magnitude and there are no features which are peculiar to any of them.

V_I (meV)	σ_0 ($\times 10^{14}\ s^{-1}$)	τ ($\times 10^{-13}\ s$)
∞ (unitary limit)	63.82	3.56
1000.0	64.10	3.56
100.0	32.39	1.65
20.0	23.22	1.08
0.0 (Born limit)	23.47	1.08

Table 4-5 Parameters for the Drude conductivity fits to the normal state conductivity shown in Figure 4.9a. The values for the Born limit and the unitary limit are taken from Table 4.1 and 4.3 respectively.

When $V_I = 1000\ meV$ then the real part of the conductivity in the superconducting state has developed the shoulder at low frequency. This is the feature seen in the case of scattering in the unitary limit (see Figure 4.8b). Thus scattering other than Born scattering is very easy to identify in the optical conductivity due to the appearance of a shoulder at low frequencies. This is

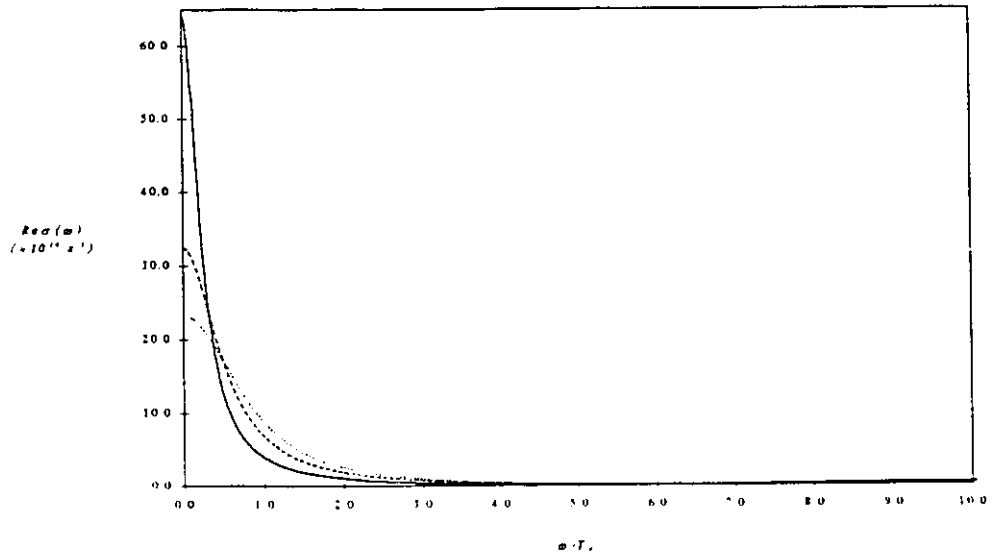

(a)

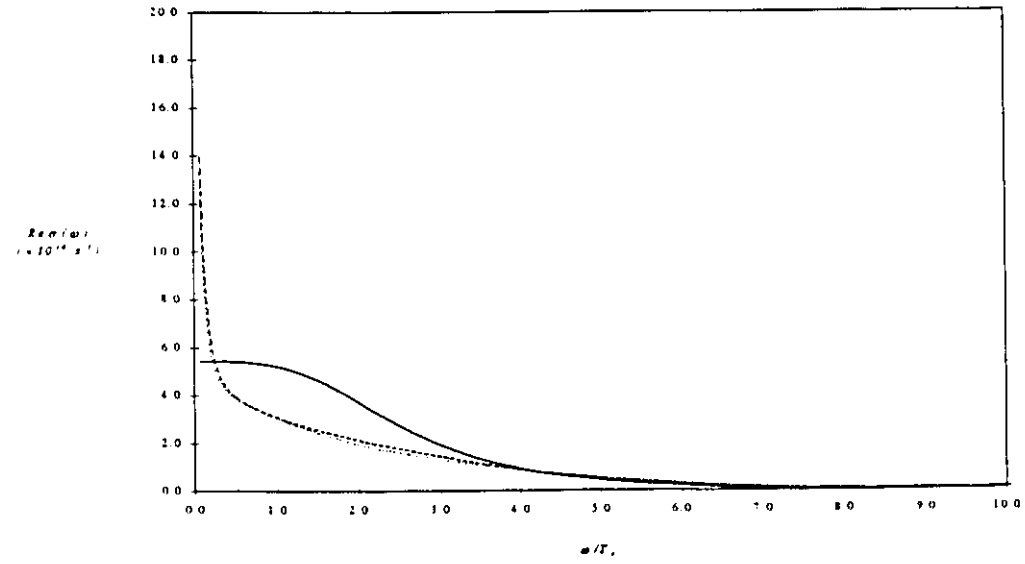

(b)

Figure 4.9 The real part of the conductivity in the normal state (a) and the superconducting state (b) for three different impurity scattering strengths and $\mu=0$ and the impurity concentration adjusted such that $T_c/T_c^0=0.90$. The solid curve is $V_I=1000$ meV; the dashed curve is $V_I=100$ meV; the dotted curve is $V_I=20$ meV. Note the difference in the y-axis scales between the normal state, (a) and the superconducting state, (b).

consistent with the conclusion reached from the penetration depth where the presence of strong scattering is very easily identified by a quadratic behavior in $((\lambda(0)/\lambda(T))^2$.

The optical conductivity with finite chemical potential ($\mu=25$ *meV*) for the same intermediate scattering strengths as above is shown in Figure 4.10. This set of diagrams can be analyzed in the identical way to the set with $\mu=0$ (Figure 4.9). The normal state conductivity is shown in Figure 4.10a for the three values of V_I. It is Drude like with the parameters as shown in Table 4-5. From this table one can see the differences of scattering in the Born limit to that of unitary scattering both on the dc conductivity and on the scattering time. Comparing the solid line of Figure 4.6 (Born scattering, $V_I \rightarrow 0$) with the dotted line of Figure 4.10 ($V_I = 20$ *meV*), it is seen that these curves are both similar in shape and magnitude and there are no features which are peculiar to any of them. Comparing this set with $\mu=25$ *meV* with the Born scattering case (Figure 4.6) and the unitary scattering case (Figure 4.8) it is seen that the same conclusions as for the case when $\mu=0$ are reached.

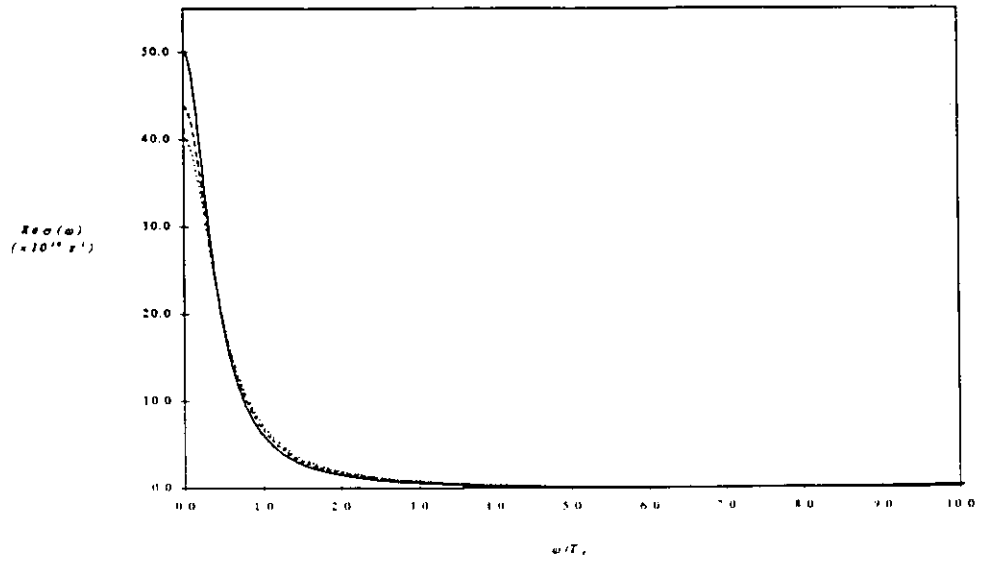

(a)

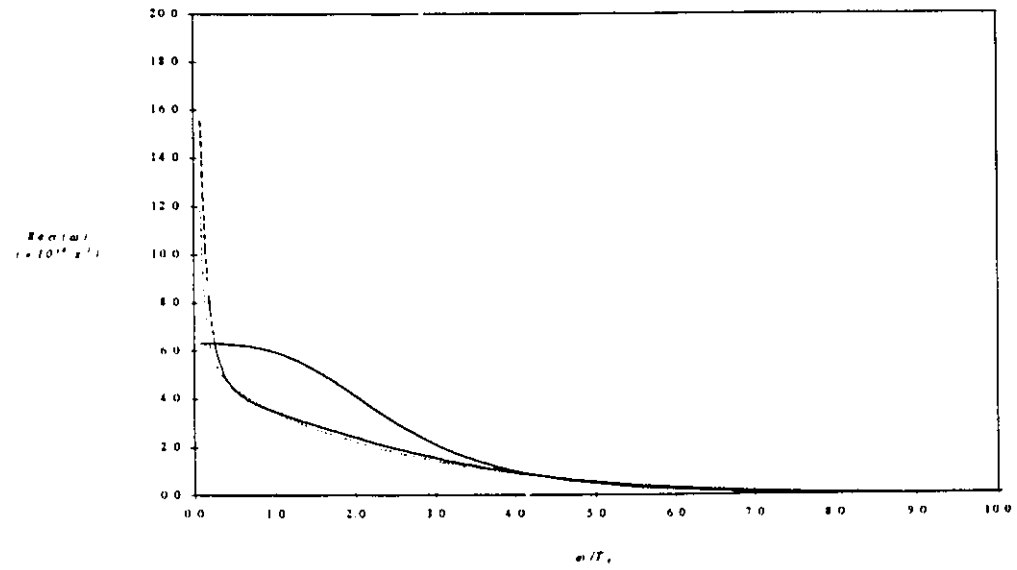

(b)

Figure 4.10 The real part of the conductivity in the normal state (a) and the superconducting state (b) for three different impurity scattering strengths and μ=*25 meV* and the impurity concentration adjusted such that T_c/T_c^0=*0.90*. The solid curve is V_I=*1000 meV*; the dashed curve is V_I=*100 meV*; the dotted curve is V_I=*20 meV*. Note the difference in the y-axis scales between the normal state, (a) and the superconducting state, (b).

V_I (meV)	σ_0 ($\times 10^{14}$ s^{-1})	τ ($\times 10^{-13}$ s)
∞ (unitary limit)	39.14	2.00
1000.0	50.12	2.53
100.0	43.80	2.23
20.0	40.10	2.03
0.0 (Born limit)	38.26	1.94

Table 4-6 Parameters for the Drude conductivity fits to the normal state conductivity shown in Figure 4.10a. The values for the Born limit and the unitary limit are taken from Table 4.1 and 4.3 respectively. The unitary limit is at a higher impurity concentration ($T_c^{(unitary)}/T_c^0=0.87$) and thus giving a smaller dc conductivity and scattering time than with V_I=1000 meV.

Thus if there is strong impurity scattering present the optical conductivity will readily demonstrate this as a shoulder at low frequency. Whereas for weak scattering there will be no direct evidence of a superconducting gap or superconductivity in the optical conductivity.

4.5. Summary

In conclusion, the optical conductivity for a 2-dimensional superconductor with a $d_{x^2-y^2}$ symmetry gap has been calculated. Impurity scattering of arbitrary strength has been included in the calculation along with different chemical potentials. The results are consistent with what is expected for a metallic normal

state (Drude like conductivity) and a superconducting state with a gap that goes to zero at points on the Fermi surface. This gapless behavior is in contrast to a conventional superconductor which has no optical absorption (a gap) from zero frequency to a value of $2\Delta_0$ due to the gap of Δ_0 in the electronic excitation spectrum. For the superconductor under consideration here, there is no evidence of superconductivity in the low frequency region, although it is known to be in a superconducting state since $\Delta_0 \neq 0$. This gapless behavior is due to the fact that electronic excitations are possible at arbitrarily small energy because the gap in the excitation spectrum becomes zero at points on the Fermi surface.

When impurity scattering in the unitary limit is included there is evidence of superconductivity as seen in the optical conductivity by the presence of a shoulder in the optical spectrum at low frequencies. This behavior is seen long before the actual limit for unitary scattering ($V_I \rightarrow \infty$), hence strong scattering should make itself readily apparent if present. This is in agreement with the conclusions obtained from the analysis of the magnetic penetration depth. However no shoulder in the optical conductivity is seen in the experiments on the high T_c superconductors (Sumner *et al.*, 1993; Kim *et al.*, 1993a, 1993b, 1993c), whereas the penetration depth does show possible evidence of unitary scattering on similar samples (Hardy *et al.*, 1993). Such low frequencies are difficult to probe by far infrared optical absorption.

The optical conductivity has also been calculated with different chemical potentials. This is seen to have no or at the most perhaps a small effect on the conductivity. Hence the details of the electronic band structure cannot be probed effectively in this manner.

A difference in the type of scattering (Born or unitary limit) has been seen in the dc conductivity and also the scattering times. This same type of difference is seen experimentally (Bonn, *et al.*, 1994) on Ni and Zn doped Y-Ba-Cu-O compounds. They observe that Ni provides as much scattering as Zn but has a much less effect on the critical temperature. This effect is seen in both the penetration depth and the dc conductivity. It is also predicted in this model as a non-trivial difference between scattering in the Born limit and scattering in the unitary limit which is not seen in the usual constant density of states theories. This shows the importance in the high-T_c superconductors of the entire electronic density of states including the van Hove singularity and how a complete theory cannot ignore the structure of the density of states.

The main feature of a 2-dimensional $d_{x^2-y^2}$ symmetry superconductor is the absence of any gap in the optical conductivity. Moreover it is difficult to identify any feature with the superconducting gap and hence pin down a value for the gap. It does make itself apparent when there is impurity scattering in the unitary limit.

5. Conclusions

In conclusion a model for superconductivity relevant to the high-T_c superconductors has been studied. This model consists of a 2-dimensional Hubbard model with tight binding electrons in the plane, and the superconducting state having a gap with $d_{x^2-y^2}$ symmetry. The Hubbard model and some of the properties have been described in chapter 2. These properties include a van Hove singularity in the electronic density of states. This work accounts for this van Hove singularity fully: a constant density of states has not been assumed at any point nor has any model been taken for the density of states. This is accomplished by performing the k-space integrations directly and not converting them to an integral over energy with the density of states as is usually done. Thus the effect of the details of the band structure have been examined.

Strong coupling theory of superconductivity has been used to derive a set of Eliashberg equations as seen in chapter 2. This includes an electron-boson interaction where the bosons are anti-ferromagnetic spin fluctuations (as opposed to the conventional case where the bosons are phonons) which is a possible mechanism for the high-T_c superconductors. Impurity scattering of arbitrary strength is included by using a T-matrix approach. The derivation of the Eliashberg equations using quantum field theoretic techniques is discussed. The resulting Eliashberg equations are completely general including any band structure, any electron-boson interaction and impurity scattering of arbitrary strength. The Eliashberg equations are then reduced to give a general set of equations for the critical temperature and also reduced to give a single equation describing the normal state.

To derive a set of Eliashberg equations for a d-wave superconductor, a separable model (in momentum and frequency) is used for the electron-boson interaction. Within this model the superconducting gap takes on the form

$$\Delta(\mathbf{k}, i\omega_n) = \Delta(i\omega_n)\eta(\mathbf{k})$$

where $\eta(\mathbf{k})$ is an expansion (2.87) in functions having the required $d_{x^2-y^2}$ symmetry. The simplest function (and the most common used in the literature) having the required symmetry is

$$\eta_{10}(\mathbf{k}) = \cos k_x - \cos k_y \quad .$$

A set of Eliashberg equations has been derived for a separable model with 2-dimensional superconductor with $d_{x^2-y^2}$ symmetry and the corresponding equations for the critical temperature.

This inclusion of impurity scattering leads to interesting results. There is found to be a non-trivial difference between Born scattering and unitary scattering. This is in contrast to the approximation that is usually made of a constant electronic density of states which leads to a single parameter (the scattering time) that can represents both types of scattering. This difference in the types of scattering is evident in the reduction of the critical temperature and it is also seen in both the penetration depth and the optical conductivity.

This set of Eliashberg equations has been solved for both T_c and for the superconducting and normal states by numerical iteration. Included in the solution have been various band structures, impurity scattering strengths and concentrations and $d_{x^2-y^2}$ symmetry functions. Band structure effects have made themselves apparent in solutions for T_c which show that T_c has a maximum when there is no next nearest neighbor hopping and also that T_c is highly peaked about $\mu=0$ (half-filling). The dependence of T_c on impurity concentration both in the Born approximation and unitary limit shows that normal (nonmagnetic) impurities act as Cooper pair breakers. This is in contrast to conventional superconductivity where normal impurities have no effect on the critical temperature.

The magnetic penetration depth has been calculated for this model. A general expression for the penetration depth has been derived and this has been calculated using solutions of the Eliashberg equations. It has been calculated for various coupling strengths, band structure parameters, impurity scattering strengths and concentrations and for various $d_{x^2-y^2}$ symmetry functions.

The main feature found is that $((\lambda(0)/\lambda(T))^2$ is linear when no impurity scattering is present. This linear behavior is a feature due to the fact that the superconducting gap goes to zero at points on the Fermi surface. If the gap were positive everywhere as is the case for a conventional superconductor then there would be an exponential dependence due to the finite gap in the excitation spectrum. Varying the chemical potential or the next nearest neighbor hopping strength produces small changes in the penetration depth but it remains linear.

This linear behavior is very robust to Born scattering as large amounts of Born scattering centres must be introduced to change the linear behavior to quadratic. This is not the case for unitary scattering as small amounts will change the linear behavior to a quadratic behavior. This stems from the non-trivial difference between impurity scattering in the Born limit and that of scattering in the unitary limit. Impurity scattering in the Born limit gives a large reduction in the critical temperature for large concentrations of impurities but does not affect the penetration depth in such a large manner. Impurity scattering in the unitary limit for small concentrations can affect large changes in the penetration depth

while reducing the critical temperature by a substantially lesser degree than that of Born scattering. This result is consistent with experimental observations on Ni and Zn doped Y-Ba-Cu-O where Zn has a much smaller reduction of the critical temperature than that of Ni while providing the same magnitude of changes in the penetration depth and the dc conductivity. This shows the importance of the electronic density of states in the properties of the high-T_c superconductors and that it must be included in a realistic manner in a complete theory for these materials. This result is consistent with that seen experimentally in the high-T_c superconductors.

The penetration depth has also been calculated with different $d_{x^2-y^2}$ symmetry functions. Large effects can arise in the penetration depth as it is possible for some of these functions to go to zero everywhere on the Fermi surface for the case $\mu=0$ and $B=0$. These effects are reduced as μ and B are varied away from zero. Effects are also seen for other $d_{x^2-y^2}$ symmetry functions but these changes are not as dramatic as the ones where the function goes to zero everywhere on the Fermi surface.

The results most consistent with the behavior seen experimentally are obtained with the simplest $d_{x^2-y^2}$ symmetry function, $cosk_x$-$cosk_y$. With this function and different impurity concentrations excellent agreement with experimental results is obtained at low temperatures.

The optical conductivity has been calculated for this model. A general expression for the conductivity on the imaginary frequency axis was derived. This expression was calculated by substitution of the solutions of the Eliashberg equations and then analytically continuing this to the real frequency axis by means of a Padé approximation. The optical conductivity of the normal state has also been calculated in a similar manner. Different chemical potentials and impurity scattering of different strengths and concentrations has been used in the calculation.

The normal state conductivity is found to be Drude like at low frequencies as expected for a Fermi liquid. No qualitative differences in the normal state conductivity are seen for different impurity scattering strengths and concentrations or for different chemical potentials. However the magnitude of the conductivity does depend on these parameters.

The optical conductivity in the superconducting state is found to be radically different from that of conventional superconductors. There is no gap in the real part of the optical conductivity whereas for conventional superconductors there is a gap of twice the superconducting gap. This gapless behavior is due to the fact that since the superconducting gap goes to zero at points on the Fermi surface it is possible to have excitations of arbitrarily small energy. Hence optical absorption can begin at arbitrarily low frequencies. Not only is there no gap in the

optical absorption spectrum, there is no evidence of a superconducting gap at low frequencies.

The normal state conductivity exhibits the difference of impurity scattering in the Born limit and that of scattering in the unitary limit. Unitary scattering does not reduce the dc conductivity or the scattering times as much as Born scattering for identical reductions in the critical temperature. This behavior is observed between Ni and Zn doped Y-Ba-Cu-0 compounds.

Gapless behavior is seen for all impurity strengths and concentrations and chemical potential studied, although the magnitude of the conductivity does change. There is however another feature when unitary scattering is included. That is a shoulder at low frequency in the real part of the optical conductivity in the superconducting state. The main feature in the conductivity is that there is no evidence of a superconducting gap or any gap in the optical spectrum

Finally, the penetration depth and the optical conductivity have been calculated for a 2-dimensional superconductor with $d_{x^2-y^2}$ symmetry. This has been done using the strong coupling theory of superconductivity along with the 2-dimensional Hubbard model. In doing so, general expressions for the Eliashberg equations, penetration depth and the optical conductivity have been derived. These are valid for any band structure, electron-boson interaction and impurity scattering of any strength and concentration. It is found that there is a non-trivial difference between impurity scattering in the Born limit and that of scattering in

the unitary limit. The results found for the temperature dependence of the penetration depth at low temperature as well as its magnitude are in excellent qualitative agreement with experiments performed on the high-T_c superconductors. The results for the conductivity are also in qualitative agreement with the available experiments. It is not yet clear of the mechanism or details of the mechanism responsible for the high-T_c superconductors. However from the work here it is found that within this model the details of the electronic density of states play a crucial role in the properties of high-T_c superconductors. The work here which is based upon a 2-dimensional system consisting of a Fermi liquid, with d-wave superconductivity stabilized by anti-ferromagnetic spin fluctuations where Migdal's theorem (or on equivalent theorem) is assumed valid does give a possible and consistent description of the properties studied as compared with the experimentally observed properties.

6. References

Abrikosov, A.A., and L.P. Gorkov, 1960, Zh. Eksp. Teor. Fiz. **39**, 1781.

Abrikosov, A.A., and L.P. Gorkov, 1961, Sov. Phys. JETP **12**, 1243.

Abrikosov, A.A., L.P. Gorkov, and I.E. Dzyaloshinski, 1963, *Methods of Quantum Field Theory in Statistical Physics* (Dover Publications Inc. New York).

Allen, P.B., 1980, in *Modern Trends in the Theory of Condensed Matter*, edited by A. Pekalski and J. Przystawa (Springer, New York), p.138.

Allen, P.B., and B. Mitrovic, 1982, in *Solid State Physics*, edited by H. Ehrenreich, F. Seitz, and D. Turnbull (Academic, New York), Vol. 37, p.1.

Ambegaokar, V., and A.A. Griffin, 1965, Phys. Rev. **137**, A1151.

Annett, J.F., and N. Goldenfeld, 1992, J. Low Temp. Phys. **89**, 197.

Arberg, P., and J.P. Carbotte, 1995, Phys. Rev. B **50**, 3250..

Arberg, P., M. Mansor, and J.P. Carbotte, 1993a, J. Phys. Chem. Solids **54**, 1461.

Arberg, P., M. Mansor, and J.P. Carbotte, 1993b, Solid State Comm. **86**, 671.

Bardeen, J., L.N. Cooper, and J.R. Schrieffer, 1957, Phys. Rev. **108**, 1175.

Basov, D., 1995, private communication.

Basov, D., A.V. Puchkov, R.A. Hughes, T. Strach, J. Preston, T. Timusk, D.A. Bonn, R. Liang, and W.N. Hardy, 1994, Phys. Rev. B **49**, 12165.

Basov, D.N., R. Liang, D.A. Bonn, W.N. Hardy, B. Dabrowski, M. Quijada, D.B. Tanner, J.P. Rice, D.M. Ginsberg, and T. Timusk, 1995, Phys. Rev. Lett. **74**, 598.

Batlogg, B.H., H. Takagi, H.L. Kao, and K. Kwo, 1993, in *Electronic Properties of High-T_c Superconductors*, edited by H. Kuzmany, M. Mehring, and J. Fink (Springer-Verlag Berlin, Heidelberg), p.5.

Baym. G., and D. Mermin, 1961, J. Math. Phys. 2 232.

Bednorz, J.G., and K.A. Müller, 1986, Z. Phys. B **64**, 189.

Bickers, N.E., D.J. Scalapino, R.T. Collins, and Z. Schlesinger, 1990, Phys. Rev. B **42**, 67.

Blashke, R., and R. Blocksdorf, 1982, Z. Phys. B **49**, 99.

Bonn, D.A., S. Kamal, K. Zhang, R. Liang, D.J. Baar, E. Klein, and W.N. Hardy, 1994, preprint.

Bulut, N., and D.J. Scalapino, 1992, Phys. Rev. B **45**, 2371.

Carbotte, J.P., 1982 in *Superconductivity in d- and f- Band Metals*, edited by W. Buckel and W. W· ber (Kernforschungszentrum, Karlsruhe), p.487.

Carbotte, J.P., 1990, Rev. Mod. Phys. **62**, 1027.

Carbotte, J.P., C. Jiang, D.N. Basov, T. Timusk, 1995, Phys. Rev. B **51**, 11798.

Chu, C.W., P.H. Hor, R.L. Meng , L. Gao, Z.J. Huang, and Y.Q. Wang , 1987 , Phys. Rev. Lett. **58** , 405.

Clem, J-R., 1966, Ann. Phys. **40**, 268.

Daams, J.M., and J.P. Carbotte, 1980a, J. Low Temp. Phys. **40**, 135.

Daams, J.M., and J.P. Carbotte, 1980b, Solid State Comm. **33**, 585.

Daams, J.M., and J.P. Carbotte, 1981, J. Low Temp. Phys. **43**, 263.

de Gennes, P.G., 1966, *Superconductivity of Metals and Alloys* (W.A. Benjamin Inc.).

Dolgov, O.V., E.G. Maksimov, and S.V. Shulga, 1990 in *Electron-Phonon Interaction in Oxide Superconductors*, edited by R. Baquero (World Scientific, Singapore).

Doniach, S., and E.H. Sondheimer, *Green's Functions for Solid State Physicists*, (Addison-Wesley, Redwood City, California).

Dzyaloshinskii, I.E., 1987, Sov. Phys. JETP **66**, 848.

Einzel, D. P.J. Hirschfeld, F. Gross, B.S. Chandrasekhar, K Andres, H.R. Ott, J. Beuers, Z. Fisk, and J.L. Smith, 1986, Phys. Rev. Lett. **56**, 2513; Z. Phys. B **64**, 175.

Eliashberg, G.M., 1960a, Sov. Phys.-JETP **11**, 696.

Eliashberg, G.M., 1960b, Zh. Eksp. Teor. Fiz. **38**, 966.

Ernst, P., W. Schaelle, M. Breuer, and R. Borowski, 1993, Ann. Physik **2**, 120.

Fetter, A.L., and J.D. Walecka, 1971, *Quantum Theory of Many Particle Systems* (McGraw Hill Inc. New York).

Frölich, H., 1952, Proc. R. Soc. London Ser. A **215**, 291.

Fulde, P., J. Keller, and G. Zwicknagl, 1988, in *Solid State Physics*, edited by H, Ehrenreich, F. Seitz, and D. Turnbull (Academic, New York), Vol. 41, pp.1-50.

Galkin, A.A., A.I. D'yachenko, and V.M. Svistunov, 1974, Zh. Eksp. Teor. Fiz. **66**, 2262; Sov. Phys. JETP **39**, 1115.

Ghiron, K., M.B. Salamon, M.A. Hubbard, and B.W. Veal, 1993, Phys. Rev. B **48**, 16188.

Golovashkin, A.I., E.V. Pechin', A.I. Skvortsov, and N.E. Khlebova, 1981, Fiz. Tverd. Tela **23**, 1324 ; Sov. Phys. - Solid State (Engl. Transl.) **23**, 774.

Grimvall, G., 1981, *The Electron-Phonon Interaction in Metals* (Noth-Holland, New York).

Gross, F., B.S. Chandrasekhar, K. Andres, U. Rauchschwalbe, E.B. Bucher, and Luthi, 1988, Physics C **153-155**, 439.

Hardy, W.N., D.A. Bonn, D.C. Morgan, R. Liang, and K. Zhang, 1993, Phys. Rev. Lett. **70**, 3999.

Hazen, R.M., L.W. Finger, R.J. Angel, C.J. Piewitt, N.L. Ross, G.G. Hadidiacos, P.J. Heany, D.R. Veblen, Z.Z. Sheng A. Ali, and A.M. Herman, 1988, Phys. Rev. Lett. **60**, 1657.

Hirsch, J.E., and E. Fradkin, 1982, Phys. Rev. Lett. **49**, 402.

Hirschfeld, P. W. Putikka, and D.J. Scalapino, 1994, Phys. Rev. B **50**, 10250.

Hirschfeld, P., D. Volhardt, and P.Wölfe, 1986, Solid State Comm. **59**,111.

Hirschfeld, P., P.Wölfe, and, D. Einzel, 1988, Phys. Rev. B **37**, 83.

Hubbard, J., 1963, Proc. R. Soc. London Ser. A **276**, 238.

Inderhees, S.E., M.B. Salamon, J.P. Rice, and D.M. Ginsberg, 1991, Phys. Rev. Lett. **66**, 232.

Inderhees, S.E., M.B. Salamon, N. Goldenfeld, J.P. Rice, B.G. Pazol, and D.M. Ginsberg, 1988, Phys. Rev. Lett. **60**, 1178.

Ishiguro, T., and K. Yamaji, 1990, *Organic Superconductors* (Springer-Verlag, Berlin).

Jerome, D., A. Mazaud, M. Ribault, and K. Bechgaard, 1980, J. Physique Lett. **41**, L95-98.

Jiang, C., 1992, private communication

Jiang, C., and J.P. Carbotte, and R.C. Dynes, 1993, Phys. Rev. B **47**, 5325.

Kieselmann, G., and H. Rietchel, 1982, J. Low Temp. Phys. **46**, 27.

Kihlstrom, K.E., and T.H. Geballe, 1981, Phys. Rev. B **24**, 4101.

Kim, H., G. Preosti, and P. Muzikar, 1994, Phys. Rev. B **49**, 3544.

Kim, J., and T. Lemberger, 1993a, preprint.

Kim, J., E.R. Ulm, and T. Lemberger, 1993b, to be published LT-20.

Kim, J., M.J. Sumner, E.R. Ulm, and T. Lemberger, 1993c, to be published J. Phys. Chem. Solids.

Kitazawa, A., 1990, in *Earlier and Recent Aspects of Superconductivity*, edited by J.G. Bednorz and K.A. Müller (Springer-Verlag Berlin, Heidelberg), p.45.

Kostur, V.N., and B. Mitrovic, 1993, preprint.

Kresin, V.Z., H. Morawitz, and S.A. Wolf, 1993, *Mechanisms of Conventional and High T_c Superconductivity* (Oxford University Press, New York).

Leavens, C.R., and D.S. Ritchie, 1985, Solid State Comm. **53**, 137.

Lee, J., K. Paget, T.R. Lemberger, S.R. Foltyn, and X. Wu, 1993, preprint.

Liang, R., P. Dosanjh, D.A. Bonn, D.J. Baar, J.F. Carolan, and W.N. Hardy, 1992, Physica C **195**, 51.

Liu, J., Y. Li, and C.M. Lieber, 1993, preprint.

Loram, J.W., J.R. Cooper, J.M. Wheatley, K.A. Mirza, and R.S. Liu, 1992, Phil. Mag. B **65**, 1405.

Mahan, G.D., 1981, *Many Particle Physics* (Plenum Press, New York).

Maki, K., 1969 in *Superconductivity*, edited by R.D. Parks (Marcel Dekker, New York), Vol. 2, p.1035.

Mansor, M., 1994, Ph.D Thesis.

Marsiglio, F., M. Schossmann, and J.P. Carbotte, 1988, Phys. Rev. B **37**, 4965.

McMillan, W.L., and J.M. Rowell, 1965, Phys. Rev. Lett. **14**, 108.

McMillan, W.L., and J.M. Rowell, 1969, in *Superconductivity* (R.D.Parks ed.), vol. 2, Chapter 13 (Dekker, New York).

Migdal, A.B., 1958, Zh. Eksp. Teor. Fiz. **34**, 1438; Sov. Phys. JETP **11**, 696 (1960).

Millis, A.J., H. Monien, D. Pines, 1990, Phys. Rev. B **42**, 167.

Millis, A.J., S. Sachdev, and C.M. Varma, 1988, Phys. Rev. B **37**, 4975.

Mitrovic, B., and J.P. Carbotte, 1981, J. Low Temp. Phys. **43**, 131.

Mitrovic, B., and J.P. Carbotte, 1983a, Can. J. Phys. **61**, 784.

Mitrovic, B., and J.P. Carbotte, 1983b, Phys. Rev. B **28**, 2477.

Miyake, K., S. Schmitt-Rink, and C.M. Varma, 1986, Phys. Rev. B **34**, 6554.

Monthoux, P., A.V. Balatsky, and D. Pines, 1991, Phys. Rev. Lett. **67**, 3448.

Monthoux, P., A.V. Balatsky, and D. Pines, 1992, Phys. Rev. B **46**, 14803.

Monthoux, P., and D. Pines, 1993, Phys. Rev. B **47**, 6069.

Nam, S.B., 1967a, Phys. Rev. **156**, 470.

Nam, S.B., 1967b, Phys. Rev. **156**, 487.

Nambu, Y., 1960, Phys. Rev. **117**, 648.

Newns, D.M., C.C. Tsuei, P.C. Pattnaik, and C.L. Kane, 1992, Comm. on Cond. Mat. Phys. **15**, 273.

Nicol, E.J., J.P. Carbotte, and T. Timusk, 1991, Phys. Rev. B **43**, 473.

Pattnaik, P.C., C.L. Kane, D.M. Newns, and C.C. Tsuei, 1992, Phys. Rev. B **45**, 5714.

Pickett, W.E., 1980, Phys. Rev. B **21**, 3897.

Pickett, W.E., 1982, Phys. Rev. B **26**, 1186.

Prohammer, M., and J.P. Carbotte, 1991, Phys. Rev. B **43**, 5370.

Rickayzen, G., 1980, *Green's Functions and Condensed Matter* (Academic Press, New York).

Rusinov, A.I., 1969a, Zh. Eksp. Teor. Fiz. **56**, 2043.

Rusinov, A.I., 1969b, Sov. Phys. JETP **29**, 1101.

Schachinger, E., and J.P. Carbotte, 1991, Phys. Rev. B **43**, 10279.

Schachinger, E., J.M. Daams, and J.P. Carbotte, 1980, Phys. Rev. B **22**, 3194.

Schrieffer, J.R., 1964, *Theory of Superconductivity* (Benjamin, New York).

Shen, L.Y., 1972, Phys. Rev. Lett. **29**, 1082.

Shen, Z.X., D.S. Dessau, B.O. Wells, D.M. King, W.E. Spicer, A.J. Arko, D. Marchall, L.W. Lombardo, A. Kapitulnik, P. Dickinson, S. Doniach, J. DiCarlo, A.G. Loesser, and C.H. Park, 1993, Phys. Rev. Lett. **70**, 1553.

Sheng, Z.Z., and A.M. Herman , 1988a, Nature **332** , 55.

Sheng, Z.Z., and A.M. Herman , 1988b, Nature **332** , 138.

Shiba, H., 1968, Prog. Theor. Phys. 40, 435.

Skalski, S.S., O. Betbeder-Matibet, and P.R. Weiss, 1964, Phys. Rev. **136**, A1500.

Stewart, G.R., 1984, Rev. Mod. Phys. **56**, 755.

Sumner, M.J., J. Kim, and T. Lemberger, 1993, Phys. Rev B **47**, 12248.

Ulm, E.R., J. Kim, T.R. Lemberger, S.R. Foltyn, and X. Wu, 1993b, preprint.

Ulm, E.R., J. Lee, J. Kim, T.R. Lemberger, S.R. Foltyn, and X. Wu, 1993a, preprint.

Varma, C.M., 1988, in *High T_c Superconductivity*, edited by H.W. Weber (Plenum, New York), p.13.

Vidberg, H.J., and W. Serene, 1977, J. Low Temp. Phys. **29**, 179.

Wells, B.O., Z.X. Shen, D.S. Dessau, W.E. Spicer, D.B. Mitzi, L. Lombardo, and A. Kapitulnik, 1993, Phys. Rev. B **46**, 11830.

Wenger, F., and S. Östlund, 1993, Phys. Rev. B. **47**, 5977.

Whitmore, M., 1984, J. Low Temp. Phys. **56**, 129.

Xing, D.Y., M. Liu, and C.D. Gong, 1991, Phys. Rev. B 44, 12525.

Zarate, H.G., and J.P. Carbotte, 1983a, Phys. Rev. B **27**, 194.

Zarate, H.G., and J.P. Carbotte, 1983b, Solid State Comm. **48**, 273.

Zhang, K., D.A. Bonn, S. Kamal, R. Liang, D.J. Baar, W.N. Hardy, D. Basov, and T. Timusk, 1994, Phys. Rev. Lett. **73**, 2484.